2020

Improving Grid Hosting Capacity and Inertia Response with High Penetration of Renewable Generation

Hamidreza Sadeghian
Virginia Commonwealth University

Improving Grid Hosting Capacity and Inertia Response with High Penetration of Renewable Generation

A dissertation submitted in partial fulfillment of the requirements for the degree of Doctor of Philosophy at Virginia Commonwealth University

By

Hamidreza Sadeghian

M.Sc. in Electrical Engineering, Amirkabir University of Technology, Iran

Director: Zhifang Wang, Ph.D.

Associate Professor, Department of Electrical and Computer Engineering

Virginia Commonwealth University

Richmond, Virginia

May, 2020

Dedication

I dedicate this work to my wife, ***Parna***, for her love, perseverance, and unconditional support. Who always inspires me to chase my dreams and stands behind me, even when there is little behind in which to stand.

I also dedicate this work to my parents, they have been the continuous light in my life and without them, achieving this importance would have been hardly possible.

Acknowledgments

First and foremost, I would like to express me very deep appreciation and sincere thanks to my advisor, Dr. Zhifang Wang for her precious support and guidance, and encouragement during these past four years. Without her valuable comments, expertise, and the effort and time she dedicated to helping me, this dissertation would not have been reached its current form. She has guided me through this Ph.D. process and given me every opportunity to be successful, I will always be grateful for her endless support.

I would like to thank my committee members, Dr. Umit Ozgur, Dr. Yanxiao Zhao, Dr. Weijun Xiao, Dr. Changqing Luo, Dr. Thang N Dinh. for their insightful comments and invaluable encouragement to achieve this dissertation.

Lastly, I would like to give a special thanks to my family and all my friends both inside and outside of VCU, for their unwavering support and encouragement throughout this challenging yet exhilarating endeavor. In particular, my friends at EVCU for their continuous support and friendship in the whole four years of my Ph.D. journey.

Table of Contents

List of figures

List of tables

Abstract

IMPROVING GRID HOSTING CAPACITY AND INERTIA RESPONSE WITH HIGH PENETRATION OF RENEWABLE GENERATION

By Hamidreza Sadeghian, Ph.D.

A dissertation submitted in partial fulfillment of the requirements for the degree of Doctor of Philosophy at Virginia Commonwealth University

Virginia Commonwealth University, 2020

Director: Zhifang Wang, Ph.D., Associate Professor, Department of Electrical and Computer Engineering

To achieve a more sustainable supply of electricity, utilizing renewable energy resources is a promising solution. However, the inclusion of intermittent renewable energy resources in electric power systems, if not appropriately managed and controlled, will raise a new set of technical challenges in both voltage and frequency control and jeopardizes the reliability and stability of the power system, as one of the most critical infrastructures in the today's world. Most specifically, the ever-increasing penetration of small-scale solar photovoltaic (PV) systems in distribution networks may result in serious overvoltage problems and impose unexpected equipment damages on the customer side. Moreover, the increasing interconnection of large-scale wind turbines and solar power plants with electronic interfaced components and zero inertia in transmission networks reduces the total power system inertia. This results in considerable frequency drops in case of large power imbalances, which may initiate underfrequency load shedding and large-scale blackouts.

This dissertation aims to investigate the impediments for renewable energy integration in both transmission and distribution networks and propose novel approaches and frameworks to increase

hosting capacity of power grids to accommodate more intermittent renewable generations and improve inertia response to achieve an efficient, secure, and reliable power system. The hosting capacity is defined as the maximum penetration of renewable generations that can be accommodated in the power system without violating operational constraints. The first objective in this dissertation is set to address the data deficiency. Existing power system models that could be used to test new concepts and methods are mostly outdated or insufficient. In order to generate sufficient and realistic test cases to examine new concepts and methods in renewable energy integration, this work develops a new framework and introduce a toolkit to automatically generate any number of synthetic power grids featuring the same statistical properties of realistic power grids. A full validation process - with five categories of topology metrics, electrical parameters, state variables, interdependency, and scaling properties - is proposed in the framework to assure that the generated synthetic cases satisfy the predefined criteria of multiple metrics that were observed from realistic power grids.

Second part of the dissertation is to investigate the impacts of small-scale solar PV systems on distribution networks and develop a detailed impact assessment framework. Utility-aided installation of solar PV systems is assumed to use an optimized algorithm and compared with randomized customer-based installation to maximize hosting capacity and minimize negative impacts of distributed solar PV systems. It is found that the proposed utility-based installation with optimized size and location of solar PV systems improves the hosting capacity from 30% to 50% in the distribution network. Simulation analysis conducted using the developed assessment framework reveals a strong correlation between the reveres power flow and overvoltages in a distribution network. In addition, it is shown that the utility-based installation can decrease the energy loss in the system by 11.3% which brings a significant improvement in system efficiency.

The third part of this dissertation examines demand side management of smart homes as one of the viable solutions to improve the utilization of distributed renewable generation. It investigates the interaction of rooftop PV systems and the electric household appliances and develop a novel algorithm to increase renewable energy utilization without negative impacts on distribution network. It is found that the solar power utilization efficiency can be increased from 66.27% to 98.24% by implementation of our proposed demand side management algorithm. It is also observed that higher demand side management participations will tend to "flatten" the voltage profile, thus considerably mitigating voltage fluctuations caused by load variations.

The fourth part of the dissertation tackles the low inertia of power system caused by high penetration of renewables in the grid. The distribution network with aggregated distributed energy resources are utilized to provide virtual inertia response for a bulk power system with high penetration of renewable energies. We propose a precise inertia estimation method by introducing new terms in the swing equation to have an accurate estimation of required system inertia in case of a large generator/load disconnection. Our proposed method for the inertia estimation is benchmarked against the conventional method showing a significant smaller estimation error, around 20 times smaller. Moreover, the cost of overestimation is investigated by implementing the proposed method in a realistic inertia market in the U.K.. It is found that the average cost of overestimation with conventional method is $3,114/day; however, our proposed method results in the average total cost of $187/day including overestimation cost and required system upgrade costs, which is significantly less than the conventional method. Our analysis of system behavior on IEEE 24-bus system and two large-scale synthetic power grids show that virtual inertia response is only required for renewable penetrations higher than 50%. It is found that for higher penetrations of renewables when the frequency drops to the critical point of 59.1 Hz, our proposed virtual inertia

framework can improve the frequency nadir by 60% to avoid underfrequency load shedding in the system. Simulation results demonstrate that the participation of virtual power plants in inertia response reduces both frequency deviation and time to frequency nadir.

List of Abbreviations

BESS	Battery Energy Storage Systems
C&CG	Column and Constraint Generation
CDF	Customer Decision Factor
CHP	Combined Heat and Power
CPP	Conventional Power Plant
DEM	Digital Evaluation Model
DER	Distributed Energy Resources
DG	Distributed Generation
DPV	Distributed Solar PV
DS	Distribution System
DSM	Demand Side Management
DSO	Distribution System Operator
ECS	Energy Consumption Scheduler
EI	Eastern Interconnection
ERCOT	Electric Reliability Council of Texas
ESS	Energy Storage System
FFR	Fast Frequency Response
FFT	Fast Fourier Transformation
GIS	Geographic Information System
GUI	Graphical User Interface
HC	Hosting Capacity
IR	Inertial Response
LiDAR	Light Detection and Ranging
LoG	Loss of Generator

MD	Maximum Demand
NYISO	New York Independent System Operator
OBW	Occupied Bandwidth
OpenEI	Open Energy Information
OPF	Optimal Power Flow
PDF	Probability Density Function
PF	Power Flow
PFR	Primary Frequency Response
PHEV	Plug-in Hybrid Electric Vehicle
PMU	Phasor Measurement Units
PSD	Power Spectral Density
PSO	Particle Swarm Optimization
PV	Solar Photovoltaics
RES	Renewable Energy Sources
RoCoF	Rate of Change of Frequency
SRDSM	Scalable and Robust Demand Side Management
TOU	Time of Use
TSO	Transmission System Operators
UC	Unit Commitment
VPP	Virtual Power Plant
WAMS	Wide Area Measurement System
WECC	Western Electricity Coordination Council

1. Introduction

Recent concerns regarding the environmental protection and sustainable development have resulted in a critical need for cleaner energy technologies. Some potential solutions have evolved including energy conversion through improved energy efficiency, reductions in use of fossil fuels, and increases in the supply of environmental-friendly energy resources which has led to the use of intermittent renewable energy sources (RESs). These RESs are utilized in both transmission and distribution networks. The inclusion of renewable energy sources gives rise to a new set of problems which are due to the intermittency of the sources and the dynamics of interfacing equipment. Therefore, it is essential to investigate the potential challenges of renewable energy integration and to find out the effective and efficient solutions.

This thesis aims to investigate the impediments for renewable energy integration in both transmission and distribution networks and propose novel approaches and frameworks to help to have an efficient and reliable power system with renewable energies. Data and test case are one of the most important necessities for every study. All the new methods and solutions to address negative impacts of RESs should be validated using realistic test cases. However, existing power system models that could be used to test new concepts and methods are mostly dated or insufficient. Therefore, as the first objective, a new framework is developed to generate any number of test cases featuring the same statistical properties of realistic power grids. The second objective is dedicated to appropriately investigate the impacts of small-scale solar photovoltaics (PVs) in distribution network. Solar PVs are the fastest growing RES in the US [1]. Generally, these RES are connected close to the loads in the distribution network to reduce transmission losses ad delay in the upgrade of transmission networks. We propose a new framework to examine two different types of distributed solar PV (DPV) installations in terms of operational parameters such

as energy loss, voltage deviation, and voltage fluctuation. To address the negative impacts of DPVs in distribution network, demand side management (DSM) of smart homes are investigated as the third objective. Historically, the prospect of increasing the efficiency of system operation has been the key driver for introducing DSM programs. However, the interaction of DSM strategies with intermittent RESs and novel algorithms to increase RES utilization without negative impacts need to be addressed. The last objective is to combine the previous findings of this dissertation and propose a novel framework to address the lower inertia, as one of the most important challenges of power grids with high penetration of RESs.

1.2 Motivation

As it mentioned, development of new concepts and methods for improving the efficiency of the power grids with high penetration of RESs needs performance evaluation with realistic grid topology. However, much of the realistic grid data needed by researchers cannot be shared publicly due to the security and privacy challenges. Therefore, to help drive additional innovation in the electric power industry, there is a need for grid models that mimic the characteristics of the actual grid, but do not disclose sensitive information. These models, say synthetic power grid models, will have the detail required to allow the successful development and testing of transformational power system optimization and control algorithms. The concept of synthetic power grids refers to a systematic way of building fully public test cases for the research community. These cases' size, structure, and features are anchored in a robust statistical and structural analysis of the actual grid [2].

Some public test cases have existed in the power systems research community for many decades. IEEE Transactions on Power Systems and other research journals are full of papers that demonstrate an innovation or analysis on the IEEE 14 bus case, IEEE 118 bus case, or another of

the standard cases. Often research papers present results on larger, actual datasets, but little data sharing is allowed for these due to the associated security constraintss. What have been missing in the power engineering community are large-scale, complex, high-quality test case datasets that are fully public. The largest IEEE test case has 300 buses, and most of these cases were developed in the 1960s and 1970s. The grid has changed and grown since then. The most recent models of the North American Eastern Interconnect have about 70,000 buses, with remote generator regulation, phase-shifting transformers, control systems, impedance correction tables, and other complexities.

The problem of building synthetic grids is to create a power system dataset: all the substations, buses, loads, generators, and branches, with all associated parameters. The system must be fully public and thus cannot use any actual power system information as an input; however, public data can be used. But the system must be realistic, matching characteristics of actual grids in size, complexity, structure, and parameter statistics. This is the validation: studying actual power systems to pick out the key characteristics that, when met by synthetic grids, quantifies their realism. The development of algorithms for generating a typical synthetic power grid requires comprehensive study on electrical and topological characteristics of real-world power grids. Existing methods in literature provide a very useful foundation to investigate the topological structure of power networks and propose several models to create synthetic network, resembling key features of real-world power grids. However, power grid networks are much more than a graph topology and we need to study realistic electrical parameter settings in order to develop appropriate models that fully represent a realistic power system. Indeed, there are still a number of drawbacks associated with current synthetic models, such as generation cost modelling, and transmission line capacity analysis. Transmission line capacity assignment can be considered as an example which is neglected in existing synthetic power grid models. Initial simulation results show that the issue

of transfer capacity assignment not only emerges as an electrical optimization concern, but some topological metrics must be considered to find the best line capacity assignment that is consistent with what is manifested in real-world grid. What is important here is that in the random topology power grid modeling it is impossible to apply the conventional methods into some operational problems such as line capacity assignment. To address this issue, we have to extract the statistical behavior of realistic power grids in the hope that these discoveries can be useful to develop a practical methodology to solve such technical problems.

In order to create a valid synthetic grid model, one needs to provide at least three critical components: a) the electrical grid topology; b) the generation and load settings which indicate their correlated placement and sizing; c) the transmission constraints which include the capacity limits of both transmission lines and transformers. In this work, first, we develop a novel approach to accurately determine the transmission capacities for a synthetic power grid model with components (a) and (b) already resolved. And then we combine all our previously proposed approaches and introduce a toolkit to generate synthetic models featuring same properties of realistic power grids. The AutoSynGrid toolkit is designed based on MATLAB Graphical User Interface (GUI) and it is able to build any number of synthetic cases that can be used for a variety of analysis such as Power Flow (PF) and Optimal Power Flow (OPF) studies. It allows to select several key characteristics of the generated system, such as reference system, loading level, and generation cost model. The generated cases include topology, bus type, generation and load setting, transmission line capacities and generation types and cost models. The output of the toolkit is exported in the native MATPOWER [3] format allowing to use the MATPOWER open-source, steady-state, planning, and analysis package to further studies on the generated cases. In addition, we develop a validation framework, which examines the generated synthetic cases based on the

metrics introduced in the literature and some new validation metrics we found in realistic power grids. These metrics are categorized into topology metrics, electric parameters, state variables, interdependencies, and scaling properties. Moreover, we define a closeness factor to measure the realism of generated synthetic cases and compare with totally random grids.

Distributed generation (DG) refers to small power generation units usually connected at the distribution voltage levels, which inject energy to the distribution system locally, in comparison with the bulk power plants that generate higher amounts of electrical power. Different types of renewable energy as well as fossil fuels can be used as DG. The renewable DG refers to wind, solar, combined heat and power, hydropower, and other categories. With the advances in power electronic technologies, integrating renewable energies to the system has become easier and both utility-sized renewable DG units and small-scale DGs such as rooftop PV systems are commonly used nowadays. Installing DG in the distribution system can have positive and negative effects on the system, and there is a need to adequately choose the permissible amount of DG penetration such that the advantages are not turned into disadvantages.

Integrating DG in the network, if properly sized and located, can have advantages for the system. Regardless of its type, a DG may increase the reliability of the power supply provided to the customers. A perspective to view this improvement is the ability of distribution network to locally provide a portion of its loads in presence of disturbances, and avoid overload in parts of its structure [4]–[6]. Energy loss reduction is another benefit that can be achieved by deployment of DGs in distribution network. Most of power system losses are seen at the distribution level [7], mainly due to heavy currents own through the lines and other devices. Presence of DG to generate power locally may reduce the current through the main feeder from substation to the DG location, and lead to reduction in overall system losses [8]–[11]. By installing DG in distribution network,

since the power is locally generated, the voltage drop near to the customer will be reduced, and the voltage profile may be boosted. This will in turn lead to the capacity of distribution system to withstand higher demand levels [8], [12]. Moreover, presence of DG in distribution system (DS) may also lead to deferment of investment [13], [14]. The distribution system operators usually consider investment for upgrading the feeder while the operating point of the DS is close to its marginal limits. These limits might be the maximum current flow through the transformer or feeder, the minimum voltage seen in the feeder, or high power losses observed in the DS [7]. Based on the previously mentioned advantages of DG, presence of such resources may lead to better voltage profile, lower current flow in the feeder, and reduced losses, which all can be helpful to the system operator and may lead to a deferment in the required investments.

In addition to the advantages of DGs we discussed before, presence of DG in distribution network may bring negative impacts on system performance. If the DG location and size is not selected properly, injection of power from the DG might cause severe overvoltages [15], and/or lead to higher power losses in the system [16]. Moreover, some renewable types of DG inject power to the system using power electronic devices, which in turn will increase the harmonic level in the system [17]. Presence of DG in the system can also interfere with the operation of voltage regulators. Some updates in the protection system may also be required, by modifying relay settings and/or changing fuses to relays or unidirectional relays to bidirectional ones. Some other concerns are related to the variability of renewable-type of generation (e.g. solar PV), or voltage fluctuations due to the intermittent nature of some types of DG, which can cause an increased operation of voltage regulating devices or temporary overvoltages in the system [18].

While it is desired for the distribution network operators to host DG, higher penetration levels may cause the distribution network to operate at its maximum available capacity. Hence, careful

measures are needed such that the system and all its elements can accommodate the desired level of DG penetration without negative impacts. DG integration in distribution network might be limited by bus voltage and line current limits, interaction with voltage regulators and control schemes, effects on the correct operation of protection systems, and harmonic levels in the system [19]–[21]. As for voltages, distribution network bus voltages are desired to remain within specified thresholds, hence, while increasing the DG penetration, voltages should not violate the higher limit. Moreover, if the DG absorbs reactive power, the voltage might be decreased in some buses while DG penetration is increased, and the minimum steady state voltage limit should also be considered. By injecting power into the system, line currents will also change, and the penetration level should not increase line currents above their loadability limits.

Solar PV power supplied to the utility grid, as a renewable energy, is one of the important DGs which gaining more and more visibility, while the world's power demand is increasing [22]. According to the Solar Energy Industries Association, solar energy ranked as the number one source of new electric generating capacity for the first time ever. There are now more than one million solar installations in the United States. The U.S. market installed 14,762 MWdc of PV system in 2016, which is twice of the PV capacity installed in 2015. Total installed U.S. solar PV capacity is predicted to become almost three times over the next 3 years. By 2022, more than 18 GW of solar PV capacity will be installed per year [23]. Non-dispachable and intermittent nature of PV systems can cause additional negative impacts on stability, reliability, and efficiency of the distribution network. Some of these technical issues in distribution circuits can be summarized as below [22]:

- *Reverse power flow:* High penetration of PVs on a feeder can cause reverse power flow from feeder to the substation. Reverse power flow can cause problems for the protection systems and voltage regulators and can lead to overvoltage violations.
- *Overload:* The ampacity rating of systems' equipment could be exceeded due to high integration of PV systems. The PV generation can overload systems' elements, which are located between load centers and PV systems.
- *Voltage Fluctuations:* PV power output depends on the solar radiation and can fluctuate a lot on cloudy days. These fast variations cause large and frequent voltage oscillations and increase the voltage regulation equipment's operations.
- *Voltage and current unbalance:* If PVs on a feeder are mostly connected to one phase, it can cause unbalance current and voltage on the feeder. However, if the PVs installed properly, they can reduce the voltage and current unbalance, as they will reduce the loading on the system.
- *Power Loss:* High PV penetration may increase feeder line losses due to the reverse power on the feeder.
- *System protection problem:* High integration of PV systems can change the level of fault currents and can result in necessary review of the protection coordination implemented in the distribution feeder.

Among the above technical problems, voltage rise is the major obstacle due to the reverse power flow along the distribution feeder [24]–[27]. This phenomenon can be aggravated under high penetration of distributed PVs (DPVs). Overvoltage violation can happen on the distribution circuit during low-load and high irradiance conditions. Voltages should remain in acceptable range; otherwise, they can result in lifetime reduction of electrical equipment and can trip offline

due to a localized voltage being out of range. To study impacts of these evaluate system capacity to host high penetration of these newcomers (DPVs) without exceeding the operational performance limits, the hosting capacity (HC) was proposed.

Hosting capacity of a feeder is defined as the maximum DG output that that can be accommodated on a distribution network without violating operational constraints or need to system upgrades [24]. This capacity depends on the DG type, feeder characteristics, limiting criteria defined by the operator (such as voltage and loading limits), operation of voltage regulating devices, protection system, whether it is assesses locally or for the total system, etc. The HC idea was primarily originated in 2004. Bollen et al. [24]. introduced the HC approach in 2005 for specifying the impacts of increasing distributed energy resources (DER) penetration on power systems. The basis of this approach was to gather the technical limitations imposed by both system operators and customers. The authors defined the HC as the maximum DERs penetration at which the power system operates satisfactorily. The HC calculation is not a fixed calculation with a single result. Thus, it should be calculated for various performance indices such as voltage and frequency variations, thermal overload, power quality and protection problems. The HC calculation criterion is described while focusing on the performance index upon which it has been calculated using illustrative power system models. The HC concept is illustrated in Fig. 1.1 and it is clear that enhancing the system's HC may allow for more DG additions while complying with the system's performance limits.

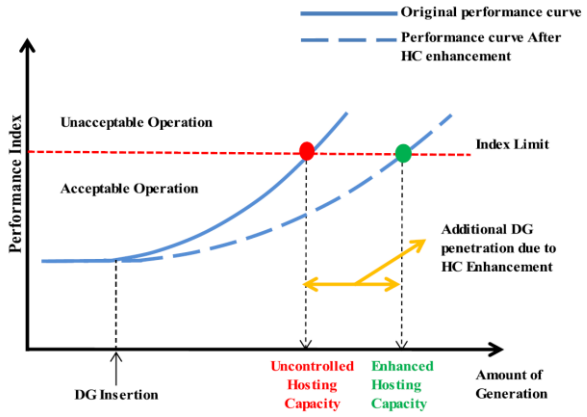

Figure 1.1 HC concept and the effect of its enhancement.

A recent survey performed on more than 100 electric utilities across 23 countries, it was noticed that distribution system operators (DSOs) raised their techno economic concerns regarding the booming DG deployment worldwide [28]. Utilities believe that they will suffer from revenues drop as a consequence for high DG penetration. DSOs highlighted that the biggest DG-related impact on a utility network's HC comes from small-scale energy prosumers who are driving low voltage DG units (mentioned by 59% of survey's contributors), followed by medium or high-voltage connected DG such as a large-scale solar plant. As well, DSO's gave their feedback about when they expect to meet HC limits within their systems, as per Fig. 1.2.

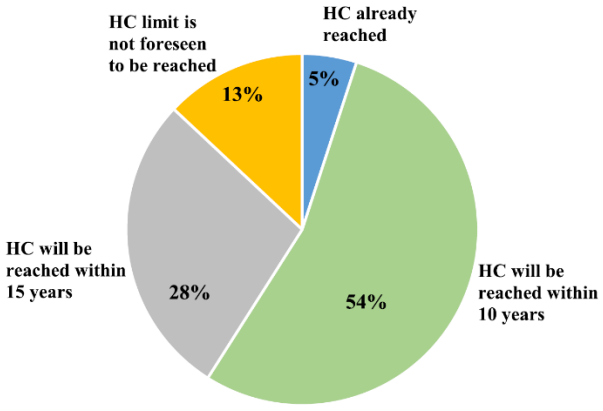

Figure 1.2 Opinions when DSOs expect to meet the HC limit

The concept of HC is used to study how much DG can be placed on a feeder before negative effects on normal distribution system operation and power quality occur. Hosting capacity is typically expressed as the percent penetration value of DG spread across any locations on the feeder that causes the first violation of operating constraints. These operating constraints and HC performance limits can be categorized to four different groups:

- *Overvoltage*
- *Overloading and power loss problems*
- *Power quality problems*
- *Protection problems*

The major obstacle that limits PV hosting capacity is induced voltage rise due to the reverse power flow caused by PV power [26]. ANSI C84.1-2011 [29] recommends that the voltage of residential loads should remain within 5% from its nominal value under normal operating conditions. To achieve higher HC, it is necessary to address all the possible problems caused by intermittent nature of RES. DSM is one of the viable options to address aforementioned challenges.

DSM technique mainly relies on matching present generation values with demand by controlling the energy consumption of appliances and optimizing their operation at the user side (for instance, by shifting appliances such as dishwashers, washing machines and dryers from peak time to off-peak time). The primary goal of DSM, for the electric grid, is to reduce peak load and enhance grid stability and reliability [30]. In fact, DSM's main advantage is that it is less expensive to intelligently influence a load, than to build a new power plant or install some electric storage device.

In recent years, residential and commercial DSM has attracted significant attention. The DSM at customer side will motivate and include the consumers, so they will become active and participate in energy market. The optimization of consumption scheduling can be achieved centrally, so that grid operators can control peak load, or individually, so that household consumers proactively schedule their consumption plan. Accordingly, future smart users can be referred as energy consumers or energy citizens depending on the level of engagement in DSM. However, an important challenge for residential DSM is that it is difficult for household users to respond to the pricing signals [31]. To tackle this problem, an autonomous energy consumption scheduler (ECS) can be implemented to help users make price-based control decisions. The autonomous ECS retrieves the pricing signal from the utility company via a communication infrastructure and schedules the operation of deferrable loads such as electric water heaters and clothes dryers. On the other hand, the use of rooftop photovoltaic (PV) units and energy storage systems (ESSs) in households has proliferated, in recent years. The households may not only consume energy but also export energy to the power grid. Many utility companies use net metering programs to encourage households to install rooftop PV units. Net metering programs typically have a feed-in tariff and allow households to sell their extra energy to the power grid.

As it mentioned, voltage rise problem is an important challenge for the integration of a large number of rooftop PV units into the power grid. Traditional voltage control strategies assume the unidirectional power flow from the substation to the households. A substantial reverse power flow from households to the substation can cause the voltage magnitude of some of the households to exceed the upper limit of the allowed voltage variation, referred as the voltage rise problem. In many countries with high penetration of rooftop PV units such as Germany, the voltage rise problem has already emerged and different mechanisms have been proposed to tackle the problem.

The DSOs have upgraded the transformers (e.g., with on-load tap changer transformers) and have enhanced the feeder to host more PV units in some areas. Moreover, the reverse power flow from PV units can be controlled by adjusting the active and reactive power of PV inverters. For instance, in Germany, the DSO measures the voltage magnitude and sends control signals to the PV units for curtailment. Besides generation curtailment, load control techniques such as DSM can be used to reduce the reverse power flow during high solar radiation hours and mitigate the voltage rise problem. However, the control of residential load requires the approval of household owners. Economic incentives such as Time of Use (TOU) pricing should be considered in the DSM programs to encourage household participation [32]. On the other hand, the voltage rise problem should also be taken into account in DSM programs if many households are equipped with PV units. Moreover, it is hard to respond to variations of voltage and pricing signals manually. Hence, it is important to have a scheduling algorithm for an autonomous DSM to manage load without human intervention. In this thesis, we propose residential and commercial energy consumption scheduling algorithm for areas with high penetration of rooftop PV units. The proposed algorithm aims to reduce the energy expenses of the users and mitigate the voltage rise problem by increasing RES utilization. It shifts deferrable load from peak consumption hours to hours with high solar power generation to decrease electricity cost and increase network reliability.

From the generation and transmission network prospective, increasing the penetration of RES is principally represented by replacing some of the Conventional Power Plant (CPP) that is predominantly operated by fossil-fuel with environmentally friendly RESs. This transformation has brought considerable ecological and economic benefits; however, this does not come without a price. The main difference between CPP and RES base power plants are their controllability. Normally, CPP is more controllable and convenient for power system stability in contrast to RES.

CPP can provide frequency response to preserve the balance between the demand and load, which is essential for power system stability. Generally, the CPPs are based on synchronous generators, which inherently exhibit inertial response (IR) to sudden frequency deviations [33]. Unlike, the CPPs, the RES-based plants are connected to the grid through power electronic converters. Therefore, the RES-based plants, by themselves, neither provide the inertial response nor participate in load-frequency regulation and their integration at large scale can lead to loss of IR and primary frequency response (PFR) [34].

Frequency response is classified, based on the time of reaction, into three broad categories: inertial response, primary frequency control, secondary frequency control tertiary control. primary frequency control and secondary frequency control are provided by two main control techniques: turbine governor and Automatic Generation Control, respectively. However, IR inherently exists in the system and is part of it. Because it principally arises due to the physical phenomena of kinetic energy generated and stored in all rotating parts of load motors and synchronous generators. If any disturbance occurs, power unbalance in the power system unpreventably follows; this kinetic energy is released in parts of a second to arrest this change and prevent the system frequency going under limits. With the help of previously mentioned system control strategies, the inertial response can bring the frequency to its scheduled value in few seconds to minutes. Therefore, the grid inertial frequency response is a fast frequency response, and it is an important factor in power system stability, especially during the early stage of system frequency disturbance.

Battery Energy Storage Systems (BESSs) are one of the processing solutions to address the lack of IR in RES dominated power grids. ‘Synthetic inertia’ or ‘virtual inertia’ are terms currently used to represent artificial inertia created by converter control or BESSs. The recent rapid development in power electronics and BESS technologies has resulted in their improved

efficiency, reliability, time response, life cycle and more importantly cost. However, the capacity of installed grid-scale BESS is still in the range of tens of MWh, which limits its grid-connected applications to support fast frequency response along with secondary frequency control [35]. However, aggregated small-scale BESS in the load side can be considered a good alternative for low inertia power systems, when all other solutions have been exhausted. These batteries usually are connected with small-scale RESs at the customer side. Controlling these small scale batteries and distributed generators is applicable through an aggregator called Virtual Power Plant (VPP).

The VPP aggregates many heterogeneous DERs to function as a single DER. It also has the inherent capacity to include the influence of the system on the aggregated DER output. In order to participate in the power system control, the VPPs have nondispatchable and dispatchable power plants including renewable and nonrenewable ones, storage units such as batteries and pump storage, and responsive loads that have some flexibility in their consumption energy levels. In other words, in VPPs, there are diverse kinds of power plants and storage units combined to overcome and handle the stochastic nature of renewable generators. In this these we consider the loads of transmission network as controllable VPPs to address the lack of inertia and improve frequency response of RES dominated power grid.

1.2 Literature Review

1.2.1 Synthetic Power Grid Modelling

Many studies have been dedicated for characterizing actual power networks and/or developing synthetic power grid models. The most relevant literature works considering general topological properties, physical properties, and differences between the various graph-related indicators and reliability aspects are categorized in [36]. The spatial distribution of the node degree and line length with similar structural properties to a given network is utilized to generate synthetic power grids

in [37]. Synthetic networks called "ACTIVSg" based on geographical, energy and population data are developed in [38]–[41], which are available in [42]. They utilize a clustering technique ensures that synthetic substations meet realistic proportions of load and generation. Some synthetic cases are developed based on a specific power grids, featuring their particular topology and electrical characteristics. For systematic study of power market design and performance issues, a synthetic 8-zone test system is developed in [43] based on ISO New England structural attributes and data. A toolbox to generate combined transmission and distribution networks based on Nordic transmission network model was presented in [44]. Their method systematically replaces the aggregated loads of the original transmission system with detailed distribution systems to generate new combined system. Reference [45] studies the structure of the three North American electric power interconnections, from the perspective of both topological and electrical connectivity and compares them with that of random, preferential-attachment, and small-world networks. In [43] authors developed a synthetic 8-zone test system based on ISO New England topology and electrical data to study electricity market design and performance of different market structures. In another study authors introduces a toolbox which replaces the aggregated loads of Nordic transmission network with detailed distribution networks to generate synthetic test cases for co-simulation of transmission and distribution systems [44]. An algorithm called Geographical Network Learner and Generator is developed in [37] to generate similar synthetic grids with considering only structural properties of real power grids. To overcome the limited information on power system planning and have a realistic case on low voltage networks, a bottom-up framework is proposed in [46] using customer locations and power demand data. Recently, a toolkit to automatically generate any number of synthetic power grids featuring the same statistical properties of realistic power grids is introduced in [47]. It generates synthetic grids based on the

statistical features of electric topology, bus type, generation capacities, load settings, generation cost models, and transmission line capacities found in the realistic power grids. To validation of synthetic distribution data sets a three-stage framework is proposed in [48]. Authors utilized three stage of statistical, operational, and expert validation to quantitively ascertaining realism of synthetic U.S. distribution networks and compare them with real utility data sets. Component rating data are utilized in [49] as the validation criteria to validate synthetic transmission networks. It was found that many existing public test cases fail to provide vital data including transmission line capacities and generator capability curves. Watts and Strogatz in their work on random graphs first proposed statistically modeling the power grid as a small-world network [50]. Our previous works in [2], [51]–[58] study properties of realistic power grids and introduce algorithms to generate different components of synthetic power grids including topology, bus type, generation and load setting, and transmission line capacities. References [51], [52] expanded on topology generation featuring the same kind of small-world topology and electrical characteristics found in realistic power grids and introduced a synthetic grid model, called RT-*nestedSmallWorld*. The approach of [58] build on previous works by using correlated assignment of generation, load, or connection buses and an optimized search algorithm to appropriate bus type assignments in a synthetic grid modeling. The scaling property of power grid in terms of both topology measures and electric parameters is studied in [54] and a set of statistical analysis on the generation capacities and load and their correlation with topology metrics to determine their settings in the given synthetic grid in [53]. Moreover, we developed a statistical-based approach to determine transmission line capacities for a synthetic power grid model in [57].

1.2.2 High Penetration of Distributed Solar PV generation

The impacts of DGs on distributed networks have been examined by many researchers. Among all the impacts of DGs, voltage violation and reverse power flow have received more attention from researchers. Voltage rise within the distribution network due to the installation of PV sources is investigated in [59]. In [60], the possible impacts of different levels of DGs on voltage profile is investigated. Authors utilized Monte Carlo analysis with snapshot approach (maximum generation and minimum load) to study the voltage violations. A probabilistic load flow analysis is utilized in [61] to study the impacts of DG penetration including voltage violations in medium voltage distribution networks. However, the authors did not consider the DGs with intermittent nature such as solar PVs. Reverse power flow and voltage violation in distribution networks with high penetration of DGs are studied in [62]. To avoid reverse power flow and voltage violations, the authors developed an approach to utilize smart transforms. However, the size and location limits imposed by solar potential and customer characteristics are not considered in [3-5]. Authors in [63] proposed an index-based methodology for assessing the impact of high solar PV generation. They examined defined indices for 13-bus IEEE network over a 24-h time frame to evaluate the sensitivity of all nodes and select the critical node to be monitored for voltage performance. However, variations of loads and DPV generations over a year require a yearly study instead of daily. The stochastic condition of the loads and the meteorological dependence of PV generation were both addressed in [64] and [65]. However, the location and size of PV installations are considered deterministically. Several works have studied the impacts of high penetration of DPVs in terms of hosting capacity [24]. The hosting capacity is defined as the amount of new production or consumption which can be connected to the grid without adversely impacting the reliability or voltage quality in the grid [66]. The optimal PV penetration of a 9-bus distribution feeder was solved in [67] by maximizing the net power of a PV system that connected at the end

of the feeder. This study did not consider the distributed PV effect, and it had limited application if considering large-scale feeders. In order to study the effects of load on the hosting capacity, in [61] a Monte Carlo framework was presented to identify the maximum DG capacity at different locations. They, however, did not consider DPV uncertainties. A risk assessment method is presented in [68] for estimating the hosting capacity considering the uncertainties associated with PVs, wind turbines and loads. The study evaluated the hosting capacity of a set of predefined positions by introducing two deterioration indices, based on voltage violations and utilizing the likelihood approximation approach. Although they modeled the uncertainties associated with the DGs generation and load, they did not consider the uncertainties associated with the location and size of DGs. An impact study using a stochastic approach to assess the general hosting capacity is performed in [69]. However, it is of additional interest to find which areas of a grid are most sensitive to high penetration levels and what characteristics of load and grid induce the impact.

Generally, small-scale DGs are installed in a distribution network based on customers' decision and utilities do not have an influence on the size and siting of DGs. For instance, in the USA, all utilities offer expedite approval for small-scale DPVs (e.g., 25 kW and below) requested by customers [70]. However, the aggregated small-scale DGs at each node could be examined to help utilities to make timely decisions for PV interconnection requests. It is foreseen that providing optimal size and location of aggregated DPV installations may become an efficient or necessary option for utilities to maximize the overall advantages or mitigate potential negative impacts of DPVs in distribution networks. For instance, Australian distribution company in [71], offers two different thresholds for unmanaged and managed distributed renewable energy installation for its different distribution feeders. Optimal sizing and sitting of DGs as a solution to address the DG impacts on the electrical network have been extensively studied in the past few decades [72], [8].

Most of these efforts focused on optimization methods for DG installations using analytical [73], [74] probabilistic [75], [11] and heuristic methods [76], [77] for minimizing power loss and voltage profile improvements. Authors in [78], presented an analytical approach to determine the optimal allocation for the DG with an objective of loss minimization for distribution and transmission networks which is said to be easily implemented and perform faster than the other optimization methods. Moreover, numerical methods applied to the optimal allocation of DGs are such as ordinal optimization, sequential quadratic programming and nonlinear programming [79]. Aman et al. propose an index-based algorithm for DG placement and sizing, in which power stability index is utilized to minimize power loss and improve voltage stability for DG installations [80]. In these papers, DGs mostly considered as the continuous and controllable source of power; however, intermittent nature of solar PV should be considered in case of DPVs. Several studies have focused on particularly deployment of solar PV systems in sense of distributed generations considering their intermittent nature. To consider non-dispatchable characteristics of PV units, a new method for the optimal sitting and sizing of DPVs using an adaptive reactive power control model is proposed in [81]. Authors used this model to balance the trade-off between the improvement of voltage quality and minimization of power loss in a distribution network.

1.2.3 Demand Side Management

Current work in residential DSM focuses on peak load reduction through load shifting. Load shifting techniques emphasize appliance scheduling on a single residence or on multiple residences using home Energy Management Systems (EMS) that take advantage of two-way communication between the home and the grid. EMS agents present an interesting model predictive control application since they must schedule appliance loads subject to constraints defined by the optimization framework. Depending on the scale, the framework can be centralized or distributed.

On a neighborhood level, each individual user may define preferences by setting appliance operating modes and activation times which can be compared to the total energy cost set by the utility as a function of market demand [82]. Since the centralized problem requires extensive information of individual user appliance preferences and energy cost as a function of the scheduling preferences of all neighborhood users, the solution to this type of problem is non-trivial. Reference [83] discusses the limitations of centralized methods in terms of computational complexity and incentive compatibility. This work offers offering a distributed mechanism that takes into account day-ahead allocation as well as individual real-time consumption in the scheduling of appliances by EMS agents. The distributed optimization framework allows the problem to be convex under the free market assumption that utility pricing will drive user self-interest thereby decreasing grid operational costs.

However, the focus on user self-interest as pertaining primarily to cost minimization and comfort defined by appliance operation, does not take into account the variability in demand due to human daily behavior. For example, [84] derive energy consumption scheduling algorithms using Nash equilibrium to minimize cost and peak to average ratio by deferring "shiftable" appliance loads as an alternative to changing resident energy consumption. Though simulation results successfully show a reduction in overall consumer cost, consumer satisfaction outside of cost and appliance duration parameters are not assessed. Similarly, [85] develops an energy management model using coevolutionary particle swarm optimization to schedule "must-run" resistive loads as well as loads associated with PHEVs, temperature systems, and pool pumps. In this framework, the consumer must define the monetary benefit of a unit of energy usage as a means of quantifying personal comfort based on ambient and water temperatures as well as PHEV charge. These parameters then determine the cost of "undelivered services" taking into account

acceptable temperature gradients, water discharge, and PHEV discharge under the constraint of tariffs set by the utility. However, in practice, user engagement in defining the "utility" of specific optimization constraints as an indirect parameter of comfort may not be straightforward. Automatic detection of user comfort constraints offers an improved solution but is subject to variability. In [86], an energy consumption scheduling algorithm is proposed for a PV-based microgrid, where the TOU probabilities of different loads are considered. References [32], [86]–[88] focus on the case where a few households are equipped with DER units and are encouraged to export their generation to the grid. However, if a large number of users are equipped with PV units, the results in [32], [86]–[88] may not be directly applicable because the reverse power flow in those areas may cause the voltage rise problem. Therefore, in areas with high penetration of PV units, new DSM programs are necessary.

In [89], the cost saving potential of changes in the load shape via demand reduction and load shifting in the short-term unit commitment (UC) problem is proposed. The UC problem is solved for each day of the study horizon of a year. Low and high wind outputs are analyzed separately on a daily basis instead of hourly. However, the effect of ESS and DR has not been studied, and this is due to the fact that it is costly to have a large ESS in a large power system, which is not the case when it comes to microgrids, where it is not necessary to have a large sized ESS at the distribution level; medium or small sized ESS can be efficient enough. Liu and Hsu [90] has investigated the energy cost minimization problem in smart grids with distributed renewable energy resources. Assume that each consumer in the grid have a photovoltaic system and a side battery. Here more challenging scenarios are focused such as non-interruptible and non-power shiftable. This problem is solved by two stage optimization methods such as Column and Constraint Generation (C&CG) and Scalable and Robust Demand Side Management (SRDSM). Initially, a C&CG method is used

for solving the problem and then the SRDSM algorithm is utilized when the amount of appliance and consumers are high. The SRDSM algorithm does not consider the uncertain energy demands while performing the demand side management. Lokeshgupta and Sivasubramani [91] has combined the Multi-Objective Dynamic Economic and Emission Despatch model with DSM. This will help to analyze the DSM benefits on the generation side. To handle the small-scale industrial loads a day ahead based load shifting technique is utilized in the DSM process. However, this method considers only a residential load such as ovens, kettle, washing machine, dish washers and other appliances. Alham et al. [92] has presented the Dynamic Economic Despatch with various penetration levels of wind energy. The DSM is utilized for solving the concerns associated to high penetration of wind energy. Here, the effect of using DSM on the operation cost with various test cases is discussed. Ye et al. [93] has presented a DSM system with advanced communication networks in smart grid which depends on the real-time information. In the grid, the peak-to-average ratio of power usage is smoothened by DSM for minimizing the waste of fuel and the emission of greenhouse gas. A Direct Load Control scheme is utilized to minimize the PAR. One more centralized scheme is used for minimum power generation cost. Hence, the customers are not motivated by using centralized scheme as well as this scheme requires too much real-time data exchange for frequent DSM deployment. This scheme requires more privacy from the customers. Di Santo et al. [94] has developed the active demand side management for households in smart grids. This model contains distributed solar photovoltaic generation and energy storage. The consumer electricity cost is reduced by managing the battery with the help of a decision-making system. The decision-making system is a validated neural network, trained with optimized data, which can be used in any household meeting certain conditions – specific location and electricity tariff, and consumption profile like to the standard verified by the local electricity utility. This

neural network based DSM considers only about the household's power demand. Vaghefi et al. [95] have presented a data-driven risk-based framework to predict and optimally control industrial loads in non-residential buildings. The proposed framework provides a risk-based model to calculate and evaluate the total risk of energy decisions for the next day. This is coupled with a utility function structure to help decision makers to take best demand-side actions. However, demand response management in this paper is limited and require a detailed study for analyzing the performance of data. Fernandez et al. [96] have proposed a Game-theoretic method to DSM for residential places meanwhile integrating renewable sources for controlling the energy profile. The projected method reduces the energy cost to the consumer while sustaining an ideal comfort level for the end user and provide adequate consumption constraints to decrease peak demand. But the proposed method does not consider the behavioral patterns of consumers.

1.2.4 Inertia Emulation and Virtual Power Plants

After a contingency event (e.g. a generator trips offline), the grid's frequency begins to drop rapidly. Rotational inertia plays a critical role in arresting frequency drops before primary frequency response becomes available to supply the lost energy. When sufficient rotational inertia is available, severe frequency drops can be avoided [97]. The literature has regularly connected system inertia to the stability of the electric grid by expounding the relationship between frequency dynamics and the grid's resilience to blackouts [35]. Some studies have integrated frequency stability into their analyses through a minimum net load constraint, recognizing that some amount of synchronous generation is required for stability [98]. Other studies have noted that renewable energy generators can contribute to fast frequency response or provide “synthetic” inertia to mitigate negative grid stability effects [99], but there is a delay in this response and the technology is still being developed [100]. In Denmark, small- and medium-scale combined heat and power

(CHP) plants have demonstrated potential to participate in frequency regulation to assist with grid stabilization [101]. The inertia reduction due to the high penetration of renewable energy sources and its challenges have already been identified by transmission system operators and many researchers worldwide [35]. The major issue is a large frequency deviation in case of large disturbance, which requires a fast frequency response immediately after the power imbalance to avoid system collapse. Fast frequency response (FFR) generally refers to the delivery of a rapid active power increase or decrease by generation or load in a timeframe of two seconds or less, to correct a supply-demand imbalance and assist in managing power system frequency.

Several studies have been done on various types of virtual inertia, to simulate the dynamic behavior of a synchronous generators, and represent the inertia and damping property from its fundamental swing equation. Two control strategies are proposed in [102] to emulate an inertial response from wind turbines, using energy stored in the DC link and the rotor masses simultaneously and also in a cascaded manner, with the latter approach seen to reduce the magnitude and duration of the underproduction period. The released energy by wind turbine during the overproduction period is optimized in [103] with taking into consideration mechanical and electrical constraints. Some studies have proposed coordination with hydro [104] and conventional [105] power plants, based around synchronous machines, to address the issue, whereby they provide a short-term increase in output until the wind turbines accelerate back to their optimal operating point. The authors in [106] presented a study on the impact of large scale PV power plant participation in dynamic frequency control including inertial response, where it has been shown that participation of large scale PV power plant in frequency regulation, including FFR, can effectively improve system frequency stability and security. Most grid code regulations require frequency control capability from PV plant connected at medium and above voltage levels.

However, PV connected at low distribution voltages are not required to provide a fast frequency response, and indeed they are often allowed to disconnect in the case of extreme frequency variations [107]. A limited number of field implementations demonstrating FFR from PV power plants have been reported in the literature, primarily because transmission system operators (TSOs) have not widely mandated such a service from PV plants yet. Frequency support from a 300MW solar PV power plant in California, USA is reported in [108] including secondary and droop control, however, FFR from the plant is planned but yet to be implemented. A coordinated strategy is also proposed in [102] to supply the active power shortfall from battery energy storage systems (BESS) connected to the grid. Similarly, a hybrid combination with fuel cells is investigated in [109] to minimize the impact of the underproduction stage and enhance further the primary frequency control response. In [110], the BESS was used for the inertia response and it was sized to deliver arbitrarily chosen rated power for at least 15 seconds. It was found that a large-scale fast-acting storage, by acting as a synthetic inertia, can mitigate the impact of zero inertia sources on the dynamic performance of a power grid in the case of a major generation outage. Many industry pioneers developing viable technologies to utilize large-scale BESS for grid stabilization. ABB integrates batteries, power converters, and system control into a single solution that provides highly reliable and accurate frequency regulation at much faster speeds than other technologies [111]. A new approach to dispatch BESSs is proposed in [112] to mimic inertia and enhance primary frequency response. It has been shown that the application of BESS significantly improves the transient stability response in a grid in high penetration of renewable energies [113]. BESS can improve and affect positively in reducing rotor speed deviation at different renewable energy penetration levels following disturbances in the system [114]. The impact of different BESS operation strategies are investigated in [115] for providing primary frequency control. Moreover,

the authors in [116] demonstrated that BESS significantly reduces environmental impacts while providing primary control. However, earlier works with energy storage system overlooked the ability of BESS to reduce frequency oscillation and increase renewable energy penetration level in the existing system. Note that the capacity of installed grid-scale BESS is still in the range of tens of MWh, which limits its applications to support inertia response along with primary frequency control [117]. In addition, fast-acting large-scale BESS is usually one of the most expensive components to utilize in power grids. On the other hand, fast response capability, cost-effectiveness, as well as the availability of demand-side make the demand control as an appropriate candidate for primary frequency regulation. Load control refers mainly to non-time-critical loads with on/off status or controllable loads which can be linearly modulated based on frequency error [118]. A multi-objective gain-tuning method for controllable loads is introduced in [118] to minimize the frequency nadir, response time, steady-state error, and total load shedding. Utilizing time-frequency response of system to implement sequential activation of flexible loads was proposed in [119]. However, variability of participants and its impact on network operation was not considered in their control strategy. A multi-step adaptive frequency restoration process, using step-wise activation of responsive demand, was proposed in [120]. A real-time estimation of event severity is proposed using rate of change of frequency; however, the dynamic characteristics of loads was not considered in their proposed frequency response. The frequency overshoots caused by considering large flexible load volumes in fixed frequency control settings was examined in [121]. Authors categorized the individual load responses into finite discrete time intervals to minimize the overshooting problem. However, it resulted in higher frequency nadirs in the system. Authors in [122] utilized a market-based framework using a price-based control algorithms for available flexible loads to improve frequency response, requiring two way communication for

multiple entity (customer, aggregator and system operator) with regular adjustments and updated broadcast. To determine required frequency regulation, local area communication in a simplified power system is utilized in [123] to evaluate the contingency volume in load level and send the frequency control signals. This approach however, requires sophisticated load controllers, a significant communication overhead and high computation time (up to 3.5 s) before a response, resulting in compromised nadir improvement. A completely centralized approach is presented in [124] where a portfolio of flexible loads transmits state information and receiving the activation commands from the aggregator. Apart from the longer response times resulting from such a control philosophy, the flexible loads are represented as energy storage with a constant drain rate, ignoring the stochastic load behavior based on user impacts and weather conditions, etc. Moreover, the potential of load control in frequency regulation was investigated by Trudnowski et al. [125], while the simple load control strategy of their proposed approach was later applied to a large and realistic network by Donnelly et al. [126]. However, large-scale implementation of the load control not only requires visibility in the power system to appropriately re-calibrate protection schemes but also needs sophisticated management of individual appliances to ensure overshoot avoidance and minimal impacts from energy recovery.

Note that the power imbalance and inertia estimation play a vital role in many applications such as inertia emulation and under frequency load shedding. For instance, to implement the under-frequency load shedding in the event of a disturbance, the system frequency is measured and compared against a fixed threshold. Whenever this threshold is violated, load is shed based on the estimated power disturbance until the frequency reaches an acceptable level. Most of the studies have focused on estimating inertia by using frequency measurements after a disturbance (disturbance-based estimation) [127]. Average frequency signal was utilized to estimate system

inertia of Japan's power grid [128]. In another attempt, wide area measurement system (WAMS) was used to estimate the inertia of the power system of Great Britain (GB) [129]. In [130], several methods including frequency signal from one generator, average frequency signal of all generators, and average signal frequency of different areas were investigated to estimate power system inertia of the Nordic power system. In [131], an inertia estimation method was proposed using rate of change of frequency (RoCoF) measurements. However, in their method the RoCoF measurements at the connection points of the generators with the grid were considered to be available. To estimate power system inertia of the Western Electricity Coordination Council (WECC), a framework which utilize frequency measurements of a single location is proposed [132]. Authors in [133]\cite{wall2014simultaneous} also focused on measurements of a single location to estimate inertia constant of power grid based on active power and frequency. In a method developed in [134], the total power change after the disturbance was estimated simultaneously with the inertia constant. The method employed frequency signals from all generators and was tested in Nordic32 test system. In [135], a strategy for updating the estimated loss of generator (LoG) during load control process through the system's inertia constant estimation is introduced. Recently, a method to estimate power mismatch after an abrupt loss of generator has been proposed based on the rate of change of frequency [136]. However, their proposed method is only limited to the loss of generation incidents.

A hybrid system with BESS and wind turbine can deliver about 45% more inertial power as compared with a wind turbine alone [137]. A control scheme to emulate an inertial response from both the stored energy of a wind turbine and energy storage system is presented in [138]. In [139], the FFR performance of a type-4 turbine is improved by connecting a short-term BESS to the DC link. Alternatively, the energy storage system can be placed at the wind farm level rather than at

each wind turbine. An independent inverter has also been used to connect the superconducting magnetic energy storage to a wind turbine bus in [140], where a coordinated strategy emulates an inertial response from both the turbine and BESS, reducing the aggregate BESS capacity while improving the turbine performance. In [141], a fuzzy controller calculates the required turbine deloading and the power released from the ESS. In order to mimic the inertial response of a conventional power plant, the authors in [142] concluded that an BESS with a minimum capacity of 5% of the wind farm rated power should be connected at the wind farm point of common coupling, in conjunction with a fuzzy controller. The authors in [110] presented a coordination control technique between PV solar panel and BESS sharing a common DC bus to provide inertial response among other grid services. As the cost per unit of storage capacity is still significant, optimization studies have calculated the optimal distributed BESS capacity that supports either primary frequency response alone [143] or both an inertial and primary responses [144]. A control algorithm based on BESS to improve the inertial response of an islanded power system was proposed in [110], with the control algorithm further developed by the authors in [145] using a self-tuning controller to more precisely mimic a synchronous generator inertial response. A response scheduling and distributed control scheme for a distributed BESS is presented in [146], which aims to coordinate the DESS response such that the system avoids activating underfrequency load shedding relays during a system frequency transient.

1.3. Research Objectives and Approaches

Objective 1: An appropriate synthetic grid model consists of at least three important components: a) the electrical grid topology; b) the generation and load settings which indicate their correlated placement and sizing; c) the transmission constraints which include the capacity limits of both transmission lines and transformers. To extend our previous work on synthetic power

grid modelling we develop a novel approach to accurately determine the transmission capacities for a synthetic power grid model with components (a) and (b) already resolved. For this part, we mainly focus on statistical analysis of transmission line capacities in terms of both topological and electrical parameters. We examine transmission line capacities based on both network topology metrics and some newly proposed electrical indexes. The obtained results show that the issue of transfer capacity assignment not only emerges as an electrical optimization concern, but some topological metrics must be considered to find the best line capacity assignment that is consistent with what is manifested in real-world grid. These results then will be used to develop a new methodology to appropriately characterize the line capacity assignment and improve the synthetic power grid modeling.

Objective 2: To address the lack of realistic grid models to performance evaluation and verification of new concepts and methods proposed by the researchers, we develop a comprehensive toolkit to generate synthetic models featuring same properties of realistic power grids. The AutoSynGrid toolkit is designed based on MATLAB Graphical User Interface (GUI) and it is able to build any number of synthetic cases that can be used for a variety of analysis such as PF and OPF studies. It allows to select several key characteristics of the generated system, such as reference system, loading level, and generation cost model. The generated cases include topology, bus type, generation and load setting, transmission line capacities and generation types and cost models. The output of the toolkit is exported in the native MATPOWER [21] format allowing to use the MATPOWER open-source, steady-state, planning, and analysis package to further studies on the generated cases. In addition, we develop a validation framework, which examines the generated synthetic cases based on the metrics introduced in the literature and some new validation metrics we found in realistic power grids. These metrics are categorized into

topology metrics, electric parameters, state variables, interdependencies, and scaling properties. Moreover, we define a closeness factor to measure the realism of generated synthetic cases and compare with totally random grids.

Objective 3: Motivated by the necessity of an accurate impact assessment framework to study DPV generation in the distribution network, we propose a detailed impact-assessment framework to accurately assess the possible impacts of two different DPV installation schemes on a realistic distribution network. We perform a full year time-series analysis of DPV installations with a novel synthetic load profile modeling and detailed models of all system components to aid utilities and policymakers on quantifying the impacts of different DPV penetration levels. To cater uncertainties in DPV installation by customers, a Monte Carlo-based technique is utilized. Solar PV installation in the distribution network is not purely random and the location and size of the installation depend on many factors. Adequate solar insolation, available rooftop and customer decision for size selection, as well as the finance budget and government incentives are the most crucial factors for rooftop PV installation. Therefore, to develop a detailed assessment approach, we perform a PV potential study to estimate actual DPV installation capacity for the buildings in the given distribution network. In addition, we define customer selection factor to mimic customer behavior for PV size selection. Moreover, a novel synthetic load modeling is proposed to generate daily load profiles for individual building types representing specific load patterns for the studied area. In addition to the Monte Carlo-based technique to study random installation, we propose a multi-object optimization approach to suggest optimal location and size of aggregated small-scale DPVs in the distribution network. The objectives of optimal size and location algorithm are minimization of the energy loss, voltage deviation, and voltage fluctuation, in addition to elimination of voltage violations and reverse power flow. This allows identifying the outcomes for

two different DPV deployment policies towards possible strategies to maximize advantages and minimize the negative impacts of DPVs and may provide useful guidance for utilities and policymakers. In fact, the proposed detailed impact assessment not only provides the more precise and accurate results on hosting capacity and high PV penetration impacts, but also provides a comparative perception of DPV installation in different penetration ratios.

Objective 4: With recent technology advances, solar photovoltaic has become one of the fastest-growing renewable energy sources in the U.S. However, high penetration of PV systems into the distribution networks may arise undesirable issues such as voltage fluctuations and reverse power flows. These issues may be mitigated with onsite energy storage systems but the latter are usually not available or expensive. An alternative solution is demand side management (DSM) strategies, which may have the dual effects of reducing electricity consumption during peak hours and allowing greater efficiency and flexibility for renewable integration, namely by enabling a better match between electric supply and demand. In this part, we propose decentralized household demand side management in a residential distribution network, which consists of multiple smart homes with schedulable electrical appliances and rooftop PV generation units. Using the developed simulation model, we examine the performance of decentralized household DSM and study their impacts on the distribution network operation and renewable integration, in terms of utilization efficiency of rooftop PV generation, overall voltage deviation, real power loss, and possible reverse power flows.

Objective 5: Large-scale deployment of RESs has led to significant generation shares of variable RES in power systems worldwide. RES units, notably inverter-connected wind turbines and solar PV that as such do not provide rotational inertia, are effectively displacing conventional generators and their rotating machinery. Low inertia power grid causes the system frequency to

change too fast after the occurrence of a severe contingency or disturbance. In this regard, the last part of this work is dedicated to develop a framework to emulate inertia response using VPPs. We propose an online power disturbance estimation by introducing new terms in the swing equation to have an accurate estimation of disturbance and system inertia in case of a large generator loss or a large load disconnection. Fast frequency response from the load side should be triggered in less than 400 ms [35]. Therefore, a real-time optimization framework will developed to control aggregated DERs in a distribution network to effectively emulate fast response VPPs. To validate the proposed approach, we will use synthetic power grids which are generated by our developed AutoSynGrid toolkit in the objective two. In addition, we will investigate the quadratic power control of BESSs and RESs in VPPs. Simultaneous control of the active and reactive power of the converter can improve the voltage regulation and provide more flexibility in the VPP to participate in inertia emulation and fast frequency response.

2. Synthetic power grid modeling

2.1. Motivation

Synthetic grid modeling has been introduced as a potential solution to address the lack of realistic grid models to performance evaluation and verification of new concepts and methods proposed by the researchers. These entirely fictitious models mimic the characteristics of real grids without disclosing any sensitive information associated with real grids. The main idea for synthetic power grid modeling is to study the statistical properties of real networks and construct a method to generate fictional networks that have all the properties of a real network [58].

In the first part of this section, we develop a novel approach to accurately determine the transmission capacities for a synthetic power grid model with known electrical grid topology and generation and load settings. The proposed approach takes into account the scaling property of total transmission capacity versus network size and the mutual dependence between the electrical parameters, as evident in real grid data of different size. The statistics of generation dispatch factor and transmission gauge ratio have been examined in terms of their marginal distribution and the correlation with corresponding capacity settings. Then a set of DC power flow solution and flow distribution in a given synthetic grid could be calculated with statistically assigned generation dispatch. Finally, a statistically correct random set of transmission capacities will be calculated and assigned to each transmission branch according to the correlated transmission gauge ratios. The main contributions of this paert are summarized as follows: 1) statistical analysis of generation dispatch factor ($\alpha \triangleq P_g/P_g^{\max}$) and its correlation with generation capacity; 2) statistical analysis of transmission gauge ratio dispatch ratios ($\beta \triangleq F_l/F_l^{\max}$) and its correlation with branch power flow; 3) development of a statistical-based algorithm to determine the generation dispatch at each generation bus; 4) using the statistics obtained in (1)-(3) development of a novel algorithm to

calculate and assign the transmission capacities based on the DC power flow solutions for a synthetic power grid. For the second part, we combine all our proposed approaches and introduce a toolkit to generate synthetic models featuring same properties of realistic power grids.

2.2 Statistical assignment of transmission capacities in synthetic grid modeling

2.2.1 System Modelling

The electrical topology of a power grid, with *N* bus and *M* branches, can be fully described by an admittance matrix $Y_{N\times N}$, which is defined as:

$$Y_{N\times N} = A^T \Lambda^{-1}(z_l) A, \tag{2.1}$$

where *A* is the branch-node incidence matrix. $\Lambda^{-1}(.)$ denotes the diagonal inverse matrix with a specific vector and z_l the vector of branch impedances. By neglecting power losses in the grid, the so-called DC power flow distribution in a grid follows its network constraints as:

$$P(t) = B'(t)\theta(t) \tag{2.2}$$

$$F(t) = \Lambda(y_l) A \theta(t) \tag{2.3}$$

where; $\theta(t)$ and $P(t)$ are the vector of phase angles and injected real power, respectively. Besides the network constraints, grid operation also needs to account for the constraints of generation capacity, load settings, and transmission capacity as following:

$$P_g^{Min} \leq P_g \leq P_g^{Max} \tag{2.4}$$

$$P_L^{Min} \leq P_L \leq P_L^{Max} \tag{2.5}$$

$$|F_l| \leq F_l^{Max} \tag{2.6}$$

It is clear that to form the later grid operation constraint, calculation of injected power along with transmission line capacities is necessary. In this paper, we will expand our previous work to

determine generation dispatches and transmission line capacities. For the purpose of statistical analysis and algorithm development, we defined the following two parameters:

$$\alpha_i = P_{g_i} / P_{g_i}^{Max} \qquad i = 1 \ldots N_G \tag{2.7}$$

$$\beta_l = F_l / F_l^{Max} \qquad l = 1 \ldots M \tag{2.8}$$

where α_i is denoted as the *dispatch factor* of generation unit at bus *i* and β_l the *transmission gauge ratio* of branch *l* in a given grid.

2.2.2 Statistics of generation dispatch factor

In power systems, generation units are committed to serve the time-varying demand of customer loads according to their costs, operational limits, network constraints, and environmental constraints and other factors. Our prior work [53] developed algorithms to generate a statistically correct random set of generation capacities and load settings, and then assign them to each generation and load bus respectively. In this section, we will study the statistics of generation dispatch ratios then develop an approach to determine the generation dispatch at each generation bus in a synthetic grid model accordingly. The main idea is that by studying the possible correlation between generation capacities $P_{g_n}^{Max}$ and short-term power dispatch P_{g_n} in real power grids, an appropriate method can be constructed to determine the power dispatch of each generating unit according to its capacity setting in a synthetic grid.

Initial statistical study indicates that there exist non-trivial correlation between the generation capacities and its generations dispatch as evidenced by the Pearson coefficient of $\rho\left(P_{g_n}^{Max}, P_{g_n}\right) \in [0.75,0.95]$, evaluated for real grid data such as the NYISO, the WECC, the PEGASE, and the ERCOT systems. Figure 2.1 shows the scatted plot of generation dispatch versus generation capacities for the NYISO-2935 system with Pearson coefficient of $\rho = 0.7509$.

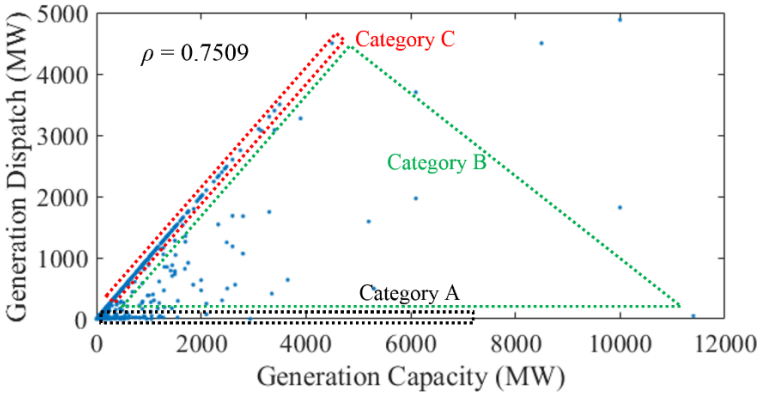

Figure 2.1 **.** Scatter plot for generation dispatch versus generation capacity in NYISO-2935 bus syste*m*

All the generators in the system may be divided to three categories: (A) uncommitted unites with $\alpha_g = 0$, (B) partially committed unites with $\alpha_g < 1.0$, and (C) fully committed units with $\alpha_g \approx 1.0$. It is found that in a typical system about 10 ~ 20% of generators are uncommitted, and interestingly most category (A) units tend to be small or medium size units only a very small number of them have super large capacities. Electricity market requirements, annual overhaul schedule, or load levels of the system could be the reasons for this special uncommitted status of generations. Additional finding is that about 40 – 50% of the generations belong to category (B) and their output power varies between the minimum and maximum generation capacity. The rest generation units operate very close to their maximum, i.e. belonging to category (C).

The scatter plot of normalized generation capacities ($\overline{P_{g_n}^{Max}} = P_{g_n}^{Max} / \max_i P_{g_i}^{Max}$) versus dispatch factor for the WECC system is shown in Fig. 2.2. It is worthy to note that a small number of units in the system operate with negative dispatch factor. These might come from the units that operate as electricity storage such as the hydro generators. Figure 2.2 also implies that in a typical power grid small and mid-size power units tend to have a wider range of dispatch factor compared with those unit of larger size. The statistics derived from data of realistic grids indicate that there

exist a significant correlation between the normalized generation capacities and their short-term power outputs with a Pearson coefficient of $\rho\left(\overline{P_{g_n}^{Max}}, \alpha_n\right) \in [0.15, 0.55]$.

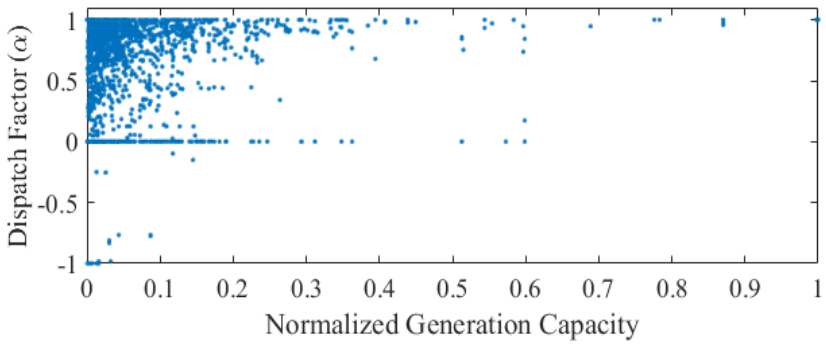

Figure 2.2 Scatter plot for dispatch factor versus generation capacity in the WECC system

Given a data set of generation unit capacity and dispatch factor, we may define a joint distribution function in the two-dimensional space of $\left(\overline{P_{g_n}^{Max}}, \alpha_n\right)$. The 2-D density function $f\left(\overline{P_{g_n}^{Max}}, \alpha_n\right)$, when integrated over a set S gives the probability that $\left(\overline{P_{g_n}^{Max}}, \alpha_n\right)$ falls into the set

$$\Pr(A) = \Pr\left\{\left(\overline{P_{g_n}^{Max}}, \alpha_n\right) \in S\right\}. \tag{2.9}$$

Figure 2.3 illustrates the 2-D empirical probability mass function (PMF) of dispatch factor versus normalized generation capacity for the NYISO-2935 system. In order to develop an algorithm for assigning dispatch factors to each generation bus based on generation capacities, we can formulate a two-dimensional table based on 2-D empirical PMF such as that shown in Table 2.1 for the NYISO-2935 bus system. It should be noted here that the main purpose of using 2-D empirical PMF table for the dispatch factor assignment in a synthetic grid model is to reproduce a similar correlation between the generation dispatch and the generation capacity as found in real grid systems.

Our studies on the statistical distribution of committed units in realistic power grids show that, more than 99% of the committed generations have capacities following an exponential distribution with about 1% having extremely large capacities falling outside of the normal range defined by expected exponential distribution indicated by imperial probability density function (PDF) committed unites shown in Fig. 2.4. However, statistical analysis of dispatch factors for committed unites on realistic grids shows that, depending on loading level of the system ($\alpha^{\Sigma} = \sum_{i=1}^{N_g} P_{g_i} / \sum_{i=1}^{N_g} P_{g_i}^{Max}$), dispatch factor follows different distributions. For instance, for NYISO-2935 as a system with large loading level ($\alpha^{\Sigma} = 0.74$), dispatch factor follows generalized extreme value distribution, however, dispatch factor for PEGASE-13659 with a small loading level ($\alpha^{\Sigma} = 0.38$) follows uniform distribution.

4.2.2.1 Assigning dispatch factors to generation buses

Given a synthetic grid topology with *N* buses and determined generation capacities and load settings, we may select a randomly correct set of generation capacities for both committed and uncommitted units which follows 99% rule for committed unites and uniform distribution for uncommitted unites. Next by generating statistically correct random set of dispatch factors, we can assign them to the selected generation capacities in generation buses based on obtained statistical pattern represented by data presented in Table 2.1. The following steps is used to determine generation dispatch for generation buses in synthetic power grid: (***Uncommitted units*****)** select a set of generation capacities form $\left[P_{g_n}^{Max}\right]_{1\times N_g}$ and consider them as uncommitted units. In this step, (10~20) % of generating units are considered as uncommitted units with $\alpha = 0$ and remaining units are guaranteed to take generation dispatch value between (0 ~ 1]. It should be noted that the selected capacities should follow the uniform distribution between [0, 0.6] and the capacity of

nominated units must be close enough to the random values generated by uniform distribution; **(Committed units)** First we need to select 40~50 % of remaining units as committed but not full-load units. In this procedure, the nominated units are selected according to the empirical PDF of generation capacities of category B, in a similar way as what has been done in step 1. Then an algorithm will be developed to assign the best generation dispatch to each generation bus with respect to the statistical pattern presented derived from 2-D empirical PMF; **(Full-load units)** in this step, leftover units are considered as full-load sources with dispatch factor $\alpha = 1$.

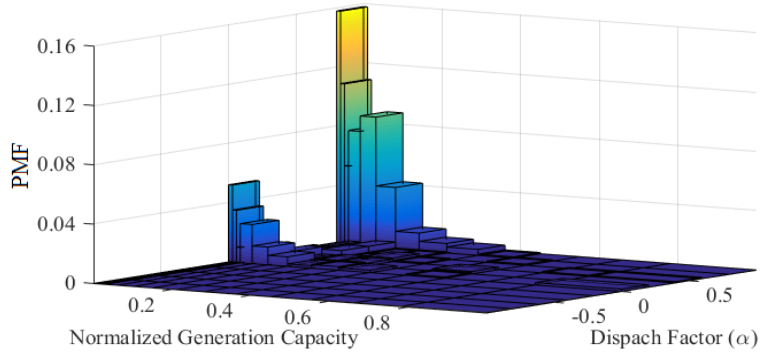

Figure 2.3 2-D empirical PMF of dispatch factor versus normalized generation capacity in the NYISO-2935 system

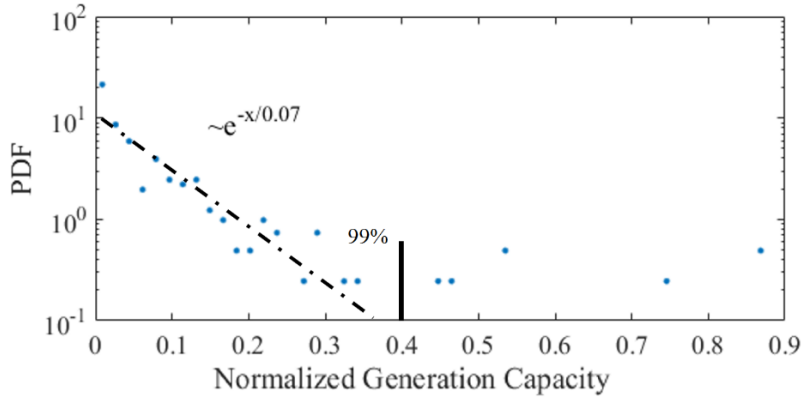

Figure 2.4 Empirical PDF of committed generation's dispatch factor for NYISO-2935 bus system

Table 2.1 Probability Distribution of Dispatch Factor vs. Normalized Generation Capacity

$\overline{P_{g_n}^{Max}}$	α_n	-1.00 -0.80	-0.80 -0.60	-0.60 -0.40	-0.40 -0.20	-0.20 0.00	0.00 0.20	0.20 0.40	0.40 0.60	0.60 0.80	0.80 1.00	Marginal Prob.
0.00 0.01		0	0	0	0	0	0.068	0.004	0.003	0.002	0.206	0.283
0.01 0.02		0	0	0	0	0	0.046	0.010	0.004	0.002	0.142	0.205
0.02 0.03		0	0	0	0	0	0.014	0	0.001	0.002	0.070	0.087
0.03 0.06		0	0	0	0	0	0.035	0.004	0.003	0.004	0.101	0.147
0.06 0.10		0	0	0	0	0	0.016	0.008	0	0.002	0.115	0.141
0.10 0.15		0	0	0	0	0	0.008	0.002	0.006	0.006	0.054	0.077
0.15 0.21		0	0	0	0	0	0.002	0.003	0.001	0.001	0.016	0.023
0.21 0.28		0	0	0	0	0	0.003	0.002	0.003	0.001	0.008	0.018
0.28 0.36		0	0	0	0	0	0.002	0	0.001	0	0.005	0.008
0.36 0.45		0	0	0	0	0	0	0	0	0	0.001	0.001
0.45 0.55		0	0	0	0	0	0.001	0.002	0	0.001	0	0.004
0.55 0.66		0	0	0	0	0	0	0	0	0	0	0
0.66 0.78		0	0	0	0	0	0	0	0.001	0	0	0.001
0.78 1.00		0	0	0	0	0	0.002	0	0.001	0	0	0.003
Marginal Prob.		0	0	0	0	0	0.197	0.037	0.025	0.022	0.720	1.000

2.2.3 Transmission capacity statistics and assignment algorithm

In order to manage or prevent overloading conditions, most transmission branches have established some capacity limits that cannot be exceeded at any time. In realistic power grids, this rating is figured out based on the device configuration and the worst-case scenario with respect to environmental conditions, and may also be imposed by other factors such as stability or voltage limits. However, in synthetic power grid modeling and due to the lack of sufficient technical information, we have to use statistical approaches in order to find the best setting for the transmission line capacity. In this section, we will introduce a statistical–based approach to generate a set of transmission line capacities and assign them to the transmission lines. To accomplish this goal, we first investigate the scaling function of total transmission line capacity in a grid versus the network size. Then we study the possible relationship between transmission line capacity F_l^{Max} and the real-time flow of power F_l through the transmission lines during the normal operation of realistic power grids. These results then will be used to develop a new methodology

to appropriately characterize the line capacity assignment and improve the synthetic power grid modeling.

2.2.3.1 Scaling property of total transmission capacity

Using the definition of aggregate transmission line capacity $F_l^{tot} = \sum_{m=1}^{M} F_{l_m}^{Max}$, we do the statistical analysis on the IEEE test cases and realistic grid data, to show the mathematical relationship between the network size and the total transmission line capacity of the grid. We derived the scaling function for aggregated transmission line capacity in a grid versus network size as follows

$$\log F_l^{tot}(N) = 1.03(\log N) + 2.52 \tag{2.10}$$

where *N* is network size and the logarithm is base 10. Although the presented scaling function can generate reasonable values for the total transmission capacity, it is really challenging to find the best line capacity assignment. Indeed, we need to evaluate the statistical behavior of realistic capacities and the relationships between the branch capacities and other grid metrics which can be measured in any given network, i.e. flow distribution.

2.2.3.2 Correlation between transmission gauge ratio and flow distribution

Our initial experiments on statistical distribution of transmission gauge ratio show that the best distribution which it fits the distribution of β_l is exponential distribution. The statistics collected from the date of a number of realistic grids also indicate that there exists a considerable correlation between the transmission gauge ratio and its flow distribution and its Pearson's coefficient varies in range of 0.35 – 0.65. Figure 2.5 displays the scatter plot of normalized flow distribution and transmission gauge ratio which can be utilized to generate the 2-D empirical PMF of some sample grids like WECC-16994 buses system. It is worthy to note that in power systems,

three different capacities define for transmission lines i.e. long term, short term, and emergency capacity and in this study we focus on long term capacity of transmission lines. However, from Fig. 2.5 we can see that for some lines β_l is higher than 1, which it means that those line are operating in short term or emergency rating.

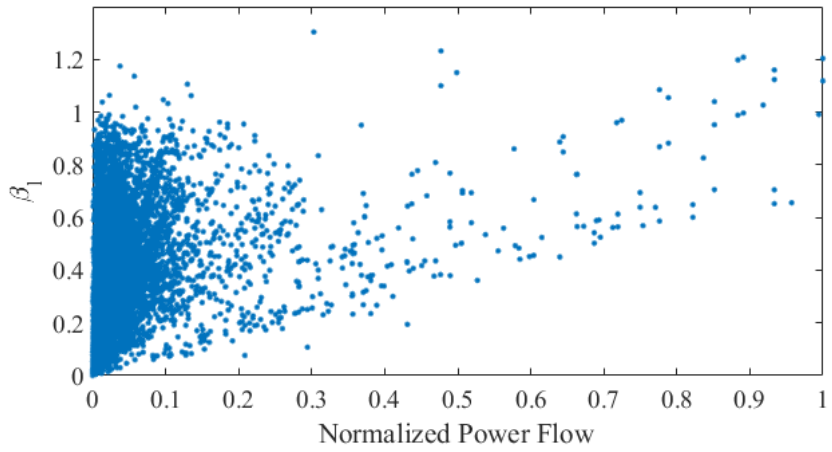

Figure 2.5 Scatter plot for transmission gauge ratio versus normalized flow distribution in WECC-16994 bus system

Studying correlation between transmission gauge ratio and normalized flow distribution, we may extract an empirical 2-dimentional PMF and based on that a 2-dimensional probability distribution table can be formulated to enable an algorithm to assign transmission line capacities to the synthetic power grid.

2.2.3.3 Transmission line capacity assignment

In this subsection we develop an algorithm to address the statistical assignment of transmission capacities in a synthetic power grid model using approximate scaling function of total transmission line capacity versus network size, the estimated exponential distribution of the transmission gauge ratio β_l, and the correlation between the gauge ratio and flow distribution of power grid. First a statistically correct random set of transmission gauge ratios will be generated;

and using derived 2-dimensional probability distribution table, we will assign transmission gauge ratios to each transmission line with respect to the grid flow distribution calculated from the DC power flow solution. Next we will scale transmission line capacities if $\sum_{m=1}^{M} F_{l_m}^{Max} > 1.05F_l^{tot}$ or $\sum_{m=1}^{M} F_{l_m}^{Max} < 0.95F_l^{tot}$ to assure the aggregated transmission line capacity remains within the range specified by the scaling function of $F_l^{tot}(N)$. The flowchart of proposed algorithm is depicted in Fig. 2.6.

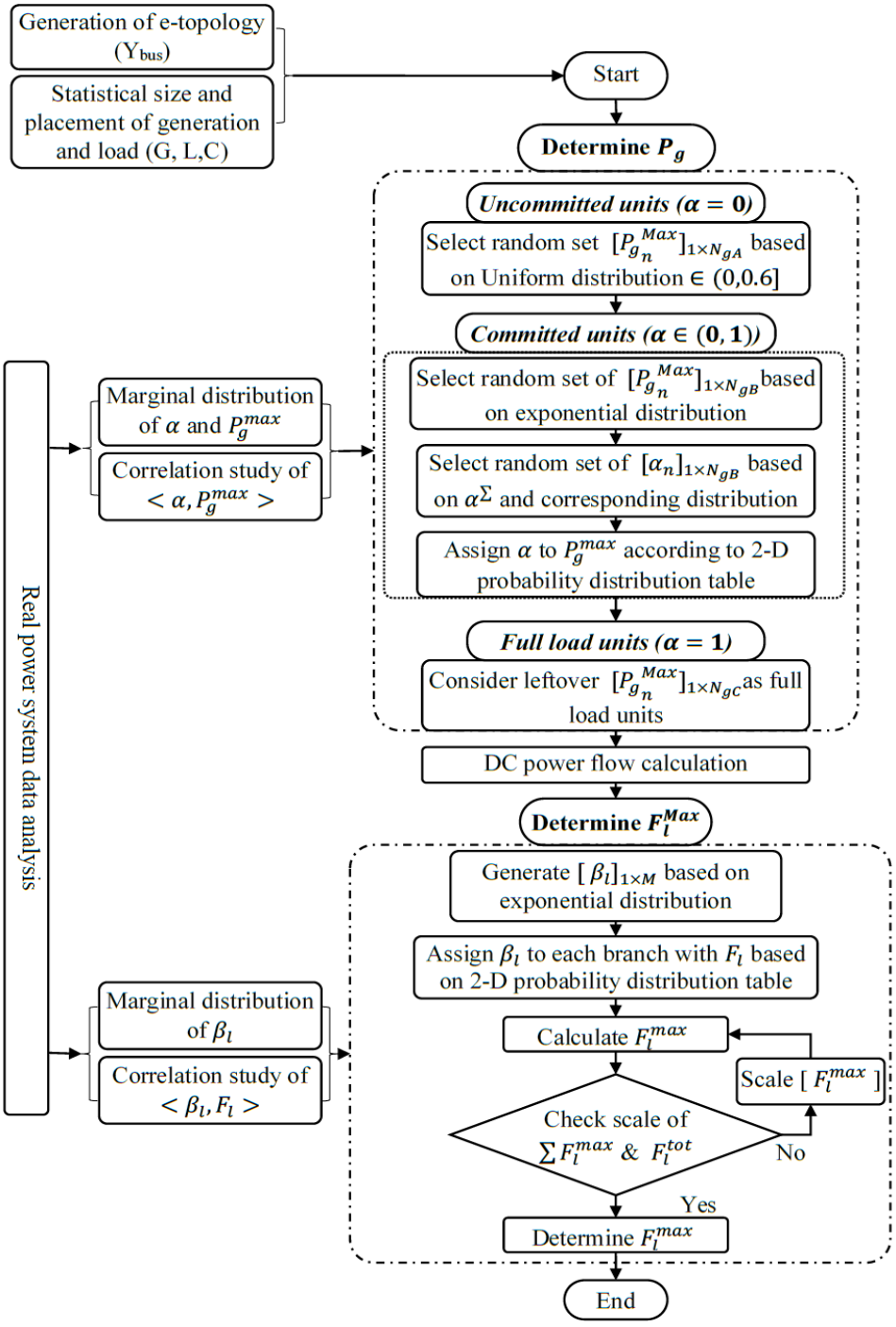

Figure 2.6 Algorithm flowchart to assign statistically accurate transmission line capacities for a synthetic grid

2.3 AutoSynGrid: A MATLAB-based Toolkit for Automatic Generation of Synthetic Power Grids

In this section, we combine all our proposed approaches and introduce a toolkit to generate synthetic models featuring same properties of realistic power grids. The AutoSynGrid toolkit is designed based on MATLAB Graphical User Interface (GUI) and it is able to build any number of synthetic cases that can be used for a variety of analysis such as PF and OPF studies. It allows to select several key characteristics of the generated system, such as reference system, loading level, and generation cost model. The generated cases include topology, bus type, generation and load setting, transmission line capacities and generation types and cost models. The output of the toolkit is exported in the native MATPOWER [3] format allowing to use the MATPOWER open-source, steady-state, planning, and analysis package to further studies on the generated cases. In addition, we develop a validation framework, which examines the generated synthetic cases based on the metrics introduced in the literature and some new validation metrics we found in realistic power grids. These metrics are categorized into topology metrics, electric parameters, state variables, interdependencies, and scaling properties. Moreover, we define a closeness factor to measure the realism of generated synthetic cases and compare with totally random grids.

2.3.1 AutoSynGrid Functionality

In this section, the key input parameters and outputs in synthetic case generation is introduced. Figure 2.7 shows the user interface of AutoSynGrid toolkit. The AutoSynGrid toolkit is able to generate the synthetic cases with only indicating the network size. However, five additinal options are provided to control the featurs of the generated cases, including number of branches, loading level, reference system, bus type entropy, and generation cost modelling approach (see Fig. 2.7). Moreover, default selections are provided for all these options.

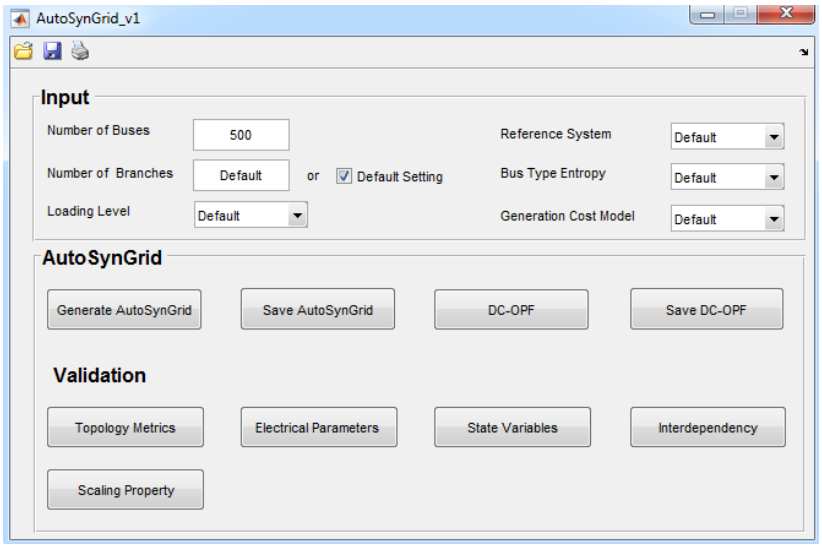

Figure 2.7 User interface of AutoSynGrid toolkit

1) ***Number of Buses:*** The network size is the only essential input that the AoutoSynGrid needs to generate the synthetic cases. The minimum and maximum network size to generate synthetic cases is set to 20 and 6000, respectively. It should be mentioned that the toolkit is able to generate synthetic cases with more than the 6000 buses, however, for the large network sizes the execution time increases significantly.

2) ***Reference System:*** The toolkit utilizes a reference realistic grid to generate synthetic cases based on its properties such as generation and load settings. For the first version, three reference systems of NYISO, WECC, and ERCOT are provided and the default reference system has been set to NYISO.

3) ***Number of Branches:*** In the default setting, the AutoSynGrid toolkit creates the branches based on the topology requirements such as average node degree and average path length. However, the user is able to specify the total number of branches in this section. It is worthy to note that to generate valid synthetic cases it is important to fulfill specific requirements for number of the branches. For instance, to satisfy the average

node degree requirement, total number of branches should be in a specific range. Therefore, the toolkit will show a massage in case of any violation.

4) ***Bus Type Entropy:*** This parameter selects the bus type assignment method for the synthetic cases. Two methods for calculation of bus type entropy i.e. $W_0(\mathbb{T})$ and $W_1(\mathbb{T})$ are provided [58]. The first option $W_0(\mathbb{T})$ has the advantage to simplify the optimization procedure seeking for the best bus type assignments with faster execution time to find the optimum assignment. While the second definition, $W_1(\mathbb{T})$ as a more generalized entropy, has the advantage to simplify the approximation procedure of the scaling function. The default option is dedicated to the $W_0(\mathbb{T})$.

5) ***Loading Level:*** This value defines what percent of total generation capacity is utilized in the power grid. It is defined as the ratio of total active load to the total generation capacity of power grid, i.e.,

$$\alpha^{\sigma} = \sum_{i=1}^{N_L} P_{L_i} \Big/ \sum_{j=1}^{N_g} P_{g_j}^{Max} \tag{2.11}$$

where N_L indicates the total number of loads, N_g is the number of generators, P_{L_n} and $P_{g_n}^{Max}$ are active load and maximum generation capacity of load *i* and generator *j*, respectively. The user is able to select the expected loading level of the synthetic case between, default (scaling property of total load [54]), low (30-40%), medium (50-60%), and high (70-80%).

6) ***Generation Cost Model:*** This setting selects the approach to determine generator cost models and their associated coefficients. For the generation cost model, two approaches of quadratic generation cost model (Approach A) and linear generation cost model

(Approach B) are provided. The approach A models the generation costs based on the dispatch cost coefficients derived from generation block-offer schedule data while the approach B utilizes average heat rates and fuel costs of power plants. The default setting for this parameter is approach A.

Once the input data is provided, the "*Generate AutoSynGrid*" button will generate the synthetic grid. A waiting bar is implemented to illustrate the process of synthetic grid generation. The generated case includes data for the system MVA base, bus data, generator data, branch data, generator cost data, type of generators, and fuel types. Once the generation is done, the "*Save AutoSynGrid*" button will save the case in native MATPOWER format in any path the user selects to save the data. MATPOWER is an open-source MATLAB-based power system simulation package that provides a high-level set of power flow, OPF, and other tools targeted toward researchers, educators, and students [3]. In addition, the user is able run DC-OPF and save the results with "*DC-OPF*", and "*Save DC-OPF*" buttons, respectively. Figure 2.8 shows a sample synthetic case created by AutoSynGrid toolkit indicating the generation and load buses with corresponding power flows. In addition to the generated MATPOWER format case, the toolkit provides evaluation results for the generated cases. These results are divided in five categories of topology metrics, electric parameters, state variables, interdependencies, and scaling properties. Each button provides a summary information on topological and electrical characteristics of corresponding category for the generated synthetic case to validate the accuracy of generated synthetic case and designed toolkit.

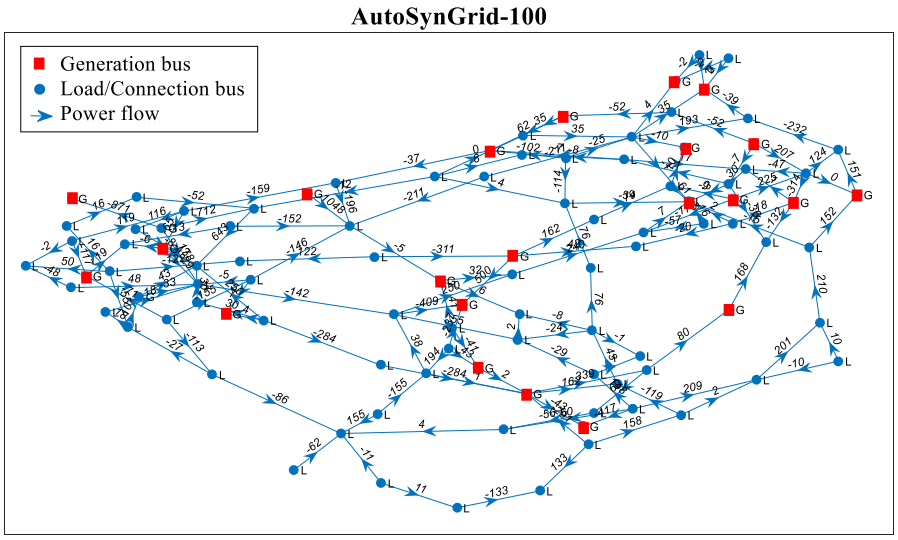

Figure 2.8 A sample synthetic case created by AutoSynGrid toolkit

2.3.2 Overview of the methodology

We introduce AutoSynGrid toolkit to produce infinite number of power grid test cases with scalable network size featuring the same kind of small-world "*electric*" topology of real-world power transmission network. Integration of electrical settings such as generation and load settings, generation cost models, and transmission line capacities with previously proposed RT-*nestedSmallWorld* model in [51], enables us to generate complete and more accurate synthetic grid cases. The AutoSynGrid toolkit includes five modules to generate synthetic grid cases as illustrated in Fig. 2.9. The synthetic grid generation begins with the topology creation in RT-*nestedSmallWorld* module, using Small-World properties and realistic power grid features. The second step is bus type assignment. Once the generation, load and connection buses are determined, generation capacities, generation dispatch and load settings are assigned in the corresponding module. Once the necessary data for DC-PF study such as electric topology, generation and load settings are determined, DC-PF is executed to test the state variables including phase angle differences and flow distribution. If the created case does not pass the predefined

criteria for the state variables, it will be sent to the previous modules to modify the created synthetic case. This modification includes revisions on branch connections, reassignment of impedances, buss type assignment, and generation and load settings. Once the generated case passed the state variables test, the *Transmission Line Capacity* module determines the line capacities, based on the synthetic grid flow distributions. The module for generation cost modelling uses the generation capacities to determine the fuel types and then assigns the cost models based on them. The final synthetic case is converted to the MATPOWER format and user is able to run DC-OPF for economic analysis and the validation process to assure the accuracy of the generated synthetic case. The *Validation* button examines the generated synthetic cases, based on the metrics that they are observed from realistic power grids. The specific description of each module in the AutoSynGrid toolkit is described in more details below.

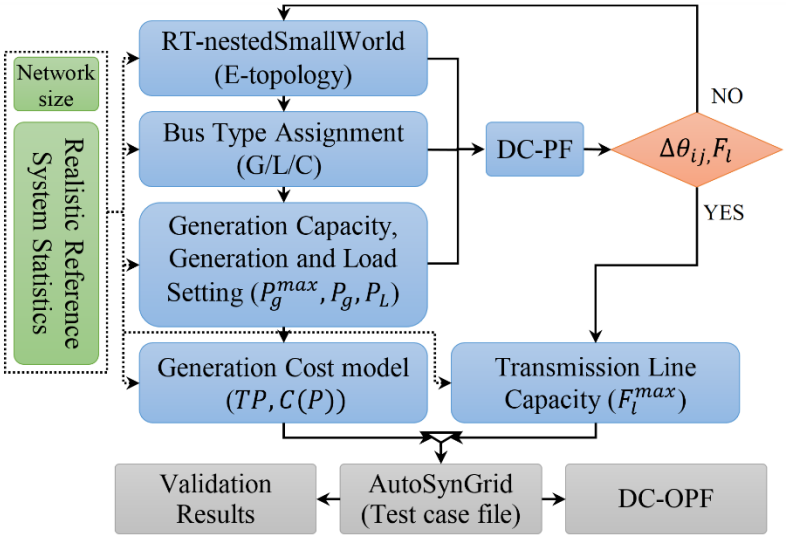

Figure 2.9 Flowchart of AutoSynGrid toolkit to generate synthetic grid cases

2.3.2.1 RT-nestedSmallWorld

The *RT-nestedSmallWorld* generates a random electric topology with any number of network size based on the small-world characteristics of realistic power grids. In real-world power grids, usually, a large-scale systems consist of a number of smaller-size subsystems, which are interconnected by sparse and important tie lines [147]. The RT-*nestedSmallWorld* generates the synthetics cases by using this fact in a hieratical way. First, it forms connected subnetworks with limited size and the connectivity requirements. Then connects the subnetworks through lattice connections and finally, generates the line impedances from specific distributions and assign them to the links in the topology network. More details are available in [51].

2.3.2.2 Bus Type Assignment

The best set of bus type assignments for the generated synthetic topology, indicating the generation, load, and connection buses, is determined in this module. The key concept in this module is the *Bus Type Entropy*. Two different *Bus Type Entropy* has been defined in [2] as the numerical weighted measures to quantify and characterize the "correlated" bus type assignments:

$$W_0(\mathbb{T}) = -\sum_{k=1}^{3} r_k \times \log(r_k) - \sum_{k=1}^{6} R_k \times \log(R_k) \tag{2.12}$$

$$W_1(\mathbb{T}) = -\sum_{k=1}^{3} \log(r_k) \times N_k - \sum_{k=1}^{6} \log(R_k) \times M_k \tag{2.13}$$

To determine best bust type assignment, first, the empirical PDF of randomized bus type assignments with respect to the grid size and its connecting topology will be generated to calculate the estimated fitting distribution parameters of (μ, σ). Then, the normalized distance called *d* [58] will be calculated to find the target entropy value of W^* using $W^* = \mu + \sigma d_W(N)$, which is consistent with that observed in realistic grids. Finally, an optimization algorithm with objective function of $\min_{\mathbb{T}} \varepsilon = |W(\mathbb{T}) - W^*|$ will be implemented to search for the desired bus type

assignments with respect to the W^* to determine the best set of bus type assignments. More details on bus type assignment can be found in [58].

2.3.2.3 Generation capacity, generation and load setting

This module generate statistically correct random set of generation capacities and loads and assign them to the generation and load buses. First, a statistically correct random set of generation capacities and load will generate based on the derived exponential distributions. For both aggregate generation capacity and load the approximate scaling function can be represented as function of network size as [54]

$$\log P_{g,Max}^{tot}(n) = -0.21(\log n)^2 + 2.06(\log n) + 0.66 \tag{2.14}$$

$$\log P_{L}^{tot}(n) = -0.20(\log n)^2 + 1.98(\log n) + 0.58 \tag{2.15}$$

where $P_{g,Max}^{tot}$ denotes the estimated total generation capacity, P_{L}^{tot} denotes the estimated total demand, and the logarithm is with base 10. The generated random sets of generation capacities and loads are examined and scaled to ensure that the aggregated generation capacities and loads remain in the range specified by Eqs. (3) and (4). The final step is to assign the generated statistically correct random sets to the related buses utilizing a non-trivial correlation between the normalized nodal degree of a generation/load bus and its capacity. Details on proposed algorithms are available in [53].

Generation dispatch is the other vital component to build a valid synthetic grid. It enables the toolkit to perform DC-PF study, test the created synthetic cases, and use the calculated flow distributions to determine transmission line capacities. Given a synthetic grid topology with *N* buses and determined generation capacities and load settings, the algorithm selects a randomly correct set of generation capacities for both committed and uncommitted units which follows 99%

rule for committed unites and uniform distribution for uncommitted unites. Next by generating statistically correct random set of dispatch factors ($\alpha = P_g/P_g^{max}$), it assigns them to the selected generation capacities in generation buses based on a 2-D empirical PMF of normalized generation capacities and dispatch factors. More details are available in [57].

2.3.2.4 Generation cost assignment

The essential component to perform energy economic studies, such as OPF problem, is to determine generator cost models and their associated coefficients. In this section, we propose an approach based on statistical analysis of actual grids and available information on generation units to determine fuel types and generation cost models based on pre-determined generation capacities.

The generation mix of U.S. EIA data [148] is studied to proposed the fuel type assignment algorithm. For simplicity, all different technologies/fuel types in the generation mix are combined into five major categories of Hydro, Wind, Natural Gas, Coal, and Nuclear to avoid relatively complicated modeling for very small portion of total installed generation capacity. Statistical analysis on power plants for all Eastern Interconnection (EI), Western Electricity Coordinating Council (WECC) [149], and Electric Reliability Council of Texas (ERCOT) [150] interconnections shows that there exist a strong correlation between normalized generation capacities of power plants and their discretized fuel types by a Pearson coefficient of $\rho\left(\overline{P_{g_n}^{Max}}, TP_n\right) \in [0.48, 0.64]$. Given a data set of generation unit capacity and discretized fuel types, we may define a joint distribution function in the two-dimensional space of $\left(\overline{P_{g_n}^{Max}}, TP_n\right)$. The 2-D density function $f\left(\overline{P_{g_n}^{Max}}, TP_n\right)$, when integrated over a set S gives the probability that $\left(\overline{P_{g_n}^{Max}}, TP_n\right)$ falls into the set:

$$\Pr(A) = \Pr\left\{\left(\overline{P_{g_n}^{Max}}, TP_n\right) \in S\right\}. \tag{2.16}$$

Thus, the 2-D empirical probability mass function (PMF) cab be extracted to use as a guidance map to assign fuel types to generators based on their normalized generation capacity. Once the fuel types determined, generation cost models will be assigned accordingly. For the generation cost model, we consider two approaches to assign no load and production cost to each generator:

$$\text{Approach A: } C(P) = a_0 + a_1 P + a_2 P^2 \tag{2.17}$$

$$\text{Approach B: } C(P) = a_0 + c_f(b_1 P + b_2 P^2) \tag{2.18}$$

where $a_i : i = 0,1,2$ and $b_i : i = 1,2$ indicate the fuel-dependent cost model coefficients, c_f refers to fuel cost and P is generator output.

The approach A models the generation cost based on the dispatch cost coefficients derived from generation block-offer schedule data of ISO-NE and PJM differentiated by fuel type [43]. On the other hand, approach B utilizes average heat rates of power plants and their fuel costs obtained from EIA data, to model cost functions [38]. No load costs for wind and hydro power plants are set to zero. The cost coefficients data summarized in [38] are used to assign for each generator by its fuel type and capacity. Figure 2.10 shows the proposed algorithm flowchart to assign fuel types and generation costs.

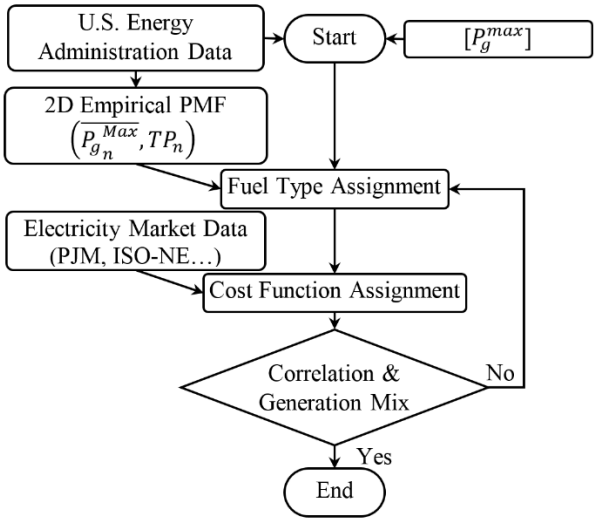

Figure 2.10 Algorithm flowchart to assign statistically accurate fuel type and generation costs for a synthetic grid.

2.3.2.5 Transmission line capacity

The line capacities are assigned to transmission lines according to flow distribution calculated by DC-PF. First, a statistically correct random set of transmission gauge ratios $(\beta_l = F_l/F_l^{Max})$ are generated based on derived exponential distribution. Then, using the derived 2-D PMF table of reference system for transmission gauge ratio and its flow distribution, the transmission gauge ratios are assigned to each transmission line with respect to the grid flow distribution calculated from the DC-PF solution. In the final step, the total transmission line capacities will be examined and scaled to assure that the aggregated transmission line capacity remains within the range specified by the scaling function of $F_l^{tot}(N)$ in [54]. More details are available in [57].

2.3.3 Validation framework

The AutoSynGrid toolkit automatically examines the generated cases in every module to assure the accuracy of implementation; however, we developed a systematic validation framework to provide an option for the user to run the validation process individually. This supports the

confidence that the generated synthetic case does not provide any misleading information in case of further simulations and studies based on the created synthetic cases. The selected metrics for the validation process have been observed from set of realistic power grids including IEEE test cases, PEGASE systems that represent some European nation's grids at different levels of network reduction, RTE system which is an equivalent of French Grid, and North America power grids (FERC data) including WECC, ERCOT, and NYISO systems. All of these cases are available in MATPOWER database [151] except FERC data which are not publicly available cases. We have categorized the validation metrics to five different categories as topology metrics, electrical parameters, state variables, interdependency between topo-parameters and electro-parameters, and scaling properties. The AutoSynGrid toolkit examines the generated cases according to these metrics to validate their realism. In the next, we introduce the validation metrics and examine the sample generated AutoSynGrid cases by these metrics. In addition, we define a new metric to measure the closeness of generated synthetic case to the realistic power grids. For each network size, 20 synthetic cases have been generated by AutoSynGrid toolkit to examine in this section. Moreover, the results are compared with realistic power grids and also ACTIVSg synthetic case which are recently introduced in [152]. It should be mentioned that all the AutoSynGrid cases have been generated with default settings of toolkit (*Reference System:* NYISO, *Number of Branches:* Default, *Bus Type Entropy:* $W_0(\mathbb{T})$, *Loading Level*: Default, *Generation Cost Model*: Approach A).

2.3.3.1 Topology metrics

This category examines the average node degree, algebraic connectivity (λ_2) and average path length ($\langle l \rangle$) to validate the generated cases. The power grids sparsely connected with known *small-world* properties including much shorter average path length and a much higher clustering

coefficient, compared to purely random graph networks with similar sizes [50]. Meanwhile, the power grids have two main distinctions from small-world networks [51]: their average nodal degree is very low ($\langle k \rangle = 2 \sim 5$) due to their sparsity and it does not scale with network size. Secondly, the algebraic connectivity (λ_2) of power grids has a very special scaling property versus the network size. Table 2.2 shows average of these topology metrics we observed from generated AutoSynGrid cases and their related valid interval based on realistic power grids. Fig. 2.11 shows the average node degree for real and synthetic grids which indicates this parameter is independent of network size.

Table 2.2 Topology metrics for generated AutoSynGrid cases

	AutoSynGrid-500	**AutoSynGrid-1000**	**AutoSynGrid-3000**
$(N, \bar{M})$	(500, 890)	(1000, 1830)	(3000, 5580)
$\overline{\langle k \rangle}$	3.5	3.6	3.6
Valid interval	[2-5]	[2-5]	[2-5]
$\overline{\langle l \rangle}$	6.1	13.1	16.5
Valid interval	[2.5 – 10.5]	[8.5 – 17.5]	[12 – 20]
$\overline{\lambda_2}$	0.011	0.008	0.003
Valid interval	[0.004–0.040]	[0.002–0.020]	[0.0005–0.005]

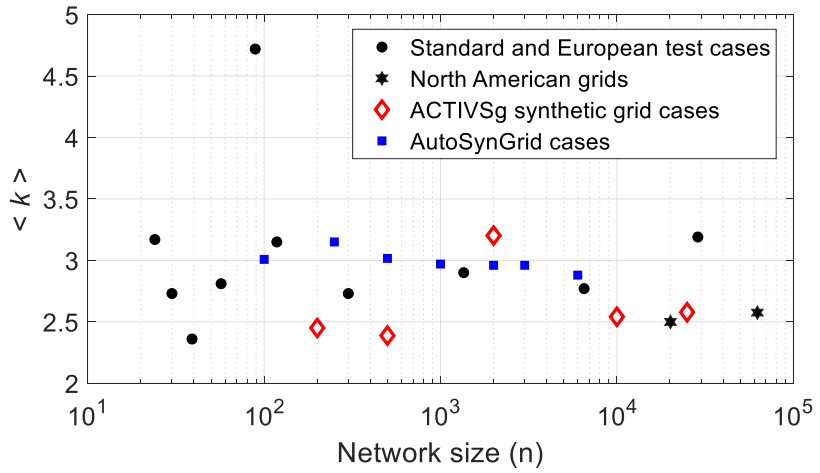

Figure 2.11 Average node degree for real and synthetic grids.

2.3.3.2 Electrical parameters

This category includes the 99% rule and line impedances. The generation capacities and loads in the real world power systems are investigated in [53] and shown that for both generation capacity and load, more than 99% of the generation units/loads follow an exponential distribution with about 1% having extremely large capacities falling out of the normal range defined by the expected exponential distribution [53]. Figure 2.12 shows the statistical distribution of generation capacities in the left side and loads in the right side for the sample generated AutoSynGrid cases. The fitting curve is depicted as a dashed line for the distribution function of P_g^{Max} and P_L. The straight line in the log plot implies that about 99% of generation capacities and loads in the generated synthetic cases tend to follow an exponential distribution function.

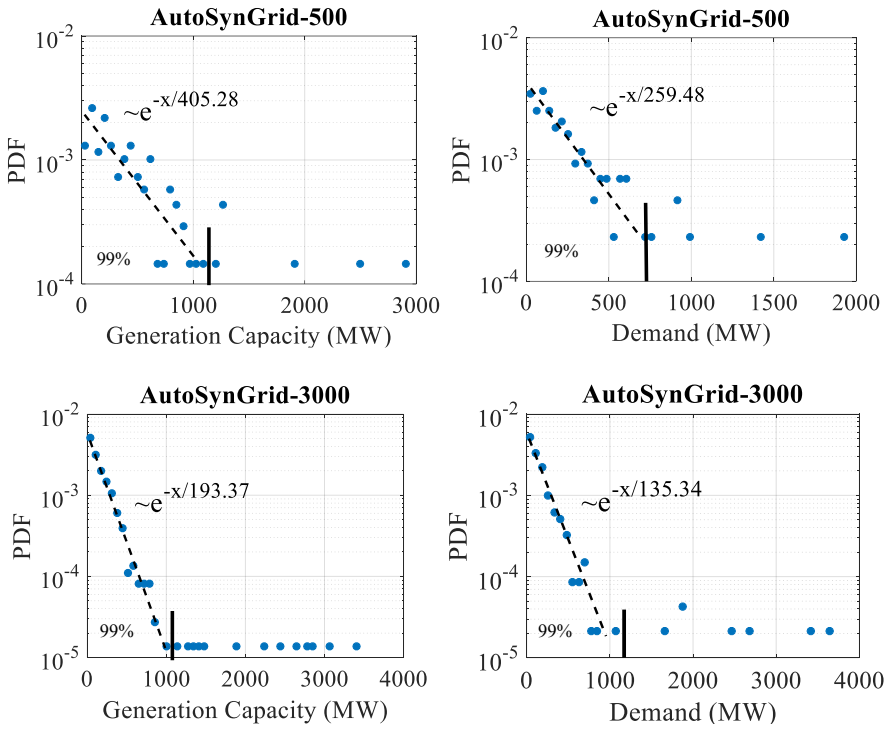

Figure 2.12 Empirical PDF of generation capacity and loads for the generated AutoSynGrid cases

Studies on line impedances of real power grids showed that the lognormal distribution is suited for fitting the line impedances [15]. The empirical PDF of line impedances for the realistic reference grids are illustrated in Fig. 2.13 with the lognormal fit distribution as the best fitted distribution based on the Kullback-Leibler divergence (D_{KL}) [153]. It is worthy to note that for the D_{KL}, smaller values represents a more accurate fit for the empirical PDF of data. Table 2.3 shows the average parameters of lognormal normal distribution for line impedances of generated AutoSynGrid cases. By increasing the network size the D_{KL} of lognormal distribution decrease. In fact, for the large network size the number of samples to fit the distribution is large, therefore the fitted distribution will be more close to the original one with smaller D_{KL}.

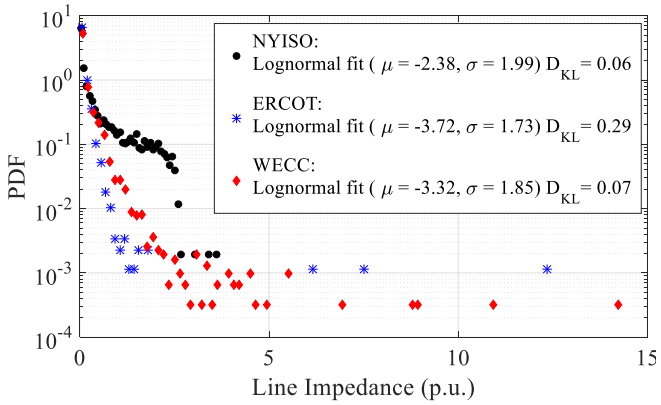

Figure 2.13 Empirical PDF and fitted distribution of line impedance for the realistic reference systems and generated AutoSynGrid cases

Table 2.3 Lognormal distribution fit of line impedance for AutoSynGrid cases

	$\bar{\mu}$	$\bar{\sigma}$	$\overline{D_{KL}}$
AutoSynGrid-100	-2.44	2.34	0.81
AutoSynGrid-250	-2.44	1.97	0.43
AutoSynGrid-500	-2.35	1.89	0.12
AutoSynGrid-1000	-2.37	1.98	0.04
AutoSynGrid-2000	-2.35	1.98	0.03
AutoSynGrid-3000	-2.37	2.01	0.03

2.3.3.3 State variables

In this subsection, two state variables of power systems i.e. absolute branch phase angle difference and flow distributions are considered. It is found that for the real-world power grids the branch phase angle difference follows exponential distribution with small mean value between 2.34 and 2.36 degree (Fig. 2.14.a). As we can see, the D_{KL} value for the ERCOT is higher than the other two reference systems. It is found that although the exponential distribution does not fit

perfectly for the ERCOT similar to the NYISO and WECC systems, it is the best fit in comparison with other distributions such as lognormal, generalized extreme value, and t-location scale. In addition, our studies on flow distribution have shown that the statistical distribution of flow distribution within a power grid based on realistic power grids data follows an exponential distribution with different mean values based on system loading level (Fig. 2.13.b). Table 2.4 shows the average distributions parameters of absolute branch phase angle difference and flow distribution for sample generated AutoSynGrid cases. For all generated AutoSynGrid cases absolute branch phase angle difference and flow distribution follow exponential distribution with acceptable D_{KL}.

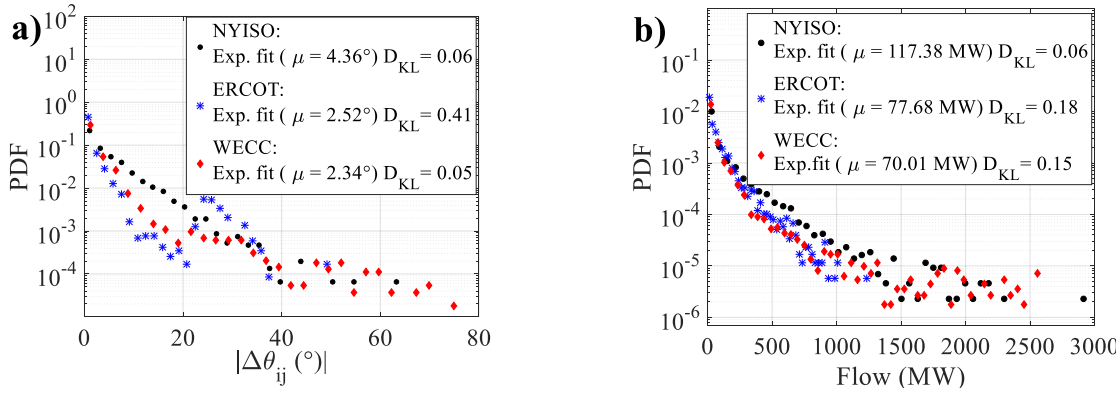

Figure 2.14 Empirical PDF and fitted distribution of a) branch phase angle difference and b) flow distribution for the realistic power systems

Table 2.4 Exponential distribution fit of branch phases angles difference and flow distribution for AutoSynGrid cases

	Branch phase angle difference		**Flow**	
	$\bar{\mu}(°)$	$\overline{D_{KL}}$	$\bar{\mu}(MW)$	$\overline{D_{KL}}$
AutoSynGrid-100	2.86	0.86	133.63	0.92
AutoSynGrid-250	3.43	0.48	145.37	0.20
AutoSynGrid-500	3.55	0.33	112.75	0.13

AutoSynGrid-1000	4.02	0.28	101.14	0.09
AutoSynGrid-2000	4.26	0.15	109.59	0.08
AutoSynGrid-3000	4.29	0.11	109.99	0.08

2.3.3.4 Interdependency

This category examines the topological and electrical interdependencies of generated synthetic cases. As mentioned, there exist a considerable correlation between the normalized node degree of a generation bus and its normalized capacity with a Pearson coefficient of $\rho(\overline{P_{L_n}}, \overline{k_n}) \in [0.1,0.5]$, for the generation type, load setting, generation dispatch, and transmission line capacities, the related Pearson's coefficients are $[0.48, 0.64]$, [0.3-0.6], $[0.15,0.55]$, and $[0.35,0.65]$, respectively. Table 2.5 includes the average Pearson's coefficients of generated cases for the related algorithms, which validates the accuracy of assignments in each algorithm.

Table 2.5 Average Pearson's coefficients of generated

	AutoSynGrid-500	**AutoSynGrid-1000**	**AutoSynGrid-3000**	**Valid interval**
$\boldsymbol{\rho\left(\overline{P_{g_n}^{Max}}, \overline{k_n}\right)}$	0.30	0.38	0.40	[0.10 – 0.50]
$\boldsymbol{\rho\left(\overline{P_{g_n}^{Max}}, TP_n\right)}$	0.48	0.54	0.58	[0.48 – 0.64]
$\boldsymbol{\rho(\overline{P_{L_n}}, \overline{k_n})}$	0.42	0.44	0.44	[0.30 – 0.60]
$\boldsymbol{\rho\left(\overline{P_{g_n}^{Max}}, \alpha_n\right)}$	0.32	0.41	0.46	[0.15 – 0.55]
$\boldsymbol{\rho(\overline{F_l}, \beta_l)}$	0.51	0.55	0.61	[0.35 – 0.65]

2.3.3.5 Scaling property

In this subsection, relative distance of correlated bus type assignment, algebraic connectivity, average path length, and maximum phase angle difference are examined as scaling property metrics. The relative distance of bus type entropy in correlated assignments and randomized permutation for power grid networks exhibit a strong dependence on the network size that can be mathematically modeled. Fig. 2.15 shows the distance for actual grids and synthetic grids. Figure 2.16.a and 2.16.b illustrates the algebraic connectivity (λ_2) and average path length ($\langle l \rangle$) of

generated AutoSynGrid cases in comparison with the realistic power grids. The blue line is the fitted curve for the algebraic connectivity of the tested realistic power grids. As we can see, the algebraic connectivity and average path length of generated AutoSynGrid cases follow the approximated trend of real systems. Maximum phase angle difference of realistic power grids along with generated synthetic cases is presented in Fig. 2.17. The solid blue line indicates the fitted curve for maximum phase angle difference of realistic power grids. The maximum phase angle difference in the grid increases as the network size increases. It is widely accepted that the phase angle difference between two buses can indicate the relative stress across the grid. To have a stable operation, the phase angle difference should be relatively small; however, for larger power grids we can see that the maximum phase angle difference is larger than 90 degrees. This large difference in phase angles comes from the operation of different zones in large power systems. In fact, each area in power grid operators with the maximum phase angle difference less than 60 degrees and the phase shifters between these areas cause the large maximum phase angle difference in whole power grid. The maximum phase angle difference of AutoSynGrid cases follow the scaling property of realistic power grid. This modelling enables to further studies and extensions for the created synthetic case to indicate operation zones, tie lines, and HVDC connection lines.

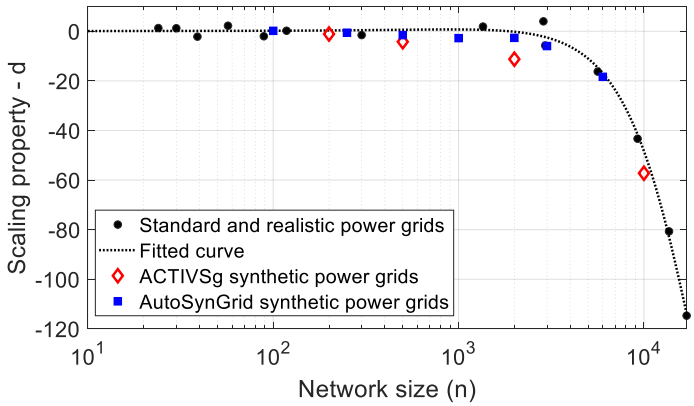

Figure 2.15 Scaling function of relative distance of bus type entropy in random assignment for different network sizes.

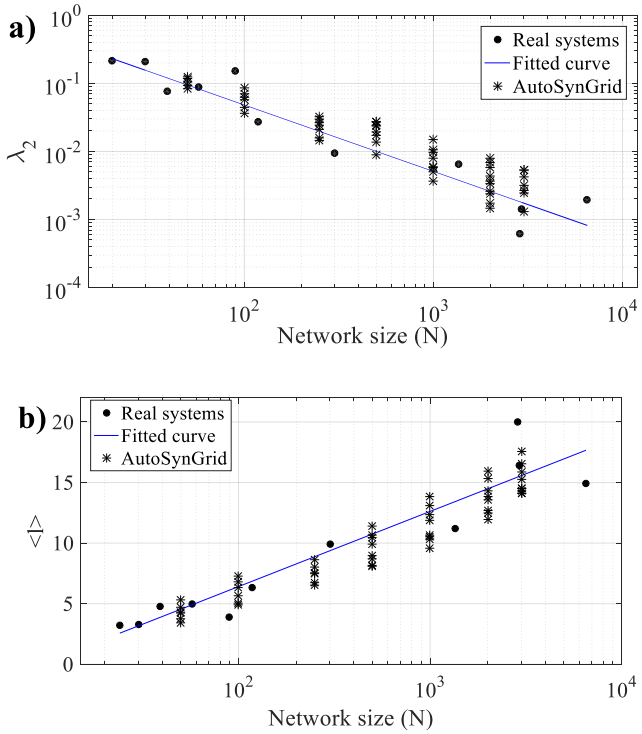

Figure 2.16 Scaling property of realistic power grids and generated synthetic cases a) algebraic connectivity (λ_2) b) average path length ($\langle l \rangle$)

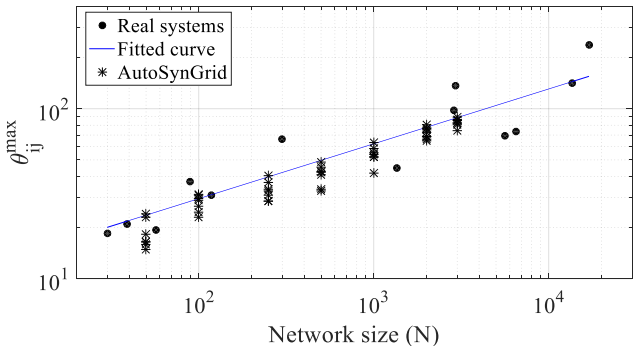

Figure 2.17 Maximum phase angle difference of realistic power grids and AutoSynGrid cases.

2.3.3.6 Synthetic grid realism

To measure the closeness of generated synthetic cases to realistic reference systems, we define a function representing the realism of generated synthetic grid based on five categories of validation metrics that we presented in previous subsections. Consider a family of N_m validation metrics belong to the specific validation category. The family accuracy for the specific validation category can be defined as follows [154]:

$$X = 1 - \frac{1}{n_m}\sum_{j=1}^{n_m}\left(\frac{\left|x_j - x_j^{ref}\right|}{x_j^{ref}}\right) \tag{2.19}$$

where n_m is total number of the metrics belong to the specific category, x_j is the measured metric j for the generated synthetic grid, and x_j^{ref} denotes the actual value of the metric j for the realistic reference system. For the metrics with pass/fail status such as average node degree in topology metrics, integer numbers of 1 and 0 are considered for pass and fail status, respectively. Also for the validation metrics that examine the PDF distributions, in addition to the distribution parameters such as mean value and variance, D_{KL} is considered to incorporate the fitting accuracy. For the scaling metrics, the fitted curves of realistic power grids are assumed as the reference value. We defined the closeness factor as the average family accuracy of validation categories:

$$C(N) = \frac{1}{n_c}\sum_{k=1}^{n_c} X_k \tag{2.20}$$

where $C(N)$ is the closeness metric ranging between [0, 1], in which the $C(N) = 1$ represents the high similarity with reference system. n_c is total number of the validation categories and X_k denotes the family accuracy of validation category of k for generated synthetic case. Figure 2.18.a shows the scaling of closeness factor for the generated AutoSynGrid cases with three different reference systems. The dashed lines indicate the fitted mean value of generated synthetic cases. The closeness factor for the generated synthetics cases with all three reference systems increases with increasing the network size. However, the synthetic cases that are generated based on NYISO

reference system, have higher closeness factor in comparison with the other generated synthetic cases. This can be explained by network size of the reference systems. The network size of NYISO, ERCOT, and WECC are 2935, 5633, and 16994, respectively. The size of generated AutoSynGrid cases are more close to the NYISO network size. Therefore, it is more feasible to mimic the characteristics of a reference system with similar network size than a reference system with higher network size difference. It is worthy to note that the goal for the synthetic grid generation is not to achieve to $C(N) = 1$. In fact, with $C(N) = 1$ the generated synthetic case is equal to the reference system with same properties and information, which is contradictory with the definition of synthetic grids. The closeness factor of generated AutoSynGrid cases, *RT-nestedSmallWorld* cases [51], and random cases is presented in Fig. 2.18.b. The *RT-nestedSmallWorld* cases, are generated using the algorithm presented in [51] and topology of random cases are generated totally random with eliminating the islanded cases. Moreover, the bus type assignment, generation and load setting, and transmission line capacity assignment are implemented randomly with considering some important and well-known properties of NYISO reference systems such as exponential generation capacity, lognormal line impedances and the ratio of committed and uncommitted generations. We can see that there is a significant difference between the closeness factor of AutoSynGrid cases and the two other methods, which verifies the effectiveness of our proposed algorithms on synthetic network modeling. Moreover, although the closeness factor of RT-*nestedsmallWorld* cases increases slightly with increasing network size, it achieves to its threshold equal the 0.4 in larger cases. The threshold for AutoSynGrid cases is equal to the 0.92. It should be mentioned that the closeness factor is an approximate measure to indicate how close the generated synthetic cases are to the reference system. The objective in synthetic power modelling is to generated fictitious grids with same statistical characteristics of actual power grids but with

diversified values from actual values. It is clear that a synthetic grid with closeness factor equal to 1 precisely represents the actual reference system, which may disclose sensitive information related to the actual power grid. Therefore, generating a synthetic grid with closeness factor of 1 is not the goal in synthetic grid modelling. Figures 2.18a and 2.18b show that the size of the network has a direct impact on realism of the network in two way. First, by increasing the network size it is more feasible to generate synthetic grids with high closeness factor. Second, it is more feasible to mimic the characteristics of a reference system with similar network size than a reference system with higher network size difference. Moreover, in synthetic grid modelling it is important to have different layers of information, i.e. bus types, generation settings, etc. in a synthetic grid but it is vital to generate and assign this information in a validated systematic approach. And totally random generation and assignment do not result in a acceptable test case.

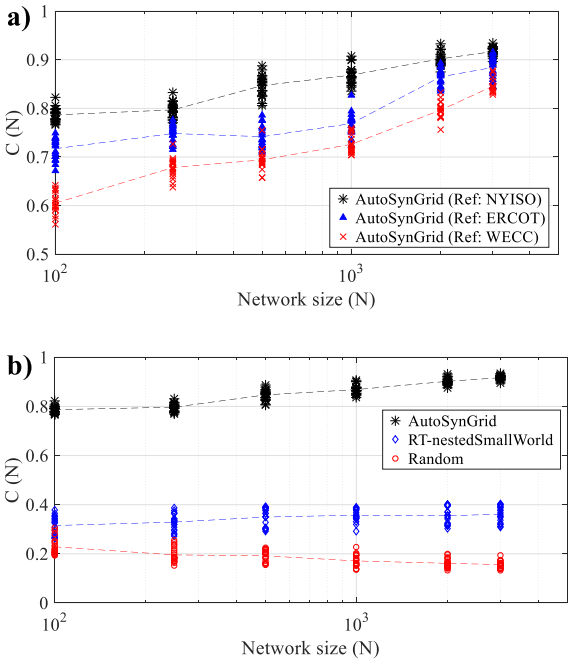

Figure 2.18 Closeness factor a) AutoSynGrids with three different reference systems. B) AutoSynGrid, RT-nestedSmallWorld, and random cases.

2.4 Summary

In this chapter, we developed two algorithms for transmission line capacity and generation cost assignment for synthetic power grids and then we combined all our proposed approaches and developed a complete framework to generate synthetic power. The AutoSynGrid toolkit is designed based on MATLAB Graphical User Interface (GUI) and it is able to build any number of synthetic cases that can be used for a variety of analysis such as Power Flow (PF) and Optimal Power Flow (OPF) studies. It allows to select several key characteristics of the generated system, such as reference system, loading level, and generation cost model. The generated cases include topology, bus type, generation and load setting, transmission line capacities and generation types and cost models. The output of the toolkit is exported in the native MATPOWER format allowing to use the MATPOWER open-source, steady-state, planning, and analysis package to further studies on the generated cases. The "syngrid" function for synthetic power grid generation is also developed as a MATLAB package and integrated in MATPOWER toolkit, which is available with MATPOWER version 7 or later. In addition, we developed a validation framework, which examines the generated synthetic cases based on the metrics introduced in the literature and some new validation metrics we have found in the realistic power grids. These metrics are categorized into topology metrics, electric parameters, state variables, interdependencies, and scaling properties. Moreover, we defined a closeness factor to measure the realism of generated synthetic cases and compare with totally random grids. It was found the closeness factor for the generated synthetics cases with all three reference systems increases with increasing the network size. It was also found that the size of the network has a direct impact on realism of the network in two way. First, by increasing the network size it is more feasible to generate synthetic grids with high closeness factor. Second, it is more feasible to mimic the characteristics of a reference system with similar network size than a reference system with higher network size difference. Moreover, in

synthetic grid modelling it is important to have different layers of information, i.e. bus types, generation settings, etc. in a synthetic grid but it is vital to generate and assign this information in a validated systematic approach. And totally random generation and assignment do not result in a acceptable test case. The summary of contribution and comparison with selected works in the literature is presented in Table 2.6.

Table 2.6 Summary of contribution and comparison with selected works in the literature

	GNLG [37]	ACTIVSg [42]	8-zone Grid [43]	TDNetGen [44]	**AutoSynGrid (proposed)**
Synthetic topology	✓	✓	✓	X	✓
Electric parameters	Synthetic	Synthetic	Actual	Actual	**Synthetic**
Network (Transmission/Distribution)	T	T	T	T&D	**T**
Optimal power flow	X	✓	✓	✓	✓
User-friendly toolkit	X	X	X	✓	✓
Selective reference system	X	✓	X	X	✓
Generation of test cases	Automatic	Manual	Manual	Automatic	**Automatic**
Number of the cases	Infinite	Limited	Limited	Limited	**Infinite**
Validation framework	X	✓	X	X	✓

3. Impact assessment framework for distributed PV generation

3.1 Motivation

In response to technical, economic and environmental developments, as well as political and social initiatives, renewable energies especially distributed solar photovoltaics (PVs), have been developing rapidly in the past decade, making solar the fastest growing renewable energy in the US [1]. Despite all promising benefits for end-user customers and distribution network operators (DNOs) to increase small-scale distributed solar photovoltaic (DPV) generation, the DPV installation could cause several negative impacts on distribution networks. The utility distribution networks are designed initially for centralized power generation and optimized for unidirectional power flow; however, the allocation of DPV systems changes the unidirectional operation of distribution networks, leading to some significant issues regarding reliability, stability and power quality. For instance, the electric generation from local PV units may exceed the feeder load, cause a reverse power flow situation, and confuse the protective relays in the network, which only sense unidirectional power flow along the radial connecting topology under normal operating conditions. The most common potential concerns caused by solar power include steady-state overvoltage, negative impacts on system losses, voltage regulating devices, protection, and voltage fluctuation [155]. Therefore, impact assessment is crucial for the deployment of these distributed energy resources. The more accurately the impact of high penetration levels of PV generation in distribution networks is assessed, the higher the level of PV generation that can be connected to the network without risking the system's operational and the technical limitations.

Motivated by the drawbacks of available studies in the literature, we propose a scalable and detailed impact assessment framework to accurately assess the impacts of DPVs on distribution networks. In this section, we perform a full year time-series analysis of DPV installations with a

novel synthetic load profile modeling and detailed models of all system components to aid utilities and policymakers on quantifying the impacts of different DPV penetration levels. To cater uncertainties in DPV installation by customers, a Monte Carlo-based technique is utilized. Solar PV installation in the distribution network is not purely random and the location and size of the installation depend on many factors. Adequate solar insolation, available rooftop and customer decision for size selection, as well as the finance budget and government incentives are the most crucial factors for rooftop PV installation. Therefore, to develop a detailed assessment approach, we perform a PV potential study to estimate actual DPV installation capacity for the buildings in the given distribution network. In addition, we define customer selection factor to mimic customer behavior for PV size selection. Moreover, a novel synthetic load modeling is proposed to generate daily load profiles for individual building types representing specific load patterns for the studied area. In addition to the Monte Carlo-based technique to study random installation, we propose a multi-object optimization approach to suggest optimal location and size of aggregated small-scale DPVs in the distribution network. The objectives of optimal size and location algorithm are minimization of the energy loss, voltage deviation, and voltage fluctuation, in addition to elimination of voltage violations and reverse power flow. This allows identifying the outcomes for two different DPV deployment policies towards possible strategies to maximize advantages and minimize the negative impacts of DPVs and may provide useful guidance for utilities and policymakers. In fact, the proposed detailed impact assessment not only provides the more precise and accurate results on hosting capacity and high PV penetration impacts, but also provides a comparative perception of DPV installation in different penetration ratios. To convey the meaning and aim of both proposed approaches, we will call the Monte Carlo-based technique as customer-based installation and optimized installation as utility-aided installation for the rest of the proposal.

3.2 Impact-assessment framework

In this section, an impact-assessment framework will be developed for DPV integration in a distributed network. Two DPV installation schemes, namely, the customer-based and the utility-aided installations, will be considered. For customer-based installation, a series of Monte Carlo experiments will be conducted to model randomly installation of DPVs in the network. Synthetic load profile modeling is proposed to generate a load profile for each customer based on building type. For utility-aided installation, an optimization model will be utilized to determine the optimal size and siting of DPVs in a distribution network subjected to network operation constraints and PV generation constraints. The impact assessment will be performed based on the distribution network operation parameters such as reverse power flow, voltage fluctuation, voltage deviation, and energy loss at different penetration ratios. Comparative study of results may provide information on distribution network planning such as recommended installation scheme, expected power quality of the network, and required network upgrades to maintain the reliability of the system. The flowchart of the developed framework is shown in Fig. 3.1.

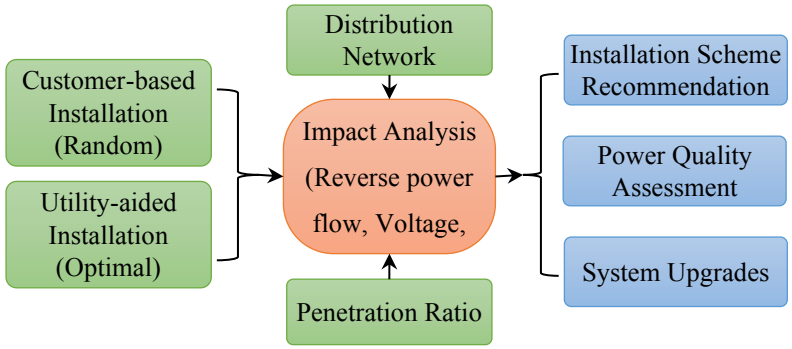

Figure 3.1 Flowchart of the developed framework for DPV impact assessment.

3.2.1 Distribution network modeling

A systematic approach has been developed to model a distribution network based on its geographic location, available public data, and the distribution network electric parameters

performing synthetic load modeling and solar insolation potential study. The synthetic load model yields yearly with hourly time-step active and reactive power demand data for each building using Geographic Information System (GIS) data and Open Energy Information (OpenEI) dataset [156] for load profiles of different load sectors (residential, commercial, and industrial). Using available solar insolation data, solar power production potential is calculated for all the buildings in the study area. Peak load, voltage level, feeder distribution, and electric parameters can be obtained from local electric power distribution utility. A flowchart showing the modeling approach is provided in Fig 3.2. A local utility network in an urban area with a summer peak load of 23,260 kW and 1,902 customers by classes of 1429 residential, 379 small commercial, and 76 large commercial/industrial is considered as the case study network. It should be noted that in this study, commercial buildings with a peak load of less than 200 kW are considered in the small commercial category. The specific parts of the distribution network modeling in the proposed framework are described in more detail below.

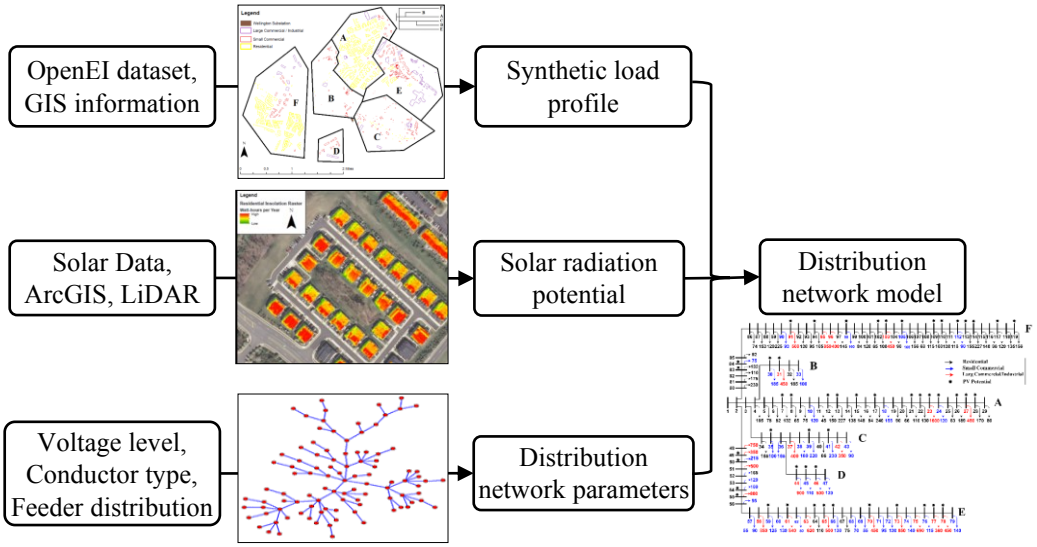

Figure 3.2 The flowchart of distribution network modeling.

Using this base map, we identified a logical alignment of distribution feeders and branch lines that could serve all of the buildings in the study area. We then divided the study area into six sub-areas representing the buildings served by each feeder. The hypothetical distribution feeder alignment and corresponding study-area sub-regions are shown in figure below.

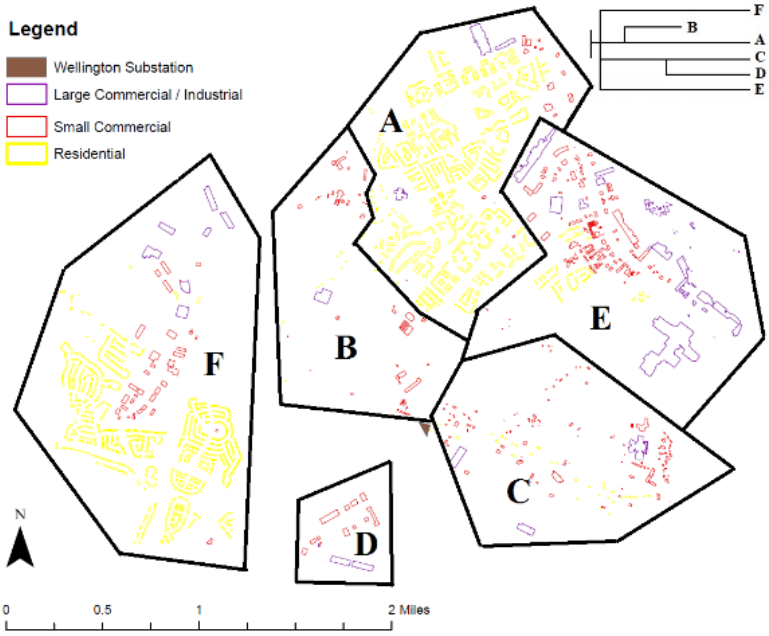

Figure 3.3 Base map of study area and sub-regions

In order to approximate the study area served by the sub-station, the geographic information systems (GIS) database layers are used to find precise number of buildings and their types. This data identified all properties and structures within the surrounding area, including information on how those properties are currently used (e.g., as an office, residence, etc.). We drew a preliminary study area boundary around the sub-station, and through an iterative process re-drew the boundary until it captured a collection of buildings around the sub-station that perfectly matched the sub-station's actual customer base. Thus, our model includes the exact same number of residential, small commercial, and large-commercial / industrial buildings served by the sub-station, all of which lie within a reasonable perimeter of the sub-station itself, many if not most of which are presumably served by the sub-station's distribution feeders. Then we determined the distribution of buildings within each sub-area by customer class, as shown in Table 3.1 below.

Table 3.1 Distribution of Study Area Buildings by Sub-Area and Customer Class

Building Type	Area A	Area B	Area C	Area D	Area E	Area F	Total
Residential	523	9	37	0	45	815	1429
Small Commercial	19	52	131	13	145	36	396
Large Comm. / Industrial	3	1	3	3	59	7	76
Totals	545	62	171	16	249	858	1901

3.2.2 Synthetic load profile modeling

Electric load profiles are often highly stochastic; influenced by many different independent variables such as environmental, cultural and social characteristic that shape individual customer's load profile in a specific geographical location. It is of fundamental importance to have a detailed and precise model of electricity consumption to perform an accurate impact assessment. In our proposed framework, types and the precise number of buildings in the study area are derived using the GIS information. We develop a synthetic load modeling to generate electricity load profiles with hourly time steps for every building holds in the given network. Numerous strategies have been developed to model residential, commercial and industrial load consumption [157]–[163]. However, most of them [157]–[162] modelled the load consumption based on real telemetry and appliance usage patterns mostly for weekly timescale which are not applicable in our study. Recently, a methodology to create transmission bus level synthetic load profiles is proposed in [163]. Authors utilize normalized template load curves and composition ratio for residential, commercial, and industrial (RCI) sectors to create hourly load profiles for a year. However, they assign yearly load profiles from a limited number of template load curves in RCI sectors without considering their load characteristics, questioning the method's application for detailed impact assessments. Open Energy Information (OpenEI) dataset [164] provides simulated sample profile data including three residential building types with low, medium and high load factors and 16

commercial building types such as small office, restaurant, primary school, etc. It contains hourly energy consumption over a year for cooling, heating, and lightning, etc. All the profiles are tagged with TMY3 members, which represent geographic locations with different meteorology. Therefore, the load profiles for a specific area can be obtained. However, these data include only one sample load profile for each building type.

The objective in this section is to generate load profiles for individual buildings based on sample load profiles provided by the OpenEI dataset for each building type. Therefore, by assigning the generated load profile for each building connected to the bus, we can calculate the bus level load profiles. Our studies show that the residential and commercial load profiles represent daily, weekly, monthly and seasonal patterns. However, the load profiles for industrial sector obtained from Oak Ridge National Laboratory [165] exhibit less variation compared to the other load types with higher load factor. Figure 3.4 shows the daily and weekly behavior of a residential and three commercial load profiles. The load profiles share similar daily trend of an increase in load during the daytime and a decrease in load during the evening but have different peak loads and daily energy-use patterns. In addition, the weekly trend in the load profiles shows a notable difference between weekdays and weekends energy-use patterns.

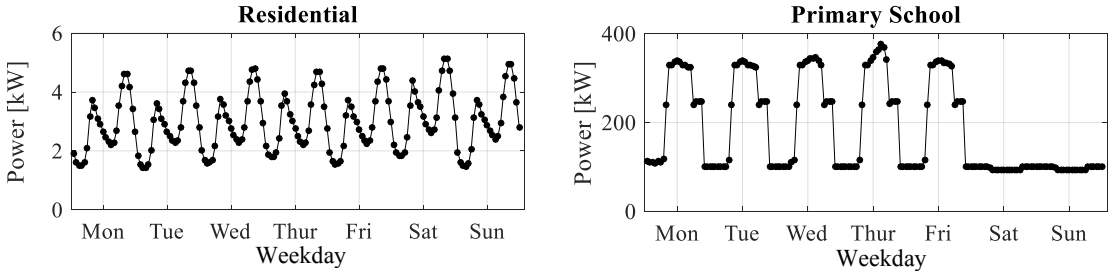

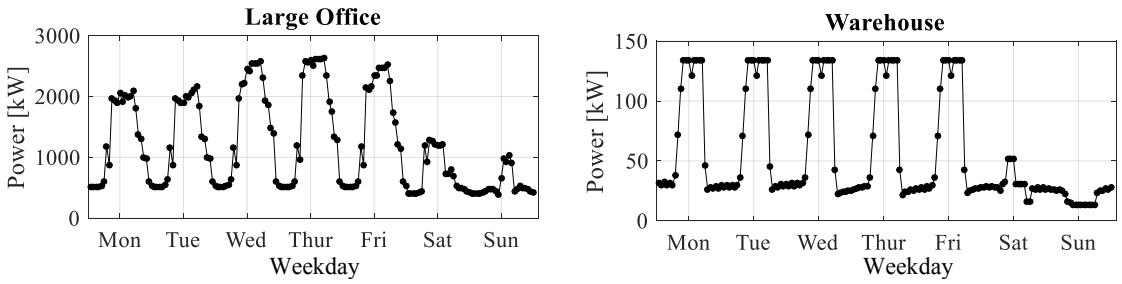

Figure 3.4 Daily and weekly behaviors in residential and commercial load profiles

Figure 3.5 illustrates empirical probability density function (PDF) and fitted distribution of peak loads in the weekend and workdays for different load types in the first month of the year. The goodness of this fitting is measured with Kullback-Leibler divergence (D_{KL}) where smaller values for the divergence represents a more accurate fit for the imperial PDF if variables [153]. It is worthy to note that for the D_{KL}, smaller values represent a more accurate fit for the empirical PDF of data. The variation in peak loads and notable difference in weekend and workdays load patterns, as well as monthly patterns, are used to develop a new algorithm to generate synthetic load profiles. Generating load profiles with utilizing monthly pattern instead of seasonal pattern guarantees to capture monthly variations as well as seasonal patterns.

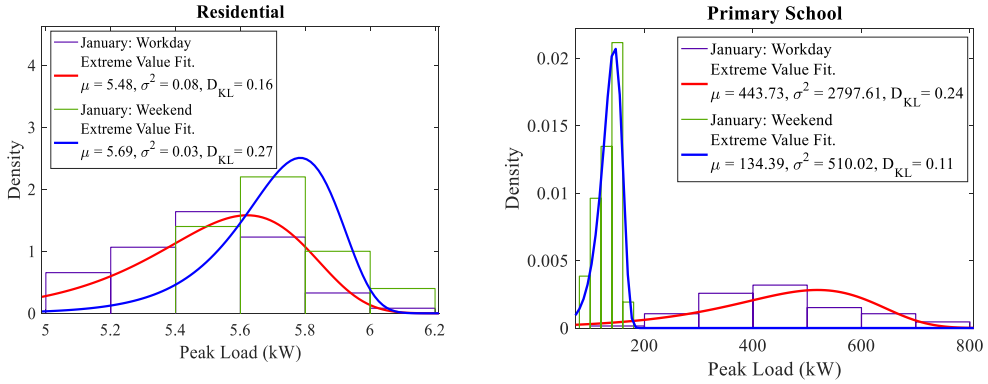

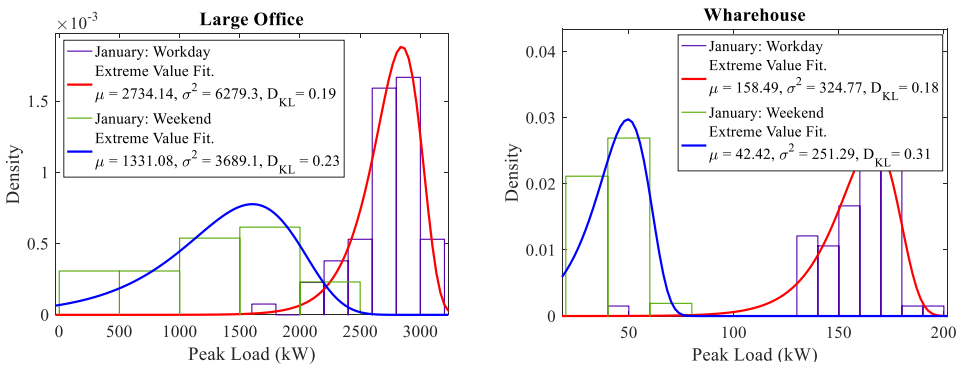

Figure 3.5 Imperial PDF and distribution fit of workdays and weekends in residential and commercial buildings

To generate synthetic load profiles based on sample load profiles, first, the yearly load profiles in the OpenEI dataset for each building type are categorized according to the corresponding month and weekday. It generates 24 categories including daily load profile templates for each building type base on month and workday. These daily load profile templates are used to generate yearly synthetic load profiles for individual buildings. For each day, based on the corresponding building type, weekday, and month, one of the multiple load templates in the category is randomly assigned. Next, the assigned load profile is scaled using the fitted distributions, which are extracted for all the building types. Generated synthetic load profile for a residential building as well as the original residential load profile is presented in Fig. 3.6. It can be seen that both synthetic and original load profiles experience their maximum during the summer and the minimums during the spring. In addition, the range exhibited in the synthetic load profile is similar to the original one where warmer seasons exhibit ranges larger than the colder seasons. Note that since the objective of synthetic load profile modeling e is to generate load patterns with similar characteristics and not a replication of the original load profiles, it is not necessary for synthetic load profiles to exactly match with the original ones. However, sufficient metrics should be utilized to validate the accuracy of method to generate synthetic load profiles.

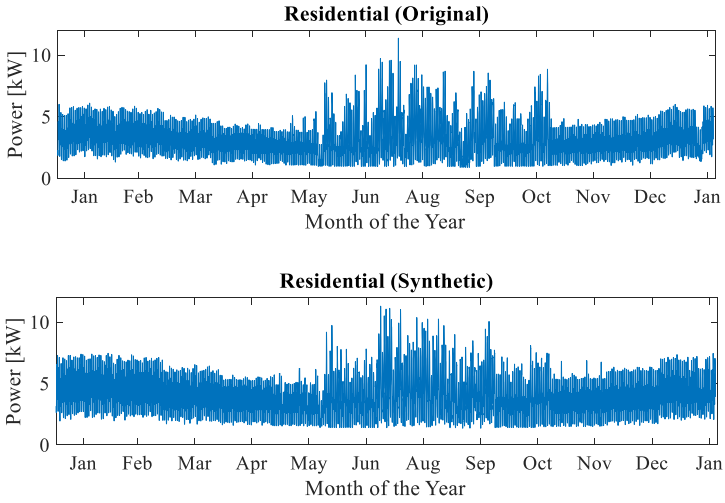

Figure 3.6 The original and synthetic load profile of a residential building.

One of the metrics to validate the accuracy of synthetic load modeling is major frequencies [163]. To compare periodic characteristics of generated synthetic load profiles with original load profiles, fast Fourier transformation (FFT) is presented in Fig. 3.7 for a residential and three commercial buildings. For all the building types, the synthetic load profiles and original ones both peak at the same major frequencies. Major frequencies include those of daily, weekly, and twelve-hour periods, which validate that these patterns are presented in the simulated data. For instance, the original residential load profile has major frequencies in daily and twelve-hour period and the synthetic load profile peaks at those frequencies with slightly different magnitude.

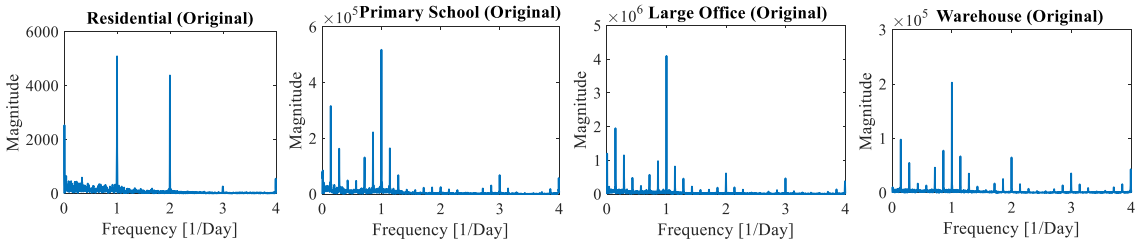

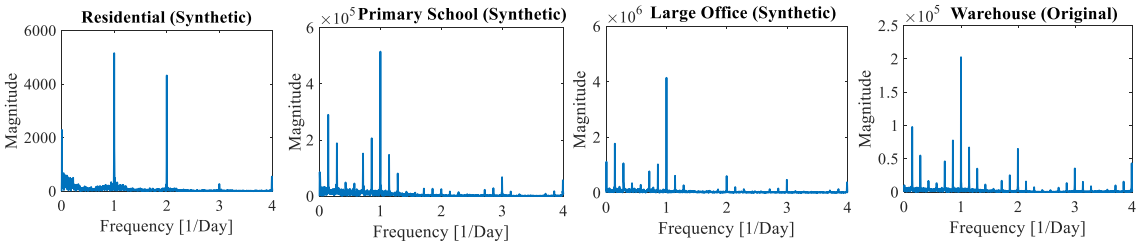

Figure 3.7 Frequency response of original and synthetic load profiles.

Occupied bandwidth (OBW) is another metric to validate the accuracy of the proposed method [166]. It is calculated using the power spectrum of the given time series signal. The power spectrum $S_{xx}(f)$ of a time series $x(t)$ describes the distribution of frequency components composing that signal. The power spectral density (PSD) spectral density describes how the power of a signal or a time series is distributed with frequency. The spectrum of physical processes often contains essential information about the nature of them. One particular information that can be useful for our purpose is the OBW of the signal. The mathematical representation of PSD can be expressed by (31):

$$S_{xx}(\omega) = |\hat{x}(\omega)|^2 = \int_{-\infty}^{\infty} R_{xx}(\tau) e^{-j\omega\tau} d\tau = \hat{R}_{xx}(\omega) \tag{3.1}$$

where $\hat{x}(\omega)$ is Fourier transform of the signal and $R_{xx}(\tau)$ is the autocorrelation function which describes the correlation between values of the process at different times, as a function of time lag. In this study, the 99% OBW is examined for both synthetic and original load profiles. The OBW is the bandwidth containing 99% of the total integrated power in the spectrum. Figure 3.8 shows PSD and the 99% OBW of original and synthetic load profiles of a residential and three different commercial buildings. Note that, to exclude zero frequency in 99% OBW calculation, we subtract the mean value of time series load profiles. For all the generated synthetic load profiles, the 99% OBW is approximately equal to the original one, validating the proposed method for generating synthetic load profiles.

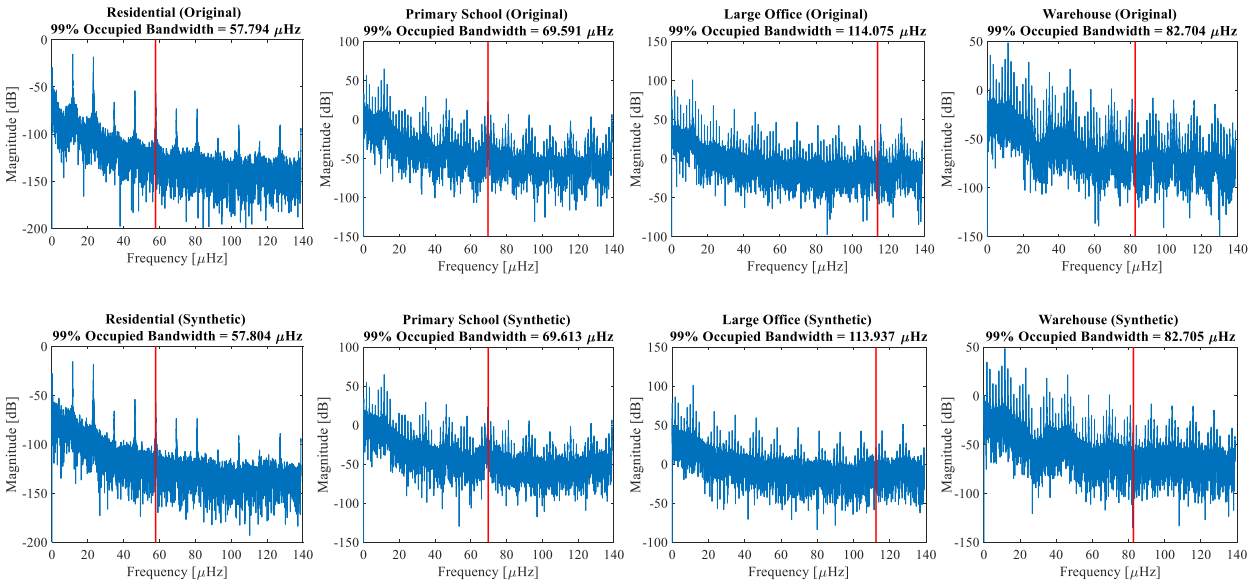

Figure 3.8 PSD and 99% OBW of synthetic and original load profiles for different building types.

The GIS analysis provides precise information on the number and type of the buildings connected to the bus in the distribution network. Once the load profiles for each building are generated, the bus level load profiles will be calculated by aggregating the load profiles of the buildings connected to the bus. At the final step, the aggregated load profiles are scaled so the generated total peak load of the grid matches the actual peak load provided by the local electricity utility.

3.2.3 Solar insolation potential

Solar insolation potential is determined using light detection and ranging (LiDAR) evaluation source data. It starts with the geographical analysis of the study area by the GIS module that evaluates rooftops and their capacities for PV installations. LiDAR data is used as an input to the ArcGIS software to generate the Digital Evaluation Model (DEM). By applying spatial analyst tools (solar radiation, slope, and aspect), the GIS module generates the average solar insolation of all the building rooftops as an output. It should be mentioned that simply aggregating the average insolation for entire buildings in the study area would underestimate the potential of PV generation

potential, as in the real world, PV systems are only placed in suitable locations that will receive adequate insolation to maximize their cost-effectiveness. Therefore, a minimum average solar insolation is set to exclude low solar insolation buildings. For instance, Fig. 3.9 shows a grouping of residential apartments in the study area, sorted by the percentage of rooftop area that receives above-average annual solar insolation. Only the buildings in red – each of which has a largely unshaded flat or south-facing rooftop – were designated as solar-ready in our model.

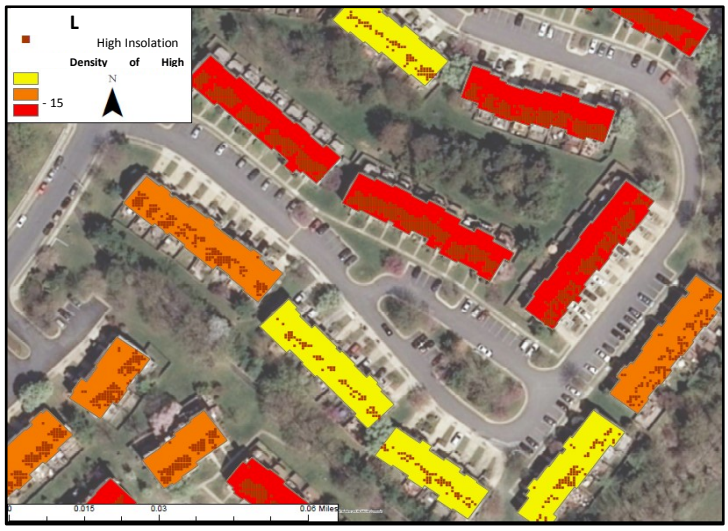

Figure 3.9 Solar insolation density in study area buildings

To estimate the potential capacity of the distribution network to install DPVs, it is assumed that DPV could only be installed on rooftops of the buildings that had high concentrations of the rooftop surface area receiving above-average annual solar insolation. We will call these buildings as solar-ready buildings for the rest of this study. This implies that 510 of the residential buildings (36%), 119 of the small commercial buildings (30%), and 26 of the large commercial and industrial buildings (34%) would become eligible for PV installations. Aggregating the potential PV generation from every solar-ready building, we may determine the total solar power in the studied substation area. It is found that the total potential PV generated power of 16,280 kW is equal to

70% of the total area peak load. The potential annual energy production from PV generation is 21,137 MWh, equal to 18% of the area's annual energy demand of 114,758 MWh. Considering the geographic location of solar-ready buildings, we are able to allocate them to a number of buses in the developed distribution network which are potentially ready for a DPV installation. Consequently, 50 solar ready buses will be considered in the distribution network. Maximum capacity to DPV installation at each bus is derived based on the number of solar-ready buildings connected to the bus and their potential DPV capacity. More details on the solar insolation potential can be found in [167].

3.3 Problem formulation and methodology of analyses

Two main assessments are considered in the proposed framework to examine the impacts of DPV installation on the distribution network. First, a stochastic Monte Caro-based approach is performed to model customer-based installations and mimic customer decision on DPV installation for different DPV penetration ratios. Then, to model utility-aided installation, an optimization problem is solved to determine the optimal placement and sizing of aggregated PV systems that minimize power loss, voltage deviation, and voltage fluctuation. The objective function is subject to distributed PV constraints and operational constraints of a distribution network, such as avoiding reverse power flow in the network. In this study, the DPV penetration ratio is defined based on substation peak load and is as follows

$$\gamma(\%) = \frac{\sum_{i=1}^{N} {P_{PV}}_i^{max}}{\max\left(\sum_{t=1}^{T} P_{Load_t}\right)} * 100 \tag{3.2}$$

where P_{PV} and P_{Load} are PV panel output power (kW) and electrical load demand (kW), respectively. Total real energy loss of radial distribution system can be calculated as [168]

$$E_{loss} = \sum_{t=1}^{T} \sum_{l=1}^{L} |i_L^t|^2 R_L \tag{3.3}$$

where i_L^t is the current flowing through line L at time t and R_L is resistance of line L. To examine the voltage quality across the network we utilize two metrics, voltage deviation (V_D) and voltage fluctuation (V_F) as follow.

$$V_D = \frac{1}{T \times N} \sum_{t=1}^{T} \sum_{i=1}^{N} |V_i^t - 1| \tag{3.4}$$

$$V_F = \sqrt{\frac{1}{T \times N} \sum_{t=1}^{T} \sum_{i=1}^{N} (V_i^t - \bar{V})^2} \tag{3.5}$$

where V_i^t indicates the voltage of bus i at time t and $\bar{V} = \frac{1}{TN} \sum_{t=1}^{T} \sum_{i=1}^{N} V_i^t$ is average voltage in the network.

3.3.1 Customer behavior modeling

The customer-based integration modeling consists of random siting and sizing of DPVs, which simulate customer decisions on DPV installation and size selection. With each selected set of location and size of DPVs, the hourly profile of PV generations over a year will be calculated accordingly and fed into the AC power flow model to determine the system state variables such as the bus voltage magnitude and the phase angle and calculate the energy loss, voltage deviation and reverse power flow. A set of Monte Carlo experiments designed to evaluate the impacts of randomized PV installation on the operation of the distribution network. The flow chart of the simulations is depicted in Fig. 3.10. For each number of solar ready buses (S), N_s^{max} random installations are generated. In selection of locations for DPV installation, we will select locations from the predefined solar-ready buses in the system. This step generates a binary decision vector $= [0/1, \ldots, 0/1]_{1\times 50}$, where 1 represents DPV installation and 0 none-PV installation on the corresponding solar ready bus, with the constraint of $1^T X = S$. PV size selection factor (β) uses the uniform distribution, $\beta \sim \text{Uniform}[\beta_{\min}, 1]$, where $\beta_{\min} \geq 0$ is called the customer decision

factor (CDF) denoting the willingness of the customer to install the largest possible PV generation on the site. After random selecting of locations and PV size selection factor, PV installation sizes for all the buses will be determined as ($Z_i = X_i * y_i * \beta_i$) where X_i is binary decision vector, y_i is PV generation potential vector, and β_i is the size selection vector for experiment *i*. Furthermore, for PV output calculation we use the solar insolation data and the size of the corresponding PV installation on the site as the Eq.(12) introduced in [169].

$$P_{PV} = \frac{\frac{V_{OC}}{n_{MPP}\,KT/q} - \ln\left(\frac{V_{OC}}{n_{MPP}\,KT/q} + 0.72\right)}{1 + \frac{V_{OC}}{n_{MPP}\,KT/q}}. \left(1 - \frac{R_s}{V_{OC}/I_{SC}}\right). I_{SC}\left(\frac{G}{G_0}\right)^{\sigma}. \frac{V_{OC}}{1+\rho \ln\frac{G_0}{G}}. \left(\frac{T_0}{T}\right)^{\tau} \tag{3.6}$$

where n_{MPP} is the ideality factor at the maximum power point, *K* is the Boltzmann constant, *T* is the PV module temperature, *q* is the magnitude of the electron charge. R_s is the series resistance, σ is the factor responsible for all the nonlinear effects that the photocurrent depends on, ρ is a PV module technology specific-related dimensionless coefficient, and τ is the factor considering all the nonlinear temperature–voltage effects. At the end, after running the daily time-series AC power flow analysis utilizing MATPOWER open source toolkit, the solution results (i.e., voltage, power loss, and reverse power flow) will be stored for the next-step impact assessments.

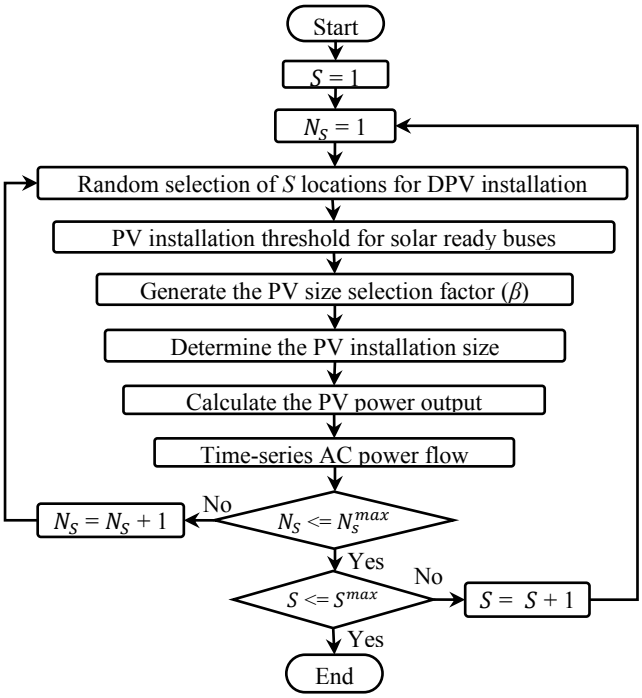

Figure 3.10 Flow chart of the simulation procedure of Monte Carlo experiments for customer behavior modeling.

In this study, the local solar irradiance profiles have been obtained from [170]. It is worth noting that the customer decision factor (CDF) is set to mimic the customer's decision on the DPV size selection. This factor could be related to various parameters such as the finance budget, incentives, and economics. With CDF we wish to model the willingness or tendency of customers to install high DPV sizes. A larger value of CDF implies a higher possibility for the customer to utilize all the potential rooftop area to install the largest possible DPV.

3.3.2 Optimization problem

The multi-objective function can be formulated as follows; the minimum of the objective functions implies the best sitting and sizing of DPV for minimizing energy loss and enhancing loadability and voltage profiles.

$$\min_{\mathcal{L}_{PV}, P_{PV}^{max}} f = \alpha_1 * E_{loss} + \alpha_2 * V_D + \alpha_3 * V_F \tag{3.7}$$

Subject to:

$$f(P_L, P_{PV}, V|Y_{bus}) = 0 \tag{3.8}$$

$$i = h(V|Y_{bus}) \tag{3.9}$$

$$P_{PV}(t) = g\left(P_{PV}^{max}, I(t)\right) \tag{3.10}$$

$$0 \leq P_i^{max} \leq \widetilde{P_{PV,i}^{max}} \tag{3.11}$$

$$1^T P_{PV}^{max} \leq \gamma . P_{sub}^{max} \tag{3.12}$$

$$P_{ij}^t \geq 0 \quad \forall\, i < j \tag{3.13}$$

$$0.95 \leq |V_i| \leq 1.05 \tag{3.14}$$

where $\mathcal{L}_{PV} = [\ell_1, \ell_2, \ldots, \ell_n]^T$ $\ell_i \in \{0,1\}$ is DPV location vector and α_{1-3} are the chosen weighting factors for weighted-sum multi-objective optimization. Higher minimization priority is assigned a larger weighting coefficient. $P_{PV}^{max} = [P_1^{PV}, P_2^{PV}, \ldots, P_n^{PV}]$ is DPV maximum capacity vector, Y_{bus} is network admittance matrix, i is vector of bus injected current, V is bus voltage vector, $I(t)$ is solar irradiance at time *t*, $\widetilde{P_{PV,i}^{max}}$ is PV installation limit for bus *i* derived from solar data analysis, and P_{ij}^t is active power flowing from bus *i* to *j* at time *t*, *L* is the number of lines, *n* is the total number of buses, and P_{sub}^{max} is defined as substation peak load. Note that Eqs. (38) and (39) are network constraints enforced by AC power flow including power balance and network operation constraints, respectively. And Eqs. (40-42) are installation constraints of DPV.

3.3.3 Improved Particle Swarm Optimization (IPSO)

Particle swarm optimization (PSO) algorithm is a heuristic optimization technique first developed in 1995 by Kenndy and Eberhart [10]. It solves the problem by generating random called a swarm, consisting of individuals as particles. Each particle, representing a potential

solution of the optimization problem, flies through an *N*-dimensional search space at a random velocity and updates its position based on its own best exploration, best swarm global experience, and its previous velocity vector according to the following equations:

$$\begin{cases} v_i^{k+1} = \kappa v_i^k + c_1 r_1 \left(\text{pbest}_\text{i}^\text{k} - x_i^k\right) + c_2 r_2 \left(\text{gbest}^k - x_i^k\right) \\ x_i^{k+1} = x_i^k + v_i^{k+1} \end{cases} \tag{3.15}$$

where κ is inertia weight, c_1 and c_2 are acceleration constants, r_1 and r_2 are two random numbers in the range of [0, 1], $\text{pbest}_\text{i}^\text{k}$ is the best position particle achieved based on its own experience, and gbest^k is the best particle position based on overall experience swarm. In order to improve the efficiency and accuracy, a linearly decreasing inertia weight from maximum κ_{max} value to minimum κ_{min} is applied to update the inertia weight [171].

$$\kappa^k = \kappa_{max} - \frac{\kappa_{max} - \kappa_{min}}{k_{max}} . k \tag{3.16}$$

where κ_{max} and κ_{min} are the initial and final inertia weights, and k_{max} is the maximum iteration number.

3.4 Simulation results and discussion

The proposed impact assessment framework including customer-based random installation and utility-aided installation is applied to the given distribution network with annual simulation and hourly based resolution in order to examine the impacts of DPVs on the distribution network in term of reverse power flow, voltage deviation and fluctuation and energy loss. Then the simulation results of utility-aided versus customer-bases installations are presented to compare their impacts on the distribution network operations. To generate random DPV installation samples, customer decision factor is set to ($\beta_{\text{min}} = 0.8$), so that the size selection factor (β) is a uniform random value between 0.8 and 1.0. This is due to the customers' tendency to cover as

much of their local load as possible with PV generated power plus DNO preference for higher PV penetration into the grid. In addition, to simulate a sufficient number of Monte Carlo experiments to drive definitive conclusions, the N_s^{max} is set to 60. In the utility-based installation model, a multi-objective optimization including minimum energy loss, voltage deviation, and voltage fluctuation is executed. Figure 3.11 shows the Pareto-optimal front for different penetration ratios (γ). For higher penetration ratio the feasible operation reign is limited by overvoltage and reverse power flow constraints; therefore, the distribution of Pareto-optimal set tends to be close to each other. This also means that there are few cases that have no voltage violation and reverse power flow at higher penetration ratios. Therefore, it is important to understand how to deploy DPVs so large penetration ratios can be achieved without voltage violation and reverse power flow. It is found that for penetration ratios higher than 50%, the voltage rise and reverse power flow is inevitable. Therefore, the optimization algorithm is not able to find an optimal solution. To extract the best compromise solution, fuzzy based mechanism [172] is imposed to select one solution for each penetration ratio and compare with the customer-based installation. The best compromise solutions for different penetration ratios, ranging from 5% to 50% with 5% step is summarized in Table 3.2.

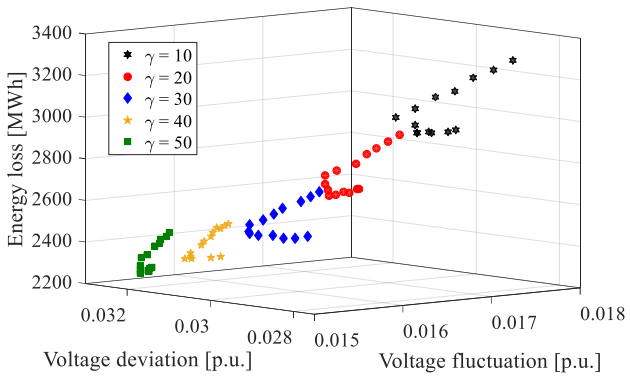

Figure 3.11 Pareto-optimal fronts of multi-objective optimization for different penetration ratios.

Table 3.2 Best compromise solutions for different penetration ratios

Penetration ratio [%]	Energy loss [MWh]	Voltage deviation [p.u.]	Voltage fluctuation [p.u.]
5	3130.21	0.02911	0.01754
10	2947.33	0.02914	0.01693
15	2810.49	0.02924	0.01650
20	2673.52	0.02946	0.01609
25	2589.95	0.02978	0.01580
30	2494.20	0.03015	0.01551
35	2438.23	0.03050	0.01536
40	2366.88	0.03087	0.01519
45	2322.51	0.03141	0.01516
50	2277.28	0.03192	0.01511

3.4.1 Reverse power flow

Since several protection devices work regarding the direction of power flow, reverse power flow could lead protection devices to operate improperly. Besides, when the power flow is

inverted, the voltage at the end is higher than the voltage at the beginning. It will imply a shift in controlling and operating the network. Total reverse power flow experienced by feeders in a radial distribution network can be calculated as:

$$F_r^{tot} = \sum_{t=1}^{T} \sum_{l=1}^{L} F_{r,l}^{t} \tag{3.17}$$

where $F_{r,l}^{t}$ denotes the power flow of line l that flows at the reverse direction (i.e., feeding back toward the substation) at time *t*. The utility-based installation finds the optimal size and location of DPVs without having reverse power flow; however, for the customer-based installation reverse power flow is expected. Figure 3.12 presents the total reverse power flow F_r^{tot} of customer-based installations in the given distribution network with the average F_r^{tot} depicted as a red solid line. Two color codes are considered for monitoring the voltage issues in the simulated customer-based installation. The "*Maximum voltage"* in Fig. 3.12.a indicates the maximum voltage that the specific installation case experiences in the whole period of study while the "*Overvoltage*" in Fig. 3.12.b represents the percent of the total overvoltage incidences happens in the case. It can be observed from figures 3.12a and 3.12b that when the penetration ratio increases, the number of cases that have reverse power flow increases as well. However, the increasing trend does not grow linearly. That is, when the penetration ratio is small, i.e. $\gamma < 30\%$, there is not a considerable reverse power flow in random installations. But after a particular penetration ratio, e.g. $\gamma = 30\%$ in our simulated system, a significant rise in the number of cases with reverse power flow issues will appear, and more cases will have large magnitudes of F_r^{tot}. For higher penetration ratios started from 45%, we can see that the network could experience even worse scenarios in case of reverse power flow issues. Therefore, it is vital to study the critical point at every distribution network to avoid abruptly increasing reverse power flow. In addition, it is observed that the overvoltage has a strong correlation with reverse power flow. The higher reverse power flows in the network can

induce severe overvoltage in the network. It should be mentioned that due to non-uniform distribution of loads in the distribution network, small amount of reverse power flow can get canceled out with upstream load with no adverse impact; however, higher reverse power flows will affect the voltage regulators, protection relay operation or will cause back-feeding at the circuit head. Note that the distribution network we studies has limited tolerance for operating normally with reverse power flows as reported in [173]. Therefore, the utility can specify a safety threshold for DPV installation using our propose impact assessment framework. When the penetration ratio of DPV installation grows beyond this threshold, mitigation actions such as equipment upgrades or utility-aided installation of DPVs will become necessary to manage the reverse power flow issues. However, using our proposed utility-aided installation, system will not need to system upgrades until 50% of penetration ratio. The average total reverse power flow of the given distribution network at each PV penetration level can be estimated by a 4th-degree polynomial:

$$F_r^{tot} = 0.003 * \gamma^4 - 0.30 * \gamma^3 + 8.25 * \gamma^2 - 75.71 * \gamma + 0.18 \quad (3.18)$$

This can help DNOs to predict possible reverse power flow in their network in different PV penetration levels.

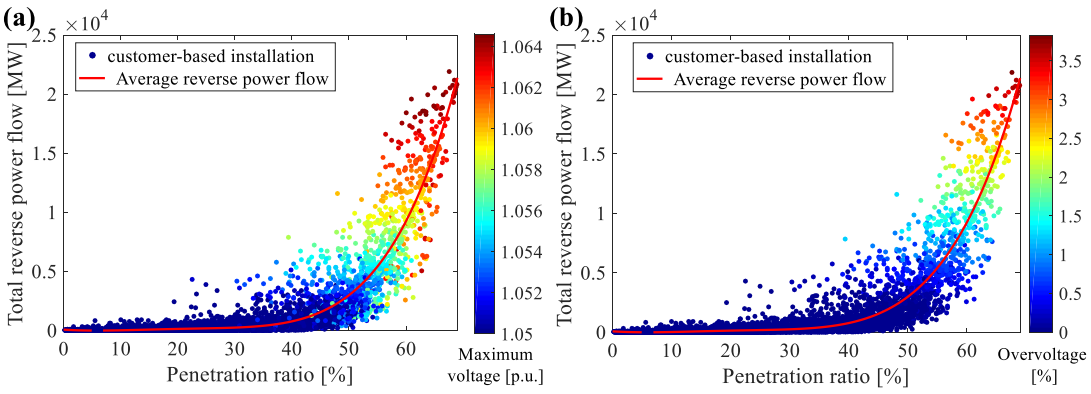

Figure 3.12 Total reverse power flow of customer-based installations with β_min=0.8.

To examine the impacts of customer decisions on reverse power flow, different CDFs have been considered to see the experienced reverse power flows in the given network. Figure 3.13 shows the probability of reverse power flow for different penetration ratios with different CDFs. It is found that for higher CDFs starting from $\beta_{\min}$=0.5 there is not a significant difference in the probability of reverse power flow incidence. Considering the fact that high CDFs are more possible in real life customer behavior, utilities could have a clear estimation of the probability of reverse power flow incidence to set a threshold to control DPV installations.

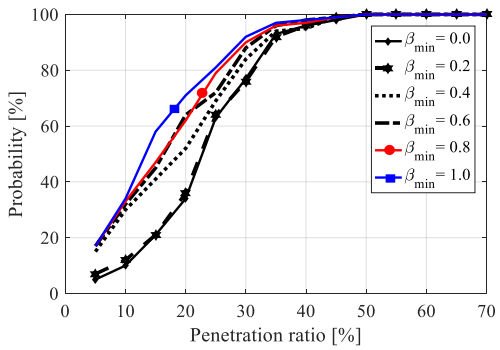

Figure 3.13 Probability of reverse power flow versus penetration ratio.

3.4.2 Voltage deviation

The results for voltage deviation across the whole distribution network obtained from both utility-aided and customer-based installations are presented in Figure 3.14. For customer-based

installations, the polynomial function for estimation of voltage deviation with respect to penetration ratio is found as:

$$V_D = -6.5 * 10^{-9} * \gamma^3 + 1.1 * 10^{-6} * \gamma^2 - 2.3 * 10^{-5} * \gamma + 0.029 \quad (3.19)$$

For both utility-aided installation and the customer-based installations, the increasing of the DPV penetration aggravates the voltage deviation. Even thou at lower penetration ratios utility-aided installation can maintain the original voltage deviation, starting from 15% of penetration ratio the voltage deviation will increase for both utility-aided and customer-based installation. In addition, the maximum voltages indicated in Fig 3.14.a shows that for customer-based installation there is no voltage violation for penetration ratios less than 30%. However, for penetration ratios beyond 30%, we can see cases with overvoltage problems. Therefore, a safe range of penetration ratio can be suggested for freely customer-based installation without voltage violation. It can be concluded that increasing the installation of DPVs in the network has negative impact on voltage deviation. Increasing the DPV installation increases the voltage deviation. However, by optimal installation at lower penetration ratios i.e. <15%, we can control the increase in voltage deviation.

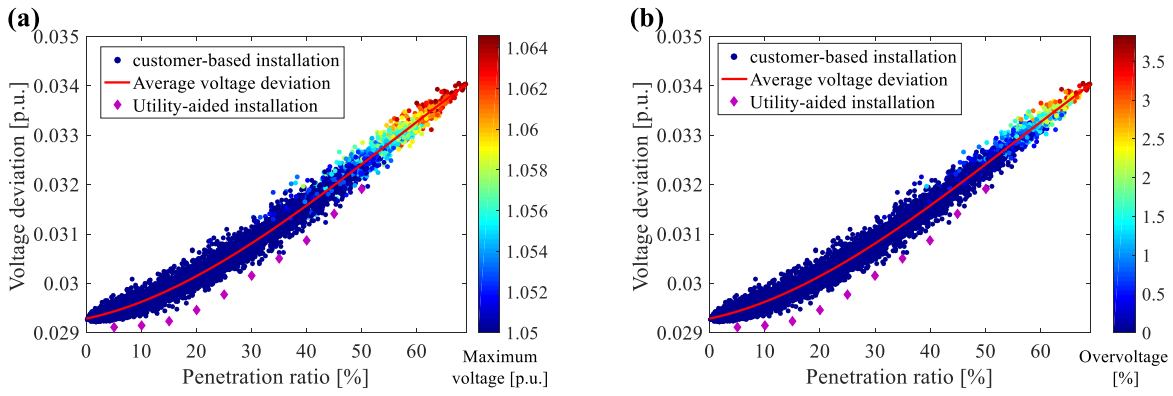

Figure 3.14 Voltage deviations of both customer-based and utility-based installations for different penetration ratios

3.4.3 Voltage fluctuation

The results for voltage fluctuation across the whole distribution network obtained from both customer-based and utility-aide installations are presented in Figure 3.15. For customer-based installations the polynomial function to estimate voltage fluctuation for different penetration ratios is derived as:

$$V_F = 8.6 * 10^{-7} * \gamma^2 - 1.1 * 10^{-4} * \gamma + 0.018 \quad (3.20)$$

Figure 3.15 shows that increasing the penetration ratio improves the voltage fluctuation across the network in the hourly based simulation; however, voltage fluctuation tends to grow at higher penetration ratios starting from 50% pf penetration level. It should be mentioned that the time-step resolution of the data and simulation varies based on the type of analysis performed and the distributed energy resource studied. Generally, for energy impact analysis and steady-state overvoltage studies an hourly resolution is recommended; however, for study of the impacts of fast variations in PV generation resulting from cloud shadows the best time-step to capture is seconds to minutes [174]. An increasing trend is expected for voltage fluctuation in high resolution (seconds) analysis for higher penetration of DPV due to cloud shadows. Although our proposed framework is not limited by data resolution and is expandable for high-resolution studies, in our study due to the available input data such as hourly load profiles and solar insolation for the given distribution network, we studied voltage fluctuation as well as energy loss and voltage deviation in hourly time step. In addition, even though the hourly simulation may not capture the high fluctuations caused by cloud shadows, it is valid for our study and utility-aided installation since the aim is to minimize all the objective functions including voltage fluctuation regardless of data resolution.

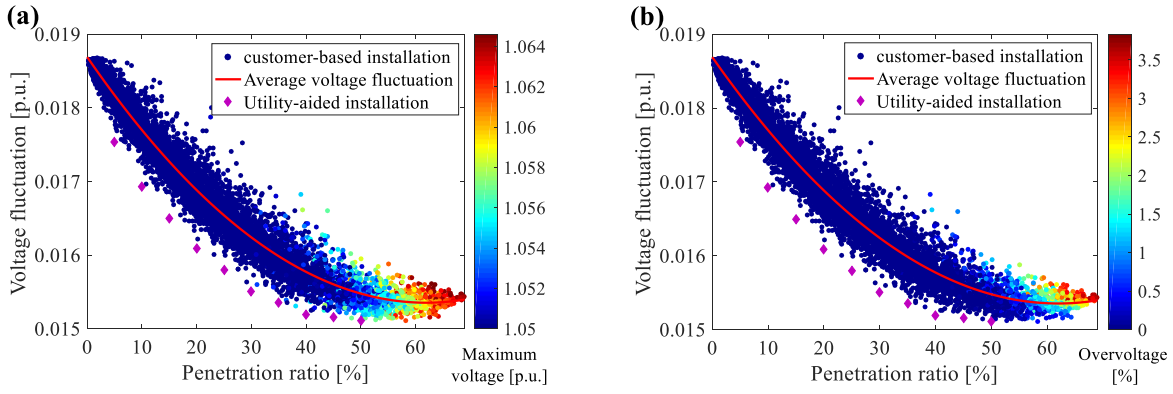

Figure 3.15 Voltage fluctuations of both customer-based and utility-based installations for different penetration ratios

To compare the utility-aided installation with customer-based installation, we define metrics to evaluate the improvement of utility-aided installation in comparison with customer-based installations. The percent of optimized voltage deviation and fluctuation improvement is defined as:

$$\Delta V_D = \left(V_D^{rand} - V_D^{opt}\right)/V_D^{rand} \tag{3.21}$$

$$\Delta V_F = \left(V_F^{rand} - V_F^{opt}\right)/V_F^{rand} \tag{3.22}$$

This metrics could provide a clear insight for utilities and policymakers to see if optimization of aggregated DPV installation is worthy or not. Figure 3.16 depicts the percent of optimized voltage deviation and fluctuation improvement using the box plot method. For the given distribution network, the maximum voltage deviation improvement that is possible by optimization is 3.2% at 20% of penetration level. This is 7.6% for voltage fluctuation improvement at 20% of penetration ratio. By the results presented in Fig. 3.16, utility based on its desired minimum improvement in voltage deviation and fluctuation could implement optimal installation of DPVs at the specified range of penetration ratio. For instance, for the desired voltage deviation improvement more than 1%, the utility should implement optimal installation on DPVs at penetration ratios of 15-40%.

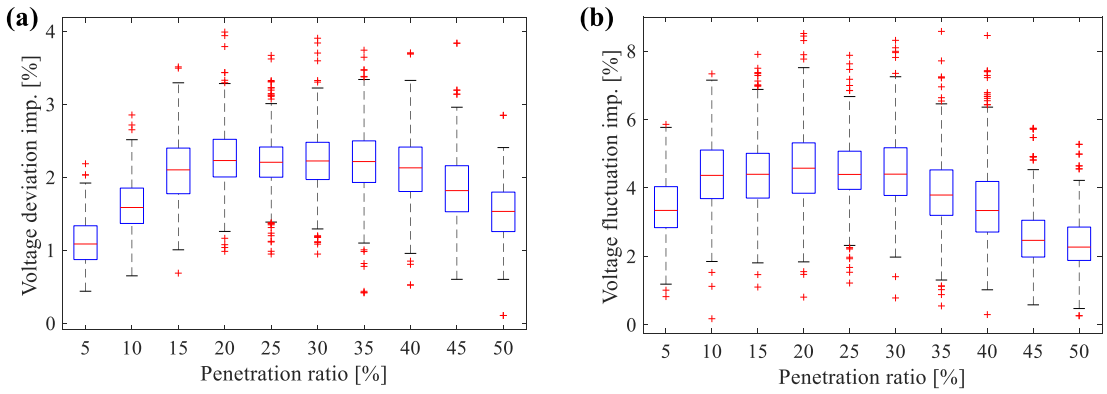

Figure 3.16 Percent of improvements in utility-aided installation for voltage deviation and voltage fluctuation.

3.4.4 Voltage violation

Figure 3.17 shows the probability of voltage violation for each bus in case of overvoltage problems for customer-based installation. Feeders B and C show zero possibility for voltage violation; however, for feeders A and E, there is 1% probability of overvoltage for specific buses. On the other hand, feeder F has a higher probability for overvoltage problems. This can be studied by considering the energy use pattern in the feeder F. Although feeder F includes both residential and commercial buildings, most of the commercial building in the feeder such as restaurants, small hotel, and mid-rise apartments share similar energy-use patterns with residential buildings. Therefore, feeder F can be considered as a residential feeder. Unlike the general commercial energy-use pattern, which has a good correlation with typical PV power profile, residential energy-use pattern presents a peak value during the nighttime when there is a small or no PV generation resulting in surplus PV generation at noon and initiating reverse power flow and voltage rise. The most important information to be extracted from Fig. 3.17 is the necessity of equipment updates for feeder F to prevent voltage violations in the distribution network.

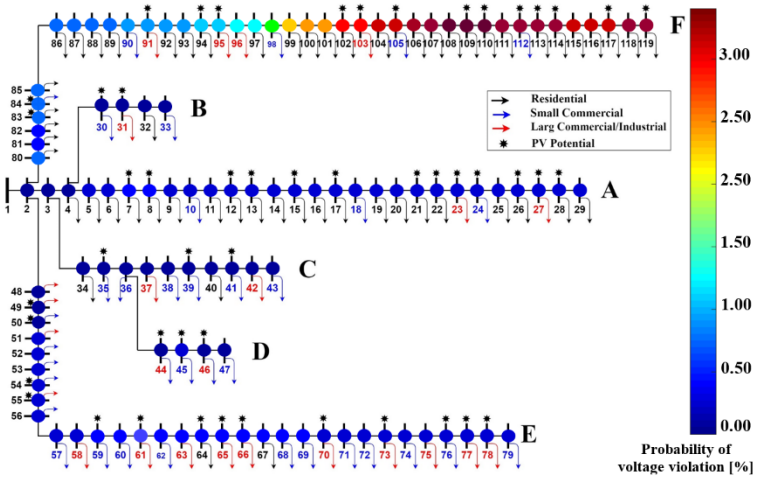

Figure 3.17 Probability of voltage violation in customer-based installation.

3.4.5 Energy loss

Figure 3.18 shows the total energy loss of customer-based installations in comparison with utility-aided installations. For customer-based installations, the polynomial function to estimate the average total energy loss with respect to penetration ratio is as follows:

$$E_{loss} = 0.15 * \gamma^2 - 28.86 * \gamma + 3423.12 \tag{3.23}$$

It can be seen that by increasing the penetration ratio of DPVs, total energy loss decreases. It is generally accepted that increasing penetration ratio of DPVs may increase total energy loss in the distribution network for several reasons such as high feeder loadings and lack of local reactive power [155]. However, at the given distribution network due to the limitation on maximum DPV penetration forced by available rooftop area for PV installation and solar insolation, penetration ratio does not reach to the critical penetration level. Moreover, it is found that there is a considerable gap between total energy losses of utility-aided and customer-based installation of DPVs in the given distribution network, particularly at moderate penetration ratios.

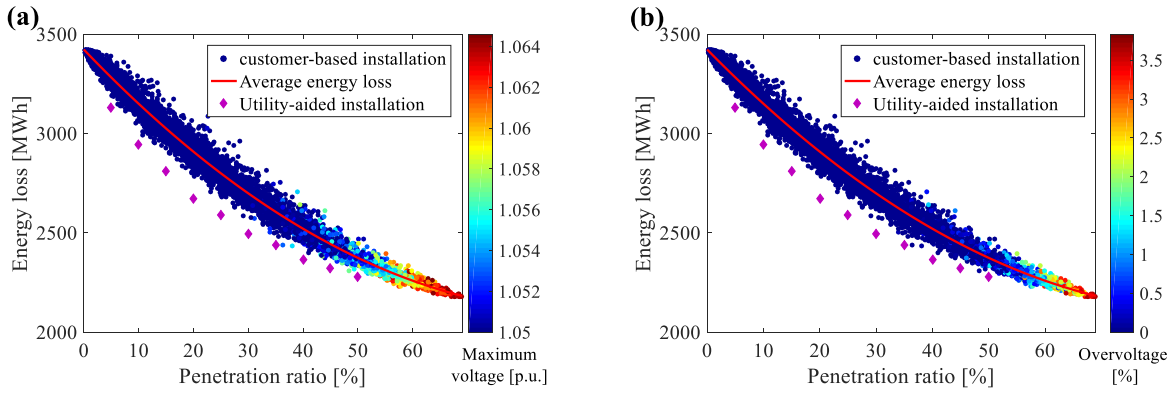

Figure 3.18 Percent of optimized voltage deviation and fluctuation improvement

Similar to voltage deviation, percent of optimized energy loss reduction is defined as

$$\Delta E_{loss} = \left(E_{loss}^{rand} - E_{loss}^{opt}\right)/E_{loss}^{rand} \tag{3.24}$$

Figure 3.19 shows the energy loss reduction by using utility-aided installation. As we can see, the maximum energy loss reduction of optimized installation in comparison with customer-based installation is 11.3% at penetration ratio of 20%. Using utility-aided installation at middle penetration ratios (15-35%), the utility could reduce energy loss more than 3% in comparison with the customer-based installation. However, at higher penetration ratios there is not a significant difference between customer-based and utility-aided installation.

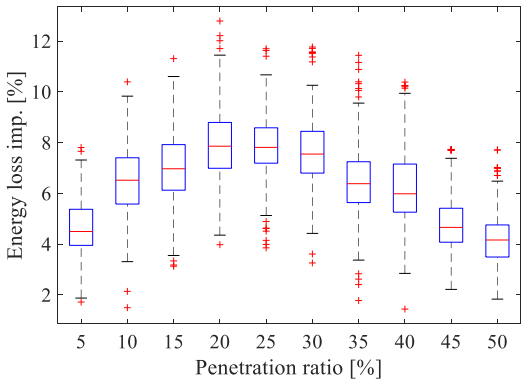

Figure 3.19 Improvement in total energy loss reduction by using utility-aided installation.

3.5 Summary

In this chapter, we proposed a scalable and detailed impact assessment framework to accurately assess the impacts of DPVs on distribution networks. A full year time-series analysis of DPV installations with a novel synthetic load profile modeling and detailed models of all system components was performed to aid utilities and policymakers on quantifying the impacts of different DPV penetration levels. To cater uncertainties in DPV installation by customers, a Monte Carlo-based technique as utilized. Solar PV installation in the distribution network is not purely random and the location and size of the installation depend on many factors. Adequate solar insolation, available rooftop and customer decision for size selection, as well as the finance budget and government incentives are the most crucial factors for rooftop PV installations. Therefore, to develop a detailed assessment approach, we performed a PV potential study to estimate actual DPV installation capacity for the buildings in the given distribution network. In addition, the customer selection factor was defined to mimic customer behavior for PV size selection. Moreover, a novel synthetic load modeling was proposed to generate daily load profiles for individual building types representing specific load patterns for the studied area. In addition to the Monte Carlo-based technique to study random installation, we proposed a multi-objective optimization approach to suggest optimal location and size of aggregated small-scale DPVs in the

distribution network. The objectives of optimal size and location algorithm are minimization of the energy loss, voltage deviation, and voltage fluctuation, in addition to elimination of voltage violations and reverse power flow. This allows identifying the outcomes for two different DPV deployment policies towards the possible strategies to maximize advantages and minimize the negative impacts of DPVs and may provide useful guidance for utilities and policymakers. In fact, the proposed detailed impact assessment not only provides the more precise and accurate results on hosting capacity and high PV penetration impacts, but also provides a comparative perception of DPV installation in different penetration ratios. It was found that reverse power flow in the network rises with increasing the DPV penetration ratio. However, the increasing trend does not grow linearly, and there is a significant increase in the number of cases with reverse power flow issues beyond a particular penetration ratio e.g. $\gamma = 30\%$. Comparing the utility-based and customer-based DPV installations showed that when the distribution network has a medium renewable penetration ratio, 15-30%, an optimal installation will bring significant improvements in energy loss reduction, voltage fluctuation, and voltage deviation. However, when the renewable integration ratio is low or high, there will be less differences between the types of installation. Moreover, it was observed that it is more likely to have a voltage violation in residential feeders. Unlike the general commercial energy-use pattern, which has a good correlation with typical PV power profile, residential energy-use pattern presents a peak value during the nighttime when there is a small or no PV generation resulting in surplus PV generation at noon and initiating reverse power flow and voltage rise. It was also found that with customer-based installation in the studied network, beyond 30% of DPV penetration the network operator needs necessary upgrades in the network to avoid overvoltages and severe reveres power flows. However, by utility-aided installation the network can accommodate 50% of DPV penetration without having overvoltages

and reverse power flows and need to system upgrades. It is clear that there will be a tradeoff between network planning by utilities and costs of network upgrades. Distribution network operators can eliminate or postpone system upgrades with interfering in customer decisions in DPV installation to minimize system operation and upgrade costs. The summary of contribution and comparison with selected works in the literature is presented in Table 3.3.

Table 3.3 Summary of contribution and comparison with selected works in the literature

		G. Carne, et al. (2018) [62]	Y. Chen, et al. (2016) [65]	M. Alturki, et al. (2018) [66]	H. Hassanzadeh, et al. (2018) [76]	M. S. Abad, et al. (2018) [69]	**Proposed framework**
Objectives	Voltage violations	X	✓	✓	✓	✓	✓
	Reverse power flow	✓	X	X	X	X	✓
	Energy loss	X	✓	✓	✓	✓	✓
Solar potential study		X	X	X	X	X	✓
Detailed customer load model		X	X	X	X	X	✓
Utility-aided installation		✓	✓	✓	✓	✓	✓
Customer-based installation		X	X	X	✓	✓	✓
Study period		Daily	Daily	Daily	Daily	Daily	**Yearly**

4. Integration of rooftop PVs with demand side management

4.1 Motivation

Demand side management (DSM) is one of the important functions in a smart grid that allows customers to make informed decisions regarding their energy consumption, and helps the energy providers reduce the peak load demand and reshape the load profile and there is a significant scope for DSM to contribute in increasing the efficiency and use of system asset. Many studies have focused on DSM in recent years [1]. Several studies examined DSM strategies for different energy sectors such as residential and commercial [2-7], however, a few studies have examined the DSM for both residential and commercial to compare their different impacts in the distribution networks [8]. Reference [9] proposed a DSM strategy for three different demands of residential, industrial and commercial with a basic system model without considering time-of-use (TOU) prices and DERs. The other huge group of studies on DSM, have been focused on programming techniques and algorithms to solve the DSM problem using dynamic programming and linear programming [10]. However, most of them are for a specific system and are not applicable to practical systems that have a large number of controllable devices from several types of devices which have several computation patterns and heuristics. The other group of studies examined integration of DSM with different new concepts such as smart pricing [11], energy storage [12] and distributed energy resources (DERs) [13]. However, a comprehensive practical DSM model including customer participation, TOU prices, and multiple load sectors is missing in this group.

In this section, a decentralized household demand side management is studied in a purely residential feeder, which consists of multiple smart homes with schedulable electrical appliances and rooftop photovoltaic generation units. Each smart home makes individual appliance scheduling to optimize the electric energy cost according to the day-ahead forecast of electricity

prices and its willingness for convenience sacrifice. Using the developed simulation model, we examine the performance of decentralized DSM and study their impacts on the distribution network operation and renewable integration, in terms of utilization efficiency of rooftop PV generation, overall voltage deviation, real power loss, and possible reverse power flows. Compared with the work in the literature, the contributions of this work include: (1) development of a multi-household simulation framework to study decentralized DSM in distribution network; (2) the proposed DSM optimization model takes into account time-varying electricity prices and rooftop PV generation available onsite; (3) every smart home that participates in the DSM program aims to reduce its electricity bill with a manageable sacrifice of convenience and comfort; (4) a comprehensive comparative study is conducted to examine the impacts of DSM on the system operation and distributed renewable integration.

4.2 DSM for residential feeder with rooftop PVs

This section describes the decentralized household DSM in a residential distribution network, which considers a single residential feeder supplying a small community with 30 residential households, as shown in Fig. 4.1. The time-varying load profile of each household is generated by a time-series load modeling [10] we developed using real residential demand data obtained from the open-access database (OpenEI). It is assumed that the simulated residential community has up to 16 smart homes that participate the decentralized DSM program with their schedulable electric appliances. Each smart home will optimize its appliance operation schedule to save electricity costs according to the day-ahead pricing forecast, rooftop PV generation (if available) with a controlled sacrifice of homeowner's convenience or comfort.

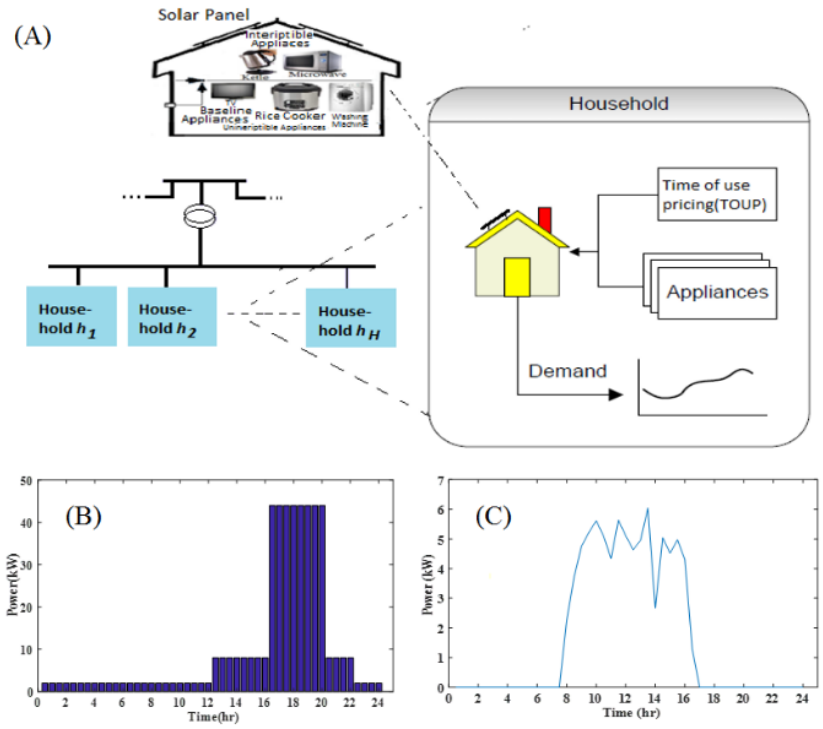

Figure 4.1 System model for the decentralized DSM study: (A) smart household with interruptible appliances and rooftop PV; (B) day-ahead electricity price forecast; (C) output power of rooftop PV generation

In order to study the impacts of decentralized DSM on renewable integration, the proposed framework also assumes that each smart household will be given an opportunity to mount a rooftop solar PV panel of a rated capacity of 6kW. For the analysis simplicity and without loss of generality, we consider all the rooftop PV systems in this small residential community have similar solar insolation and produce the same amount of electric power.

It is worth noting that each smart household has a specific set of flexible electric appliances, with different power ratings and operational limits, as shown in Table 4.1. More details on the household DSM appliances may be found in [175]. In order to avoid creating additional peak load period resulted from the DSM load shifting, each smart home will be given a maximum demand (MD) constraint equal to the peak load of its original load profile.

Table 4.1 Smart housholds with agreed MD limits

Household Index	Bus No.	Interruptible Appliance No.	Uninterruptible Appliance No.	MD(kW)
1	12	21	7	12.4
2	14	15	4	15.3
3	17	17	4	11.8
4	20	12	4	8.0
5	3	21	7	12.4
6	10	15	4	15.3
7	19	17	4	11.8
8	29	12	4	8.0
9	8	21	7	12.4
10	15	15	4	15.3
11	22	17	4	11.8
12	25	12	4	8.0
13	6	21	7	12.4
14	16	15	4	15.3
15	23	17	4	11.8
16	31	12	4	8.0

4.2.1 Problem formulation

The proposed decentralized household DSM model will be implemented at each smart home participating in the program individually. It aims to minimize the household's electricity cost by scheduling the on/off status of domestic appliances over the operational periods, considering the dynamic electricity prices, locally available PV generation, and the penalty cost of appliance operation time-shifting. The penalty cost is included in order to manage the customer inconvenience caused by the DSM load shifting. Assume that the proposed demand side management program is scheduled day-ahead with 30 min per slot. The decision variables are the operational status of appliances $u_a(t)$ over the next 24 hours for each household.

Three levels of DSM participation will consider the enrollment of 4, 8, and 16 smart homes in DSM program respectively. In addition the simulation model will use three penalty prices of 0, 5, and 10 (¢/kWh) to represent different compensations requested for the sacrifice of convenience. After implementation of DSM on selected households final load profiles represent the optimal load

profile of the households are considered to run AC power flow and examine the voltage, power loss and power flow across the residential feeder. The impacts of DSM on the residential network will be examined with two scenarios: (a) DSM households without PV Installation; and (b) DSM households with rooftop PV installation on site.

The decentralized DSM optimization for each smart building can be defined as below:

$$\min_{[u_{a,m}(t)]} C_e^m + C_p^m \tag{4.1}$$

Subject to:

$$C_e^m = \sum_t^T P_{load}^m(t) \times \pi_e(t) \tag{4.2}$$

$$C_p^m = \sum_{a,m}^A \pi_p \cdot r_{a,m} \cdot \Delta T_{a,m} \tag{4.3}$$

$$P^m{}_{load}(t) = \max\left(\left(\sum_{a,m=1}^{A_m} r_{a,m} \times u_{a,m}(t) - P^m{}_{pv}(t)\right), 0\right) \tag{4.4}$$

$$\sum_{a,m=1}^{A_m} r_{a,m} \times u_{a,m}(t) \leq MD^m \forall a \in 1 to A_m \tag{4.5}$$

$$\sum_{t=1}^{T} u_{a,m}(t) = D_{a,m} \forall a \in 1 to A_m \tag{4.6}$$

$$u_{a,m}(t) = 0 \qquad \forall t < s_{a,m} \text{ or } \forall t > f_{a,m} \tag{4.7}$$

$$\Delta T_{a,m} = \mathbf{1}^T . \left| t_{a,m}^{st_{new}} - t_{a,m}^{st_{old}} \right| \qquad \forall a \in \{1 \; to \; A_m\} \tag{4.8}$$

$$t_{a,m}^{st_{new}} = \left[t \middle| u_{a,m}^{new}(t) = 1 \right]_{1 \times D_{a,m}} \qquad \forall a \in \{1 \; to \; A_m\} \tag{4.9}$$

$$t_{a,m}^{st_{old}} = \left[t \middle| u_{a,m}^{old}(t) = 1 \right]_{1 \times D_{a,m}} \qquad \forall a \in \{1 \; to \; A_m\} \tag{4.10}$$

The objective function of (4.1) is to minimize the total cost of electricity consumption (22) and the penalty cost for convenience sacrifice (4.3) for each building, where *m* is the household's index. $u_{a,m}$ represents a binary status of appliance *a* (0 = *off*, 1 = on) at building *m*, with the following format $[\boldsymbol{u_{a,m}(t)}]_{A \times T}$. Constraint of (4.4) is assumed to avoid negative electricity cost. Because the proposed model assumes that surplus PV generation will be injected into the

distribution network without reward. Therefore, the total electricity cost within each time slot should be no less than zero as indicated by eq. (4.4). Maximum Demand (MD) constraint is considered in (4.5). This specified upper limit is to prevent super-high power demand peak even during the hours when day-ahead electricity price is low because the utilities do not want to have "new" peak created by the DSM load-shifting or because the distribution feeders have capacity constraints. Eq. (4.6) and (4.7) model total operation duration and the allowable turn-on time of appliances and Eq. (4.8)-(4.10) specify the original and the new starting point, $t_{a,m}^{st_{old}}$ and $t_{a,m}^{st_{new}}$ and to calculate load-shifting time for flexible appliances. The penalty cost included in the objective function (4.1) means to minimize the electricity cost with manageable sacrifice of load-shifting inconvenience, to avoid inefficient load shifting that only yields slight electricity cost in (C_e^m) which is less than the increase in C_p^m the inconvenience-penalty cost.

4.2.2 Numerical simulation and results

Numerical experiments have been conducted to examine the impacts of decentralized household DSM program with rooftop PV system on the residential distribution network in terms of renewable usage efficiency, voltage deviations, real power loss, and reverse power flow. In the first scenario the proposed DSM model is considered without rooftop PV installation on selected DSM households and the impact of different DSM penetration level with different penalty prices are investigated. In second scenario, DSM households considered to have rooftop PV systems and with calculation of optimal load profiles for DSM households, distribution network operation in terms of voltage, power loss and reverse power flow is investigated.

4.2.2.1 Individual Household DSM

Figure 4.2 compares the original load profiles (depicted as red solid line) and the DSM scheduled profile (depicted as blue bar plots) of smart home #1 under four different conditions (with/without onsite PV, and $\pi_p = 0$ or 5 ¢/kWh). The PV output power is depicted as blue dashed line. Original load profile indicates two demand peaks: around 7:00 to 9:00 in the morning and 17:00 to 20:00 in the evening.

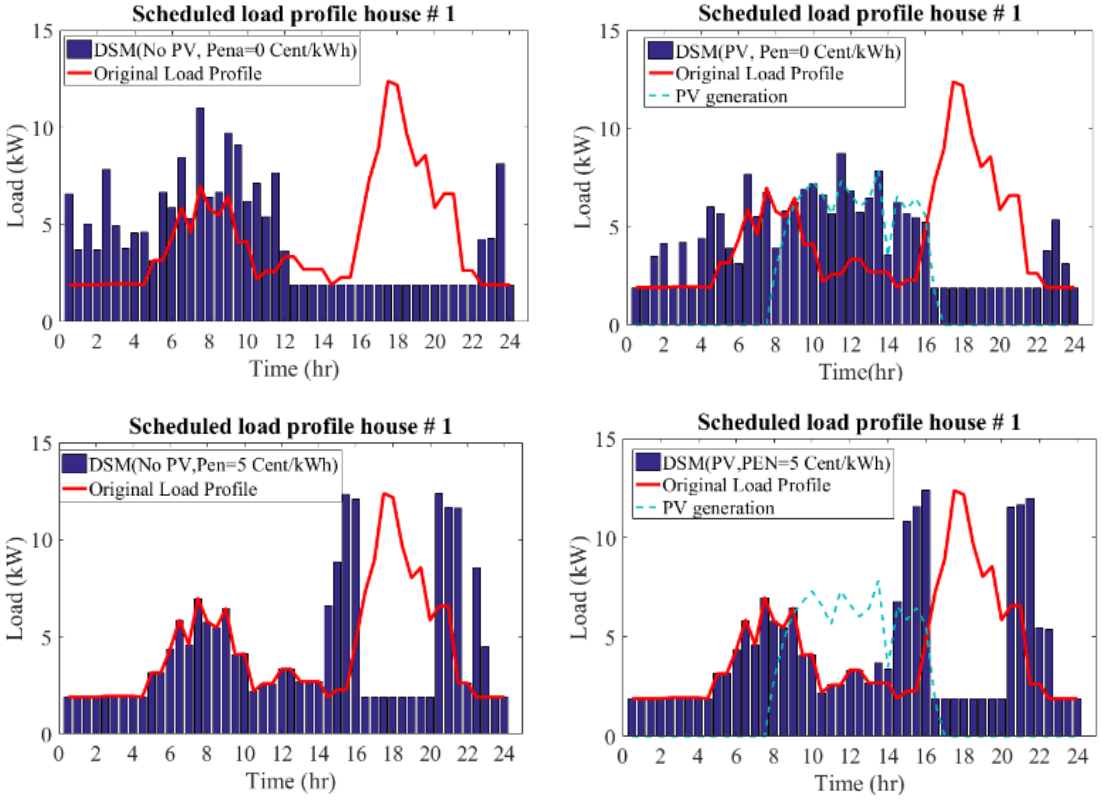

Figure 4.2 Load profiles of smart household #1 with DSM under four different conditions

As shown in Fig. 4.1, there is a peak price rate during the time of 17:00 to 20:00. Therefore, the DSM program without any penalty for load-shifting inconvenience will move all the schedulable appliances out of the peak price hours, as shown in the top two subfigures in Fig. 4.2. When the onsite rooftop PV is mounted, the appliance load will be first shifted to the time slots inside 8:00-16:00 where the PV generation is available hence achieve a renewable usage efficiency

of 99.98%. However, if penalty for load-shifting inconvenience is considered, say, with $\pi_p = 5$ ¢/kWh, the shifted load will be concentrated on the boundary next to peak-price hours as 14:00-16:00, and 20:00-22:00. And this may significantly affect the renewable usage efficiency, causing it to drop to 36.55%.

4.2.2.2 PV utilization efficiency

PV utilization efficiency (γ) defines the percentage of total PV generation that has been consumed by local demands. From Fig. 4.2, it can be seen that a typical load profile of residential household has peak loads occurring in the morning or evening hours when there is little or no PV generation. However, the commercial load profile usually presents a good time alignment with the PV power generation. Figure 4.3 depicts the energy consumption mix of a sample residential building (B1) for original load profile and DSM in different penalty prices. For the original load profile, the building receives 74% of its energy form the grid and 26% from installed rooftop PV system with PV utilization of 66.27%. It is found the proposed DSM without penalty price improvs the PV utilization capacity to 98.24%, which also helps to eliminate reverse power flow in the system and improve hosting capacity. It is clear that by increasing the penalty price the possibility to shift the loads to the PV generation time slots decrease and therefor, share of solar PV in building consumption decrees. However, even with higher penalty prices the PV utilization efficiency still is higher than the case without DSM implementation.

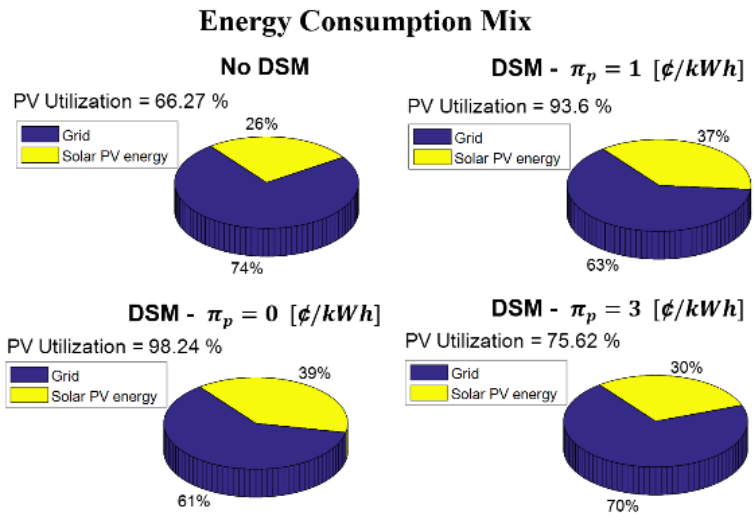

Figure 4.3 Energy consumption mix for a sample residential building (#1)

4.2.2.3 Voltage

Fig. 4.4 compares the voltage profile at the end of the feeder for different DSM participation levels with $\pi_p = 0$ ¢/kWh considering the two scenarios, i.e., with or without PV installation. It is found that higher DSM participations will tend to "flatten" the voltage profile (i.e. filling the voltage drop valleys) and bring better improvement to voltage fluctuations caused by load variations. Besides, during the daytime hours (8:00-16:00) when the rooftop PVs generate power, the DSM without penalty for convenience sacrifice will help mitigate overvoltage problem during those hours.

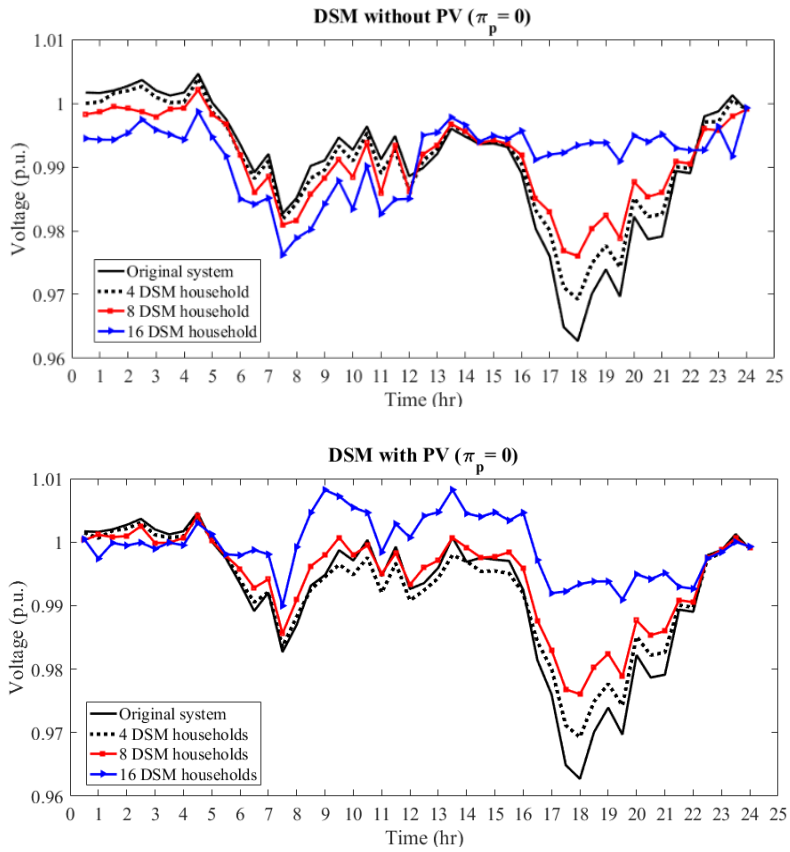

Figure 4.4 Voltage profile at the end of the feeder for different DSM participation levels (with/without PV installation, $\pi_p = 0$).

Fig. 4.5 compares the voltage profile at the end of the feeder when there are 16 smart homes participating in the DSM program with different penalty prices considering the two scenarios, i.e., with or without PV installation. Comparing with the results in Fig.3, we may see that higher penalty prices such as $\pi_p = 5$ or 10 ¢/kWh will significantly reduce the voltage smoothing effect of the DSM program because much fewer flexible appliances will be shifted out from the peak-price hours. Besides, during the daytime hours (8:00-16:00) when the rooftop PVs generate power and cause overvoltage conditions, the DSM with high penalty for convenience sacrifice cannot help much during those hours.

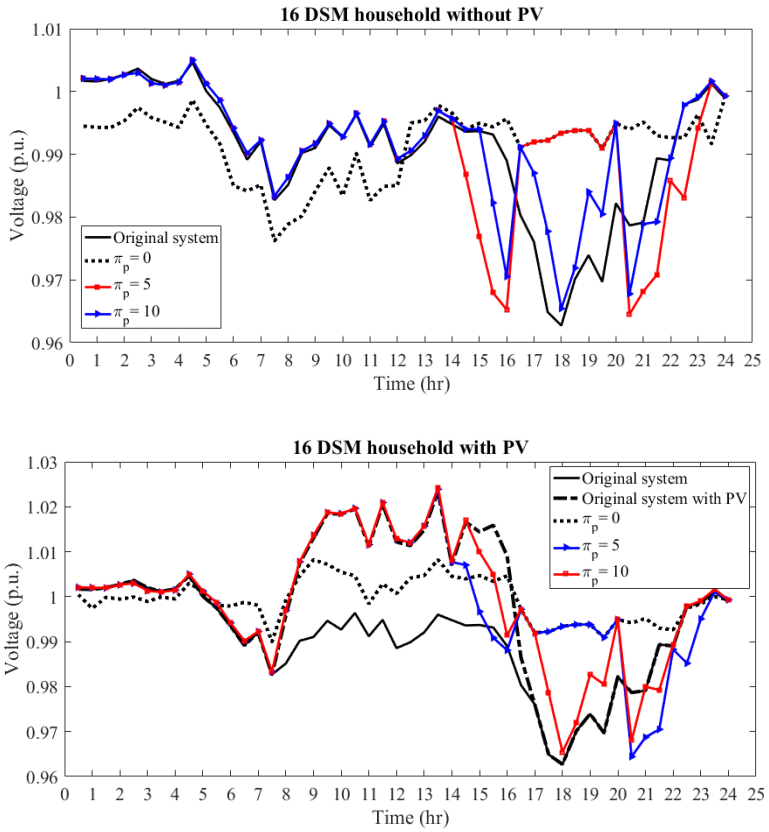

Figure 4.5 Voltage profile at the end of the feeder with 16 DSM households with different penalty prices

4.2.2.4 Reverse Power Flow

Fig. 4.6 presents the power flow distribution across the distribution feeder of the original system and with 16 household DSM ($\pi_p = 0$), without any PV installation. Obviously, DSM participations without high penalty for load shifting inconvenience help smoothing the flow distribution. Figure 4.7 shows the power flow distribution across the distribution feeder of the original system and with 16 household DSM ($\pi_p = 0$ ¢/kWh), with 16 onsite rooftop PV installations. The output power from rooftop PVs may cause reverse flows at some line segments at mid-day hours as can be seen from the top subfigure. However, the DSM scheduling may shift some appliance usage into those time slots and lessen the reverse flows.

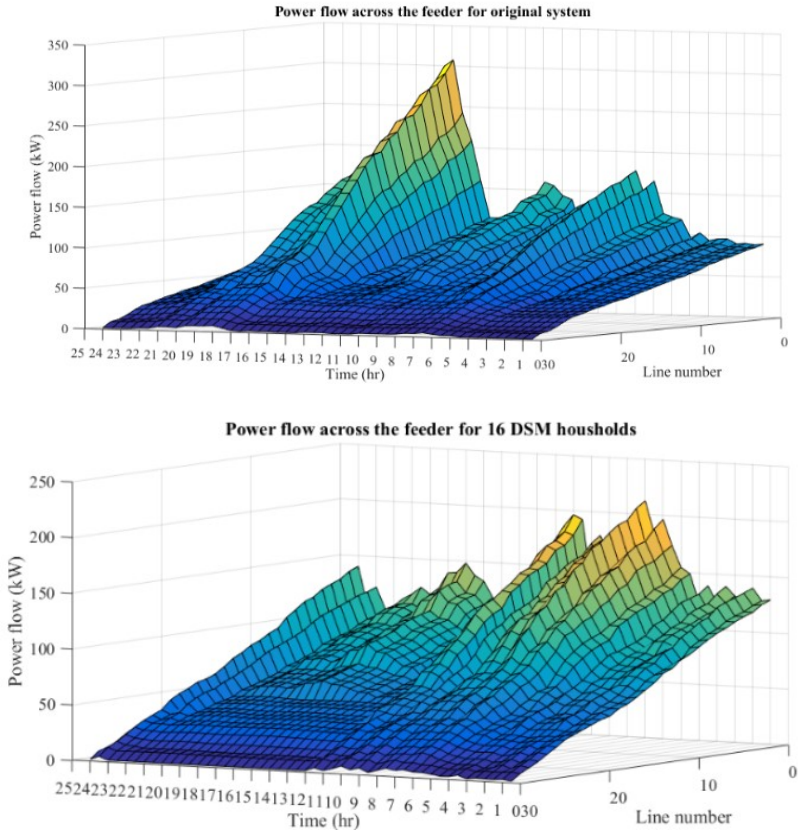

Figure 4.6 Power flow across the feeder without PV installation

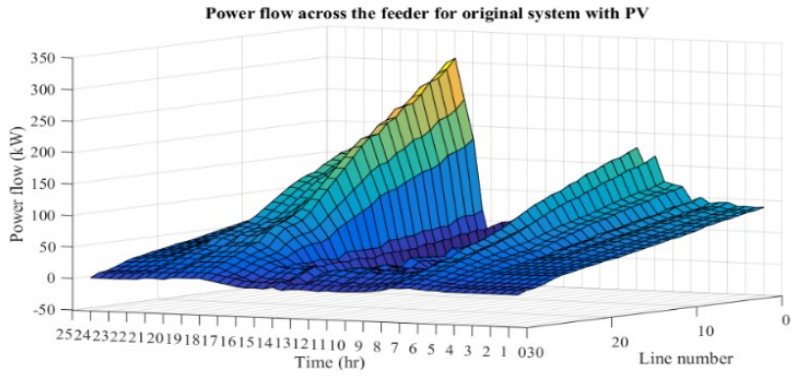

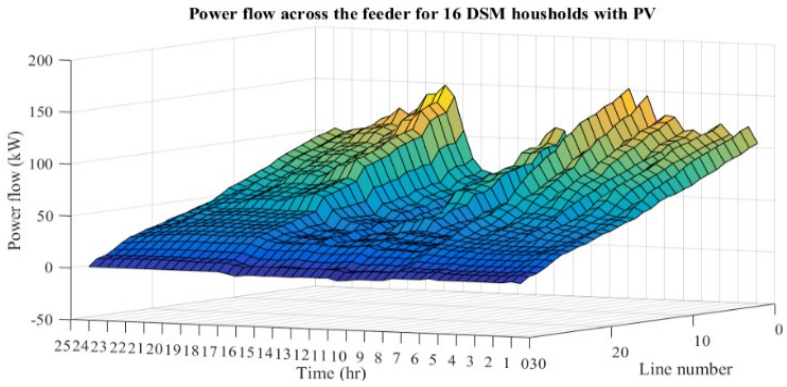

Figure 4.7 Power flow across the feeder with on-site rooftop PV installations

4.2.2.5 Real Power Loss

Fig. 4.8 compares the feeder real power loss experienced at each hour with different DSM participation levels with or without PV installation. Clearly, it shows that higher DSM participations will more effectively bring down the high energy loss during peak-price hours with a little bit increase during the mid-day hours. However, with onsite rooftop PV installations, the output PV generated power during the mid-day time will help to get rid of the real-power loss caused by DSM load shifting.

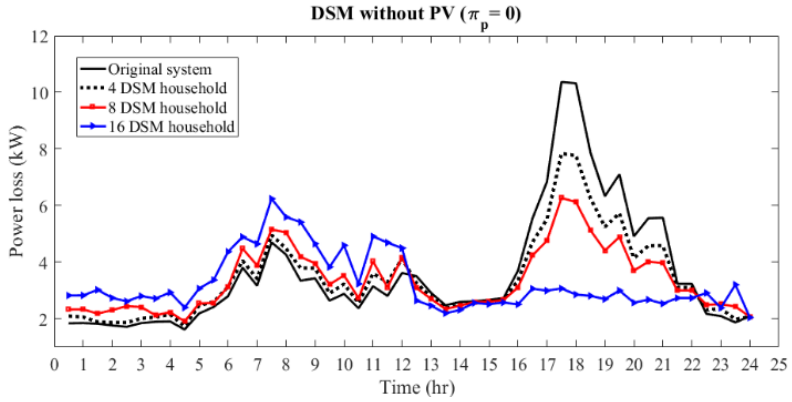

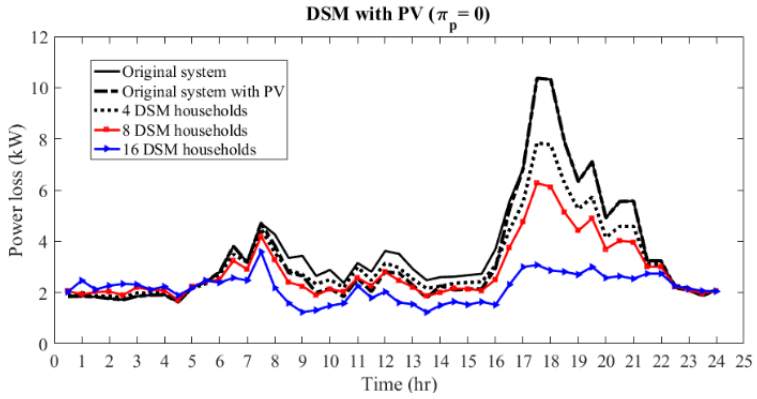

Figure 4.8 Power loss in the feeder for different DSM participation levels with or without PV installation

4.3 Summary

In this chapter, we developed a decentralized DSM with multiple residential loads with rooftop PV installations. The residential loads considered with different time-varying billing rates and different characteristics such as load profile, appliance settings, and customer willingness for DSM participation. In addition, rooftop PV systems, TOU electricity prices and different customer participation models for both residential and commercial loads were considered to have a more practical DSM model. Moreover, a heuristic based evolutionary algorithm that can easily handle large number of appliances with different criteria was developed. The performance of decentralized DSM scheduling with rooftop PV systems and their impacts on customers and distribution network operation, examined in terms of electricity cost savings, renewable utilization efficiency, voltage fluctuation, and real power loss. It was found that DSM without high penalty for load-shifting inconvenience effectively smooth the load profile, reduce the voltage fluctuations, boosts renewable energy consumption, and eliminates the overvoltage and revers power flow problems caused by PV generated power during the mid-day. It was found that the PV utilization efficiency can be improved from 68% to 98% by utilizing proposed DSM algorithm. However, with higher penalty price, i.e. $\pi_p = 3$ ¢/kWh for load shifts the PV utilization efficiency drops to

76%. Note that the increasing the PV utilization efficiency results in improving the hosting capacity of the network by eliminating backfeed power to the network due to surplus rooftop PV generation. As we observed in the previous chapter, the reverse power flow has an strong relationship with overvoltage in the system. Therefore minimizing the reverse power flow with increasing PV utilization efficiency improves the total husting capacity of the network. The summary of contribution and comparison with selected works in the literature is presented in Table 4.2.

Table 4.2 Summary of contribution and comparison with selected works in the literature

		H. Shakouri, et al. (2017) [32]	B. Bahl, et al. (2017) [87]	R.-S. Liu, et al. (2018) [90]	B. Lokeshgupta, et al. (2018) [91]	K. Di Santo, et al. (2018) [94]	**Proposed framework**
Viewpoint	Customer	✓	✓	✓	X	✓	✓
	Network operator	✓	✓	X	✓	X	✓
Smart home control		✓	✓	✓	X	✓	✓
Customer inconvinence		X	X	✓	X	X	✓
Renewable energy		X	X	✓	✓	✓	✓
TOU electricity cost		✓	✓	✓	✓	X	✓
PV utilization efficiency		X	X	X	X	X	✓

5. Online Virtual Power Plants Control for Inertia Emulation and Fast Frequency Response

As discussed earlier, the ultimate goal of this research is to investigate potential solutions to improve HC and install more renewable energies without negative impacts on the power grid. Among all different solutions for increasing the HC [24], battery energy storage systems (BESSs) have been attracted a great deal of attention in recent years. Although the cost of the BESS is steadily decreasing, the main concern is still the initial investment. This chapter, investigates the potential of distribution networks with aggregated distributed energy resources (DERs), including BESSs, DGs, and flexible loads to provide a fast frequency response to a bulk power system with high penetration of renewable energies.

5.1 Motivation

Increasing share of the renewable energy resources in the generation mix is resulting in a lighter system with low system inertia, leading to jeopardize the power system stability. The major issue is a large frequency deviation in case of large disturbance, which requires a fast active power (injection) response immediately following frequency event to avoid system collapse. Many studies have proposed different approaches to address the lack of inertia which have been discussed in section 1.2.4.

In the most of the studies, the total power system inertia is estimated using the well-known swing equation and neglecting the reduction of inertia due to the loss of an unknown synchronous generator [176]. However, it is crucial to calculate the precise and more accurate disturbance to improve the performance of frequency regulation studies, especially for minimum load shedding. Most of the measurement based methods use frequency measurements from after the disturbance

to approximate the center of inertia frequency and, as such, the inertia of the tripped generator should not be accounted for. However, since the tripped generator is unknown, they consider all the generators including tripped generator for estimation of disturbance and system inertia. This drawback results in a percentage error in estimation which can threaten the accuracy and effectiveness of proposed methods that rely on disturbance estimation such as inertia emulation and minimum under frequency load shedding. Therefore, introducing a new method which excludes tripped generator for inertia estimation is of importance. On the other hand, a thorough search of the relevant literature shows that the potential of virtual power plants (VPP) to participate in inertia response and fast frequency response has not been investigated [177], [178]. With a low latency communication system, aggregated dispatchable distributed energy resources (DERs) including different types of distributed generations and energy storage systems are an ideal solution to supplement generation-side capabilities such as fast frequency regulation.

In this chapter, an inertia emulation framework is developed to investigate the potential of aggregated DERs for fast frequency regulation. An online power disturbance estimation is proposed by introducing new terms in the *swing equation* to have an accurate estimation of disturbance and system inertia in case of a load/generation imbalance. In addition, a real-time optimization framework is developed to control aggregated DERs in a distribution network. It guarantees the fast response of DERs in their feasible operation region while satisfying network operational constraints. Moreover, VPP participation factor and decentralized inertia control are introduced to allocate the active power set-points of VPPs in the power system.

5.2 Methodology

The main idea of proposed framework is outlined with respect to the illustrative system in Fig. 5.1. The objective is to develop a real-time architecture for aggregated DERs of a distribution

network in which the active power at the substation, P_k^{sub}, rapidly track the setpoint $P_{k,set}^{sub}$ to provide fast frequency regulation. In this regard, we propose a three-stage framework. First, the power system inertia is estimated based on a precise online calculation. Then, a decentralized virtual droop control indicates the target value for the corresponding VPP, and finally, a real-time optimization algorithm is applied to dispatch individual DERs.

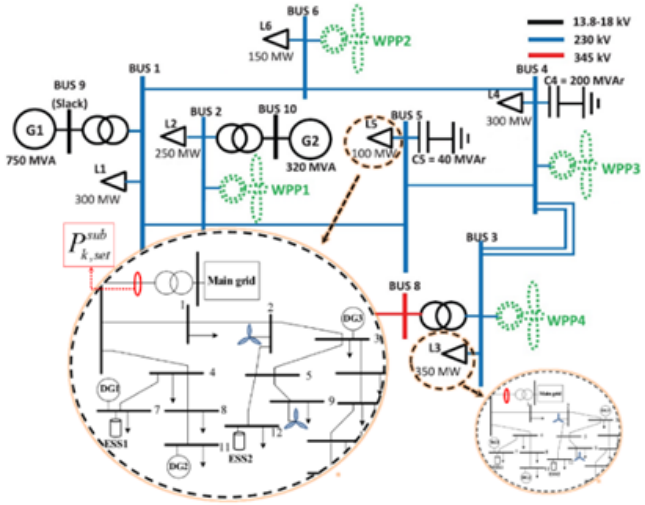

Figure 5.1 Proposed architecture: output powers of VPPs track set points in real-time to provide fast frequency response.

5.2.1 Power system Inertia Estimation

In general, inertia is defined as the resistance of a physical object to a change in its state of motion, including changes in its speed and direction. Applying this definition to a traditional electric power system, the physical objects that are in motion are the rotating machinery (synchronous generators and turbines, induction generators, etc.) connected to the power system and the resistance to the change in rotational speed is expressed by the moment of inertia of their rotating mass. The motion of each single generator can be expressed by *swing equation* [179]. It describes the acceleration (deceleration) of the synchronous generator and turbine (prime mover) due to any imbalance between mechanical torque (τ_m) and electromagnetic torque (τ_e).

$$J\frac{d\omega_m}{dt} = \tau_m - \tau_e \tag{5.1}$$

where J is the combined moment of inertia of the rotating mass (kg.m2) and ω_m is the angular velocity of the rotor in mechanical rad/s. Here, both mechanical and electromagnetic torques are expressed in N.m. In power system, it is preferred to define inertia constant $\mathrm{H} = (0.5\,\mathrm{J}\omega_{m0}^2)/S_b$, as the rotor kinetic energy stored in rotating mass (W.s) referred to the generator base rating (S_b in VA) where ω_{m0} is the rated angular velocity of rotor, in mech. rad/s. The unit of H would be in seconds. Expressing the moment of inertia using inertia constant and substituting it into Eq. 5.1 obtain

$$2H\frac{S_b}{\omega_{m_0}^2}\frac{d\omega_m}{dt} = \tau_m - \tau_e. \tag{5.2}$$

In power system engineering, it is however more common to express this swing equation in power instead of torque: therefore, by multiplying both side of Eq. 5.2 by ω_{m0} , we can have

$$2HS_b\frac{d}{dt}\left(\frac{\omega_m}{\omega_{m_0}}\right) = 2HS_b\frac{d}{dt}\bar{\omega}_m = p_m - p_e, \tag{5.3}$$

where, $p_m$and p_e are the mechanical power and electrical power in W, and $\bar{\omega}_m$is mechanical speed in per-unit. Let us consider a small perturbation around the equilibrium point Eq. (5.3) for a synchronous generator due to a power disturbance.

$$2HS_b\frac{d}{dt}(\bar{\omega}_{m0} + \Delta\bar{\omega}_{m0}) = \left(p_{m_0} + \Delta p_m\right) - \left(p_{e_0} + \Delta p_e\right), \tag{5.4}$$

where the equilibrium point indicated by zero subscript. Since at the equilibrium point the generators speed is constant and mechanical power is equal to the electric power, the Eq. (5.4) can be rewritten as

$$2HS_b \frac{d}{dt}(\Delta\bar{\omega}_{m0}) = (\Delta p_m) - (\Delta p_e). \tag{5.5}$$

Note that we use $\frac{d}{dt}(\Delta\bar{\omega}_{m0})$ to express the Rate of Change of Frequency (RoCoF) based on pre-event equilibrium point and it is equal to the post-event RoCoF, $\frac{d}{dt}(\Delta\bar{\omega}_m)$Let us consider a typical power system with *n* synchronous generators, supplying *k* electrical loads. In case of any power disturbance all the power units can be aggregated into one single unit and the share of each on-line generator in meeting the power imbalance depends solely on its inertia and not on its electrical distance from the disturbance [180]. Therefore, the Eq. (5.5) can be extended to all the generators:

$$\sum_{i=1}^{n} 2H_i S_{b,i} \frac{d}{dt} \bar{\omega}_{m,i} = \sum_{i=1}^{n} \Delta p_{m,i} - \sum_{i=1}^{n} \Delta p_{e,i}. \tag{5.6}$$

As an approximation in the conventional power imbalance estimation, the left-hand side of the Eq. (5.6) can be rewritten in terms of the angular speed of the equivalent center of inertia (COI), defined as [181]:

$$\bar{\omega}_m^{CoI} = \sum_{i=1}^{n} 2H_i S_{b,i} \frac{d}{dt} \bar{\omega}_{m,i} / \sum_{i=1}^{n} 2H_i S_{b,i}. \tag{5.7}$$

Substituting the Eq. (5.6) into the Eq. (5.7) gives

$$\sum_{i=1}^{n} \left(2H_i S_{b,i}\right) \frac{d}{dt} \bar{\omega}_m^{CoI} \approx \sum_{i=1}^{n} \Delta p_{m,i} - \sum_{i=1}^{n} \Delta p_{e,i}. \tag{5.8}$$

It is worth noting that in the first few seconds following the power disturbance, the mechanical power change in the right-hand side of the Eq. (5.8) can be ignored due to the slow-changing mechanical power relative to the electric power. Therefore, the active power disturbance can be estimated as follows:

$$\sum_{i=1}^{n}\left(2H_iS_{b,i}\right)\frac{d}{dt}\bar{\omega}_m^{CoI} \approx -\sum_{i=1}^{n}\Delta p_{e,i} = -p_{\text{dist}}. \tag{5.9}$$

Equation (5.9) represents the conventional practice to calculate the power disturbance [176]. Unfortunately, neglecting the system inertia reduction due to the loss of generator is one of the deficiencies in this method. This drawback, results in a percentage error approximately equal to the lost power size normalized to the base power of system. In the following an approach is proposed to address this deficiency.

Let us assume a power disturbance caused by tripping a generator. If *j*-th generator abruptly disconnects, the Eq. (5.9) can be rewritten as

$$-\left(\sum_{i=1}^{n}2H_iS_{b,i} - 2H_jS_{b,j}U_{\text{h}}\left(\frac{-d}{dt}\bar{\omega}_m^{CoI}\right)\right)\frac{d}{dt}\bar{\omega}_m^{CoI} = p_{\text{dist}}, \tag{5.10}$$

where $U_h(x)$ is the Heaviside step function with definition of

$$U_h(x) = \begin{cases}1 & x > 0\\ 0 & x \le 0\end{cases}, \tag{5.11}$$

whose value is zero for negative arguments (positive frequency deviation) and one for positive arguments (negative frequency deviation). Multiplying the Heaviside step function with tripped generation components guaranties the generality of *swing equation* for both positive and negative power imbalances.

It should be mentioned that since the tripped generator is unknown, it is impossible to calculate the exact amount of reduced inertia in the Eq. (5.10). To address this obstacle a new online method is implemented. The pre-event active power of tripped generator is utilized to replace the unknown $S_{b,j}$. The pre-event loading level of active power for tripped generator (L_j) can be calculated as

$$L_j = \frac{p_{e_0,j}}{S_{b,j}}, \tag{5.12}$$

where, $p_{e_0,j}$ is pre-event electrical power of tripped generator. On the other hand, when *j*-th generator suddenly disconnects, its generated electric power becomes null in Eq. (5.4) and consequently, $\Delta p_{e,j} = -p_{e_0,j}$. Since the system frequency is considered as a global system parameter, all the power units can be aggregated into one single unit [182]. Therefore, the disturbance power which is equal to the deficit electric power supplied by the rest of the generators can be interpreted as:

$$\sum_{i=1\neq j}^{n} \Delta p_{e,i} = -\Delta p_{e,j} = p_{e_0,j} = p_{\text{dist}}. \tag{5.13}$$

And substituting the Eqs. (5.12) and (5.13) into Eq. (5.10) results in:

$$-\left(\sum_{i=1}^{n} 2H_i S_{b,i} - 2H_j \frac{p_{\text{dist}}}{L_j} U_{\text{h}} \left(\frac{-d}{dt}\bar{\omega}_m^{CoI}\right)\right)\frac{d}{dt}\bar{\omega}_m^{CoI} = p_{\text{dist}}. \tag{5.14}$$

In Eq. (5.14), disturbance power appears in both left- and right-hand sides, indicating the real and estimated values of the power disturbance, respectively. Substituting the real value with the estimated one obtains:

$$p_{\text{dist}} = \frac{-\left(\sum_{i=1}^{n} 2H_i S_{b,i}\right)\frac{d}{dt}\bar{\omega}_m^{CoI}}{1 - \frac{2H_j U_h \left(\frac{-d}{dt}\bar{\omega}_m^{CoI}\right)}{L_j}\frac{d}{dt}\bar{\omega}_m^{CoI}}. \tag{5.15}$$

Note that in Eq. (5.15), both H_j and L_j are unknown. To have a rough but rational initial value of inertia constant and loading level of unknown tripped generator, H_{HOR} can be selected as inertia constant of generator with high rate of outage. Moreover, the loading level of system before disturbance $L_{0,sys}$ can be selected as a close approximation for L_j.

To accurately estimate the inertia response, considering the impact of loads is vital. In case of any disturbance, the disturbed power, i.e, p_{dist} plus deviation in demand side, i.e., Δp_L is supplied by inertia responses on the online synchronous generators. This means:

$$p_{\mathrm{IR}} = p_{\mathrm{dist}} + \Delta p_{\mathrm{L}}. \tag{5.16}$$

By assuming an efficient voltage control in the entire power system, power deviation of loads can be formulated using frequency deviation and load damping constant:

$$\Delta p_{\mathrm{L}} = \sum_{i=1}^{k} \alpha_i \, p_{L0,i} \Delta \bar{f}_{L,i}. \tag{5.17}$$

As mentioned, frequency is a global parameter in the power system, therefore we can estimate the per-unit frequency deviation of *i*-th load, i.e., $\Delta \bar{f}_{L,i}$ with per-unit angular speed of equivalent center of inertia, i.e., $\Delta \bar{\omega}_m^{CoI}$. By using this approximation and substituting the Eqs. (5.17) and (5.15) into Eq. (5.16) we can calculate the total inertia response as:

$$p_{\mathrm{IR}} = \frac{-\left(\sum_{i=1}^{n} 2H_i S_{b,i}\right) \frac{d}{dt} \bar{\omega}_m^{CoI}}{1 - \frac{2H_j U_h \left(\frac{-d}{dt} \bar{\omega}_m^{CoI}\right)}{L_j} \frac{d}{dt} \bar{\omega}_m^{CoI}} + \sum_{i=1}^{k} \alpha_i \, p_{L0,i} \Delta \bar{\omega}_m^{CoI} \tag{5.18}$$

In the conventional power systems, the power disturbance is supplied by the online synchronous generators which initially provide the Inertia response. Following the inertia response period, the primary control using governors of generators limits the frequency deviation. Therefore, the inertia response estimation should be accomplished before governor's initiation otherwise the right-hand side of the Eq. (5.6) would be unknown. It should be mentioned that in practical application, $\bar{\omega}_m^{CoI}$ cannot be calculated since it requires the availability of the measures of all synchronous machine rotor speeds. However, with wide-area installations of phasor measurement units (PMUs), the online estimation of center of inertia frequency is possible. PMUs

provide voltage and current phasors as well as frequency and its rate of change, which are useful in power system state estimation studies. Transmission system operators, can install PMUs at network buses, and have thus access to the bus frequencies estimated by such PMUs, while the rotor speeds of the synchronous machines are not accessible to them. Online estimation methods utilize measurements of PMUs along with the models of the synchronous machines and their controllers as well as of dynamic loads to estimate center of inertia frequency and rotor speeds of synchronous machines [183].

5.2.2 Decentralized Inertia Response

Following the instantaneous estimation of power disturbance and total inertia response, the steady-state active power set-points for VPPs must be calculated. Assuming that all the generators remain in synchronism, they will slow dawn at approximately the same rate after a few rotor swings and each generator will contribute an amount of power proportional to its inertia. The contribution of *i*-th generator in meeting the power disturbance can be calculate by, [184],

$$\Delta p_i = \frac{M_i}{\sum_{j=1}^{n} M_j} p_{\mathrm{IR}}, \tag{5.19}$$

where $M_i = 2H_i S_{b,i}$. In practice the inertia constant (H_i) is approximately similar for all the synchronous generators except renewable energy power plants which they have zero inertia constant. Therefore, the Eq. (5.19) can be rewritten as

$$\Delta p_{\mathrm{i}} \approx \frac{\mathrm{S_{b,i}}}{\sum_{\mathrm{j=1}}^{\mathrm{n}} \mathrm{S_{b,j}}} \mathrm{p_{IR}}. \tag{5.20}$$

To extend the Eq. (5.20) to a power system with *v* VPPs, we can define a rated power for each VPP and add them to the total system generation capacity connected to the system. Therefore, the target set-point of inertia response for *i*-th VPP can be calculated as

$$p_{\mathrm{set,i}}^{\mathrm{sub}} = \frac{\mathrm{S}_{\mathrm{b,i}}^{\mathrm{VPP}} \beta_i^{\mathrm{vpp}}}{\sum_{\mathrm{j=1}}^{\mathrm{n}} \mathrm{S}_{\mathrm{b,j}} + \sum_{\mathrm{l=1}}^{\mathrm{v}} \mathrm{S}_{\mathrm{b,l}}^{\mathrm{VPP}} \beta_l^{\mathrm{vpp}}} \mathrm{p}_{\mathrm{IR}}. \tag{5.21}$$

where β_i^{vpp} is the VPP participation factor in fast frequency response. The rated power of individual VPP with *m* bus can be obtained by aggregating nominal power of DERs and available controllable loads,

$$S_{b,i}^{\mathrm{VPP}} = \sum_{j=1}^{m} \left(S_{\mathrm{DG},j}^{\max} + S_{\mathrm{ESS},j}^{\max} + S_{\mathrm{L},j}^{\mathrm{flx}} \right). \tag{5.22}$$

5.2.3 VPP Control

In this step, the objective is to control VPP to track the set-point with minimum tracking error at the substation while enforcing distribution network operational constraints such as voltage violation. To this end, we consider following optimization problem:

$$\min_{p,q} D_i \left| p_i^{sub}(p,q) - p_{set,i}^{sub} \right| \tag{5.23a}$$

s.t.

$$f(p_i, q_i, \mathrm{V}_i | \mathrm{Y}_{\mathrm{bus}}) = 0 \tag{5.23b}$$

$$p_i, q_i \in \mathrm{FOR}_i \tag{5.23c}$$

$$0.95 \leq |\mathrm{V}_i| \leq 1.05, \tag{5.23d}$$

where $D_i = 1$ if the VPP requested to track the set-point and $D_i = 0$ otherwise. The constraint (5.23b) represents AC power flow equations, constraint (5.23c) indicates feasible operation reign of DERs in VPP including DGs and ESSs. And constraint (5.23d) represents voltage constraint. The optimization problem with the original power flow equations in (5.23b) is nonlinear. To reduce the complexity and decrease the computational time, the sensitivity matrix derived from power flow equations is used for the grid voltage calculation. Let us consider am *m*-bus LV grid (VPP) with the following power flow equations at bus *k*

$$\begin{cases} p_k = \sum_{i=1}^{m} V_k V_i Y_{ki} \cos(\theta_{ki} + \delta_i - \delta_k) \\ q_k = -\sum_{i=1}^{m} V_k V_i Y_{ki} \sin(\theta_{ki} + \delta_i - \delta_k) \end{cases}, \tag{5.24}$$

where p is active power, q is the reactive power, V is the magnitude of bus voltage, δ is the angle of bus voltage, Y is the magnitude of Y_{bus}, and θ is the angle of Y_{bus}. Expanding these two equations in a Taylor series for the initial estimate, and neglecting all higher order terms, results in the following set of linear equations [185]:

$$\begin{bmatrix} \Delta p \\ \Delta q \end{bmatrix} = \underbrace{\begin{vmatrix} \left[\frac{\partial p}{\partial \delta}\right] & \left[\frac{\partial p}{\partial V}\right] \\ \left[\frac{\partial q}{\partial \delta}\right] & \left[\frac{\partial q}{\partial V}\right] \end{vmatrix}}_{Jacobian} \begin{bmatrix} \Delta \delta \\ \Delta V \end{bmatrix}. \tag{5.25}$$

By solving the Eq. (5.25), the voltage sensitivity matrix can be extracted as follows:

$$\begin{bmatrix} \Delta \delta \\ \Delta V \end{bmatrix} = \begin{vmatrix} S_{\delta p} & S_{\delta q} \\ S_{Vp} & S_{Vq} \end{vmatrix} \begin{bmatrix} \Delta p \\ \Delta q \end{bmatrix}, \tag{5.26}$$

where $S_{\delta p}$ and $S_{\delta q}$ are the sensitivities of bus voltage angles to active and reactive powers, respectively, and S_{Vp} and S_{Vq} are the sensitivities of bus voltage magnitudes. The magnitude of voltage at bus k can be calculated using the following equation:

$$V_k = V_{\text{sub}} + \sum_{i=2}^{m} \left(S_{\text{Vp},k,i} p_i + S_{\text{Vq},k,i} q_i \right), \tag{5.27}$$

where V_{sub} is the voltage magnitude at the substation. Note that in practice the voltage of HV/MV substation of distribution networks is kept fixed, usually by on-line tap changer or FACTS. therefore we can assume that the V_{sub} is known and is equal to the 1 p.u. The constraint

(5.23c) indicates feasible operation reign of DERs in the VPP. Each DER such as BESS or PV systems has its own operational constrains that should be considered in the study.

5.2.3.1 Battery Energy Storage System

An ideal BESS can be modeled with following equations [186],

$$e_i(t) = e_i(t-1) - p_{\mathrm{ESS},i}(t)\Delta t \tag{5.28a}$$

$$c_i\zeta_i^l \le e_i(t) \le c_i\zeta_i^l \tag{5.28b}$$

$$e_i(1) = e_i(t^e), \tag{5.28c}$$

where $e(t)$ is the energy stored in the BESS at time step *t*, $p_{\mathrm{ESS}}(t)$ and $q_{\mathrm{ESS}}(t)$are the active and reactive power outputs of the BESS at time *t*, Δt is the time step length, ζ^l and ζ^u are the maximum and minimum allowed *SoE* levels of the BESS. *c* and S_{ESS} are the reservoir capacity and power rating of the ESS. And finally, t^e is the last time step of the day. Equation (5.28a) represents the *SoE* equation of the ESS. It implies that the amount of stored energy in the BESS reservoir at time *t* depends on its *SoE* in the previous time step and the net energy injected/extracted from it. The maximum and minimum *SoE* limits are modeled by (5.28b). Equation (5.28c) implies that the energy stored in the ESSs at the end of the day have to be identical to its initial value.

5.2.3.2 Distributed Generations

Distributed generators must operate in their feasible operation region. In this regard maximum and minimum power output of DGs should be considered in the VPP optimization.

$$p_{\mathrm{DG},i}^{\min} \le p_{\mathrm{DG},i} \le p_{\mathrm{DG},i}^{\max} \tag{5.29a}$$

$$q_{\mathrm{DG},i}^{\min} \le q_{\mathrm{DG},i} \le q_{\mathrm{DG},i}^{\max} \tag{5.29b}$$

where $p_{\mathrm{DG},i}^{\min}$ and $p_{\mathrm{DG},i}^{\max}$ are minimum and maximum active power, and $q_{\mathrm{DG},i}^{\min}$ and $q_{\mathrm{DG},i}^{\max}$ are minimum and maximum reactive power output of *i*-th DG, respectively.

5.2.3.3 Flexible Loads

Load models are categorized into two groups of flexible and non-flexible loads. It is assumed that the flexible loads can participate in inertia emulation and fast frequency response based on their participation factor, ρ. Demand response constraints of VPP are formulated as [187]

$$p_{\mathrm{L},i} = p_{\mathrm{L0},i}\rho_i \tag{5.29a}$$

$$q_{\mathrm{L},i} = q_{\mathrm{L0},i}\rho_i \tag{5.29b}$$

$$(1 - \rho_i^{min}\Lambda_i) \leq \rho_i \leq (1 - \rho_i^{max}\Lambda_i) \tag{5.29c}$$

where $p_{\mathrm{L0},i}/q_{\mathrm{L0},i}$ and $p_{\mathrm{L},i}/q_{\mathrm{L},i}$ indicate the original and modified active/reactive of load i with demand response perturbation. ρ_i donates variable for changing the load in Eqs. (5.29a) and (5.29b). The constraint (5.29c) models the flexibility degree of load in fast frequency response. ρ_i^{min} and ρ_i^{max} specify the maximum possible decrease and decrease of load in bus i. Λ_i is binary variable which indicates the participation status of load i. If $\Lambda_i = 0$ then the load i does not participate in demand response program and vice versa.

For all DERs including BESSs and DGs, two performance parameters in terms of delay in operation time and time taken to ramp to full power can be considered [188]. The power response of DERs can be approximated with a ramp in power as shown in the Fig. 5.2. The delay time and ramp time is different for different technologies. Among them, BESSs have smaller delay and ramp time, making them as one of the fast response DERs.

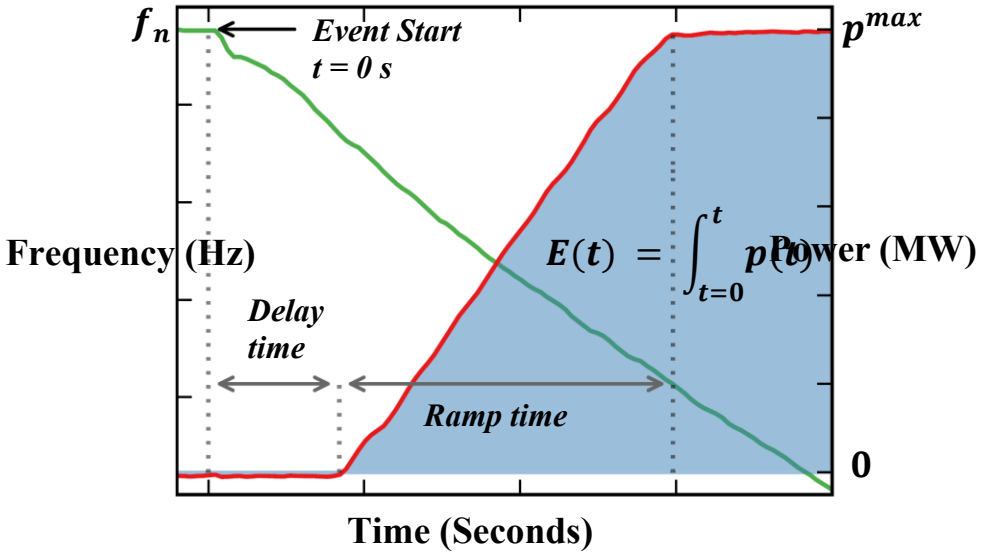

Figure 5.2 Plot of DERs response, displaying start time, delay time and ramp time.

5.2.4 Proposed Framework

Figure 5.3 shows the proposed online architecture to provide fast frequency regulation using aggregated DERs in distribution networks. The framework includes three main stages of inertia estimation, inertia allocation, and VPPs optimization to provide the required fast frequency response. The red dashed box in the framework is considered to act as a disturbance detector. The first three blocks of framework are considered to act as disturbance detector. It examines the angular speed of the equivalent center of inertia with time steps equal to the PMUs measurement rate which is equal to 50 frames per second. The inertia response will be triggered if RoCoF exceeds 100 mHz per second for a time period of delay time. The time constant T_c is added to consider communication delay and operation limits of phasor measurement unit (PMU). According to the IEEE Std. C37.118, PMUs are devices that provide an estimation of the voltage and current synchrophasors, frequency and RoCoF, all based on the common coordinated universal

time reference [189]. A simple and consistent method to estimate frequency is through the phasor time derivation [190]. However, it yields implausible spike in the frequency when voltage angle abruptly jumps due to the electrical transients such as loss of generation events or numerical derivation. This may induce instabilities if the control actions are taken based on it. Averaging over several phase angle samples is used as a simple solution to mitigate undesirable transients' effect, which results in a delay in the frequency estimation [136]. Moreover, in PMU-based WAMS applications, phasor data concentrator (PDC) reporting latency is one of the main design parameters. The PDC reporting latency is composed by the PMU reporting latency, the communication network latency and the PDC latency. Once the disturbance is detected, the total required inertia response will be calculated using Eq. (5.18) in corresponding block. {The time delay of T_p is assumed for corresponding delay in inertia estimation block. The next stage is calculating target setpoints (p_{set}^{sub}) for every VPP using Eq. (5.21) based on the data provided by all the aggregators (VPPs) with time delay of T_s and calculated total inertia response. Next, all the aggregators will receive their target setpoint (p_{set}^{sub}) with their corresponding communication delay, T_a, to optimize their operation dispatch individual DERs to track the commanded target setpoint.

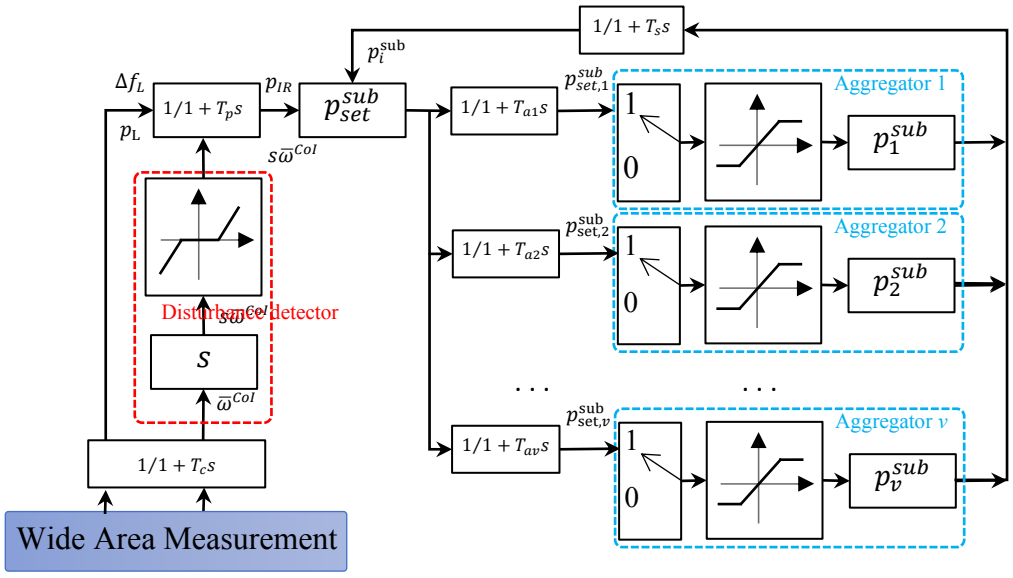

Figure 5.3 Plot of DERs response, displaying start time, delay time and ramp time.

5.3 Numerical results

In this section, the effectiveness of the proposed framework is examined using both IEEE standard cases and AutoSynGrid synthetic cases. In the first scenario the modified IEEE 24-bus system is utilized as transmission network to study the performance of the approach and compare with available studies in the literature. For the second scenario we have utilized synthetic cases to ensure that the proposed framework is applicable to large-scale power grids.

5.3.1 IEEE test case

The single line diagram of the modified IEEE 24-bus system is depicted in Fig. 5.4. The maximum generation capacity and total peak load are 2500 MW and 1646 MW, respectively. Conventional synchronous generators are replaced by renewable energy power plants to achieve different penetration levels of renewable energies. The penetration ratio of renewable energies is defined as $\gamma = \frac{\sum P_{G,RES}^{max}}{\sum P_{G,tot}^{max}}$, where $\sum P_{G,RES}^{max}$ is the total renewable generation capacity and $\sum P_{G,tot}^{max}$ is the total grid generation capacity. By replacing more conventional generators from the original

setting of the network with renewable energy power plants in addition to those already installed, γ is increased to investigate the impacts of higher renewable energy penetration on grid frequency response. To examine the loss of generation event, the generator at bus 13 (G13) with $P_{G13} = 200\ MW$ is tripped off from the grid at t = 1 s in all cases, resulting in a severe frequency decline due to the transient power imbalance and reduced system inertia. Moreover, the VPP is modeled based on the augmented IEEE 69-bus system used in [191], including BESS, DGs and flexible loads. It is considered that every load in the transmission network is able to perform as VPP with a maximum capacity equal to 50% of its load. It is assumed that the BESSs, DGs, and flexible loads compose 60%, 30%, and 10% of VPPs maximum capacity, respectively. It is also assumed that the ramp time of BESSs and DGs are 26 and 5000 milliseconds, respectively. Moreover, the delay times are considered as 5 and 500 milliseconds for BESSs and DGs, respectively [192]. Note that since on/off status is considered for flexible loads, it is also assumed that they will operate simultaneously after time delay of T_a , without any time delay and ramp time. It is also assumed that the participation factor for all the VPPs, β^{vpp}, is equal to 1. The nominal frequency of the system is 60 Hz and the simulation system is developed using Python and PSS/E software.

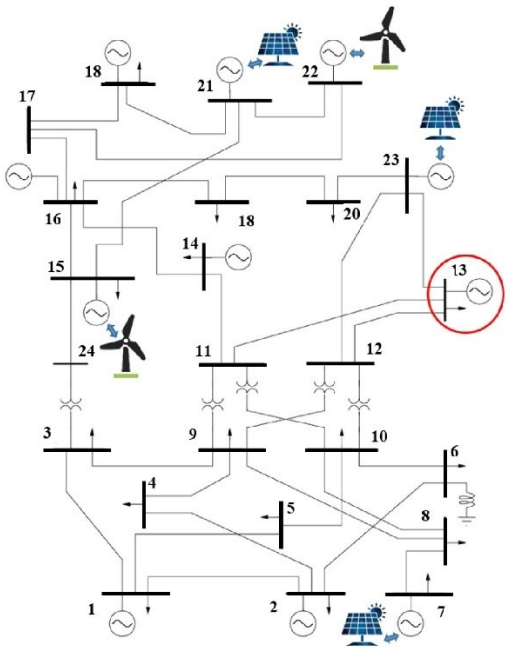

Figure 5.4 Single-line diagram of modified IEEE 24-bus system.

As normal inertia control condition, the test system operates without VPP participation. Figure 5.5 shows the frequency response of the system without VPP control subjected to the loss of generator G13 for different RES penetration ratios. It is assumed that the RES units do not deliver any frequency support. It can clearly be seen that the reduction of synchronous inertia, corresponding to a higher share of RES generation, increases the RoCoF and decreases the nadir frequency. This increased RoCoF can be considered as one of the main barriers to operate a system with low inertia in a safe and reliable way. It not only reduces the time period for the governor control to react before the frequency exceeds thresholds, but it also has an impact on current protection schemes and the operation of synchronous units. If the frequency falls below certain thresholds then the load shedding will accrue, which is costly for system operator and costumers. If the frequency falls too far there is the risk of cascade tripping and localized or system-wide blackouts.

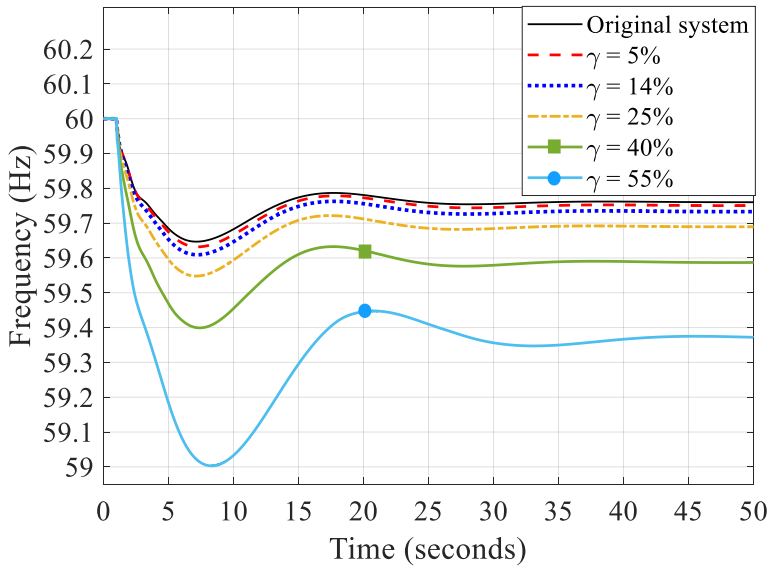

Figure 5.5 Frequency response of the test system without VPP control for generation imbalance.

Displayed in Fig. 5.6 is the estimated inertia, p_{IR}, after the generation imbalance using conventional (Eqs. (5.9)) and proposed method (Eq. (5.18)). Clearly, the estimated values using the proposed method are less than the values that are calculated using the conventional method. The actual p_{IR} with taking into account the load deviation is 199.5 MW. Note that the deviation of load in demand side is negative in case of generation loss. Therefore, the actual p_{IR} should be slightly less than the actual p_{dist} due to the small frequency deviation at the initial time steps. However, the estimated value after the event does not indicate the exact p_{IR}. The unreliability of data measured in the initial moments and also the assumptions that have been made to calculate the p_{IR} are the reasons for the estimation error. The estimated blue trace reaches its maximum after 40 ms following the power disturbance and decreases consequently. This maximum value can be selected as the estimated p_{IR}; however, this will not provide a reliable estimation for two reasons. First, the p_{IR} should be determined based on RoCoF at the event time, not at any later time. Second, estimation based on the maximum p_{IR} results in a larger estimation error, which should be minimized. To tackle this problem, the p_{IR} at the disturbance time is estimated using linear

regression. This method makes our proposed approach robust to the initial transients. The time window of regression is vital for accurate estimation. It starts from a time after the disturbance (termination of initial transient) to a time before turbine governor's initiation which is generally up to 1 second after the event. For the study case, the first governor initiates after 300 milliseconds. However, to have a quick response for inertia emulation the minimum time window should be selected. It is found that 200 milliseconds is the minimum time window that results in acceptable estimation error. Based on the simple linear regression, the estimated p_{IR} using proposed approach is 201.1 MW with estimation error of 0.8%. This value by using the conventional method is 229.3 MW which has the estimation error of 14.9%. As we can see, the estimation error of the proposed approach is about 18 times smaller than that of conventional method.

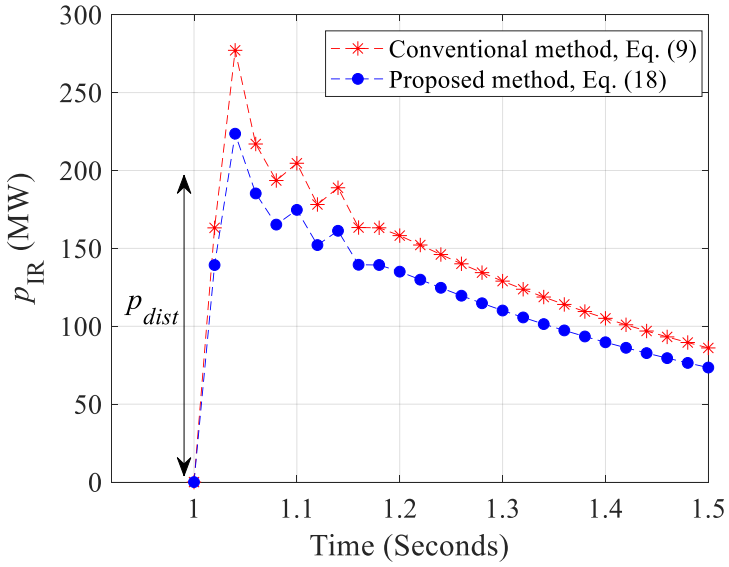

Figure 5.6 Estimated inertia using conventional and the proposed methods.

The performance of p_{IR} estimation algorithms for different disturbances in the test system is provided in Table 5.1. Results show that the proposed approach has considerably smaller estimation errors in comparison with conventional method. In addition, larger power imbalances result in larger error estimations in conventional method. However, proposed method is robust to

the size of power imbalance with estimation errors around 0.70%. Note that it is vital to calculate precise value of inertia for frequency regulation, not only for minimum load shedding, but also for versatile operation of virtual inertia market [193]. Overestimating the required inertia results in additional costs in frequency response market and unnecessary extra investments for inertia improvement. Table 5.1 also shows the additional cost of the market due to the error of inertia estimation. The additional participation costs are calculated based on the present regulation of the Great Britain frequency response market [194]. The payment of participating in the fast frequency response service includes both availability fee (C_{av}) and utilization fee (C_{ut}) per day [195].

$$C_{tot} = C_{av} + C_{ut} \tag{5.31a}$$

$$C_{av} = p_{av}.t_{av}.\pi_{av} \tag{5.31b}$$

$$C_{ut} = p_{ut}.t_{ut}.\pi_{ut}, \tag{5.31c}$$

The availability fee in \$/MWh, is the payment to the service provider to make a certain amount of response service (p_{av}) available for the tendered hours of a day (t_{av}) at availability price of π_{av}. Moreover, the utilization fee in \$/MWh is the payment to the service provider for the utilization volume (p_{ut}) during the tendered hours of a day (t_{ut}) at utilization price of π_{ut}. The utilization volume is the amount of response that has been delivered to the system and it depends on the system frequency changes. The average cost of overestimation with conventional method is \$ 3,114 /day. On the other hand, with proposed method the average overestimation cost is \$152 /day. It should be mentioned that our proposed method also requires additional upgrades and investments including implementation of PMU-based WAMS and low latency communication infrastructure. The total cost of WAMS implementation for complete observability in the study case (IEEE 24-bus system) including PMU, low latency optical fiber communication infrastructure, operation and maintenance costs is reported as \$160,000 [196]. Therefore, the daily

levelized cost of WAMS implementation over 20 years investment period and 5% interest rate using the amortization calculation formula is $35/day [197]. Thus, the final average cost of overestimation for proposed method would be $187/day, which is still significantly less than the conventional method. Error in inertia estimation can also results in unnecessary extra investments. Generally, the performance of a power system in frequency control is assessed for the case of sudden loss of the largest power plant in the system, so-called reference incident [192]. And any further investments in the system to improve the frequency response are done based on the reference incident. Clearly, any error in inertia estimation results in over/underestimation of required investments to improve inertia response. For instance, the largest generator in the case study is Gen15 with generation of 250 MW. Based on the results in Table 5.1, inertia estimation using conventional method results in 20.8% error which overestimates it by 45 MW. The capital cost of BESS utilization in power grid is estimated as $1.4 million/MW by National Renewable Energy Laboratory (NREL) [198]. Therefore, improving the inertia response by implementing solely BESS in the system using the conventional method results in extra $67.5 million in the system investment which is much higher than the implementation cost of WAMS ($160,000) reported in [196]. Note that WAMS not only provides the feasibility for online inertia estimation but also can be used for other applications in monitoring, operation and control of power systems such as system protection, island detection and system restoration.

Table 5.1 Estimation of p_{IR} for different tripping scenarios

		Conventional method				**Proposed method**			
Tripping event	Size (MW)	Estimation (MW)	Overestimation (%)	Overestimation ($\times 10^3\$/day$)	Cost	Estimation (MW)	Overestimation (%)	Overestimation ($\times 10^3\$/day$)	Cost
Gen. @ bus#1	76	81	6.62	0.62		76.6	0.78	0.07	
Gen. @ bus#15	250	295	20.84	5.70		252.2	0.88	0.27	
Gen. @ bus#18	144	162	12.53	2.28		144.3	0.21	0.03	
Gen. @ bus#22	150	171	14.01	2.66		151.4	0.93	0.17	
Gen. @ bus#23	200	234	16.53	4.31		201.8	0.90	0.22	
			$\boldsymbol{\mu}_{\text{con.}}^{\text{over.}} = 14\%$	$\boldsymbol{\mu}_{\text{con.}}^{\text{over. cost}} =$ 3,110 \$/day			$\boldsymbol{\mu}_{\text{prop.}}^{\text{over.}} = 0.74\%$	$\boldsymbol{\mu}_{\text{prop.}}^{\text{over. cost}} =$ 152 \$/day	

As it mentioned, the inertia constant, H_j, and loading level, L_j, of tripped generator are unknown in Eq. (5.18). To address this problem, the inertia constant of generator with high rate of outage and the loading level of system before disturbance are selected as rational approximation. Figure 5.7 shows the sensitivity of estimated p_{IR} to H_j and L_j selection. The horizontal axes represent variations of H_j and L_j with respect to their true values, i.e., 9.4 seconds and 66%. It is found that H_j has a linear relationship with the with p_{IR} estimation error. However, L_j tends to a nonlinear relation. In addition, increasing/decreasing value of H_j / L_j from its true value results in a smaller/larger estimated p_{IR} and the estimation error tends to be negative/positive.

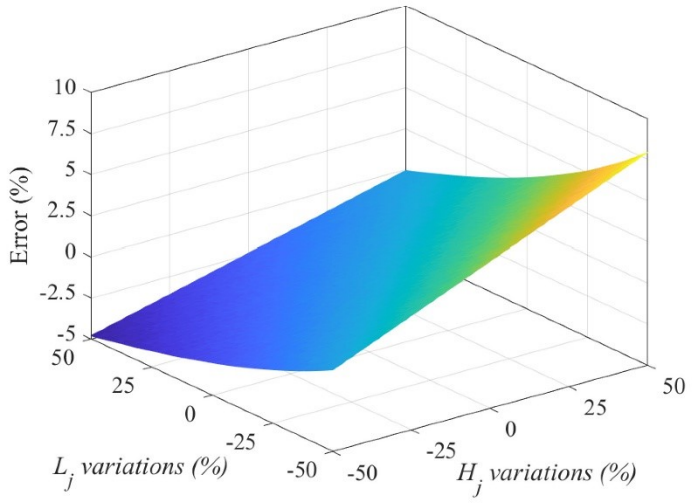

Figure 5.7 Error of p_{IR} estimation with variation of H_j *and* L_j.

Figure 5.8 shows the frequency response of test systems for a fixed RES penetration ratio , $\gamma = 55\%$, and varying total VPP capacity. The total VPP capacity ratio, κ, is defined as $\kappa = \frac{\sum S_b^{VPP}}{\sum S_b^G}$, where $\sum S_b^{VPP}$ and $\sum S_b^G$ are the total rated power of VPPs and generators, respectively. It is observed that VPP operation, with a capacity ratio of 33.1%, improves the frequency deviation by 60%. This improvement is 50% for κ = 16.2%. Note that to void under frequency load shedding which happens at 59.1 Hz, it is required to have more than 1.8% of VPP participation. The participation of VPPs in inertia response reduces both frequency deviation and time to frequency nadir, as it is illustrated in Fig. 5.8. Both of these outcomes are highly desirable. The reduction in frequency nadir reduces the possibility to encounter load shedding or blackouts, while the reduction in time to frequency nadir reduces the required time for VPPs energy delivery and operate at normal condition. Note that, the duration of VPPs energy delivery also plays a vital role to avoid a new frequency nadir. It should be long enough to provide the required time for primary frequency control to takeover and avoid secondary nadir. Fig. 5.8 also demonstrates the effectiveness of proposed approach for RoCoF improvement, particularly the duration of RoCoF

reduction. Improving RoCoF decreases mechanical stress on connected equipment and provides additional time for connected devices especially synchronous generators to respond to the power imbalance, avoiding decoupling relays trip [199]. In addition, as we can see from Fig. 5.8, the frequency nadir is largely determined by the quantity of additional energy delivered to the system before the nadir is reached. Therefore, both VPP capacity ratio and response time are vital for effective fast frequency regulation.

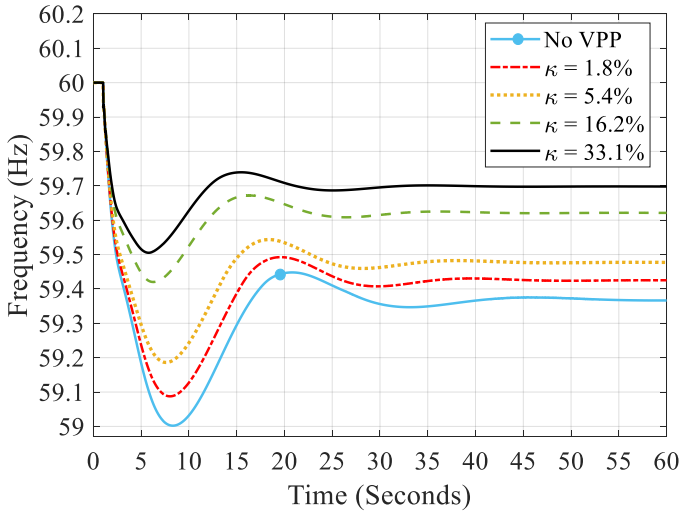

Figure 5.8 Frequency response of the test system with VPP participation for $\gamma = 55\%$.

Clearly, the power delivered as frequency response after the frequency nadir will have no effect on frequency nadir. The frequency regulation components should be fast enough to act swiftly after the power disturbance to avoid large frequency nadir. The ramp time of BESS as the most dominated and effective DER in VPP is investigated in Fig. 5.9. The x-axis (time) is limited to 7 seconds, as the frequency nadir occurs at less than this time under normal operations. Increasing the ramp time of BESS from 26 milliseconds to 2 seconds results in slightly lower frequency nadir in the test system. However, with higher ramp times the system frequency falls quickly, demonstrating the negative impact of higher ramp time on RoCoF. The maximum 400

mHz/s is considered as the critical RoCoF in IEEE Standard C37.118.1 [200], in which the RoCoF relays trip the protected equipments. It is observed the at T_{ramp}^{BESS} = 0.750 seconds the maximum RoCoF is 480 mHz/s. Therefore the maximum ramp time for the BESS to avoid the tripping of the RoCoF relays is T_{ramp}^{BESS} = 0.500 seconds in our studied test case. The VPPs trigger time is also highlighted in the Fig 5.9. The small peak in the blue trace, T_{ramp}^{BESS} = 0.026 seconds, shows the response of BESSs which reaches its maximum value in 26 milliseconds and improves both frequency nadir and RoCoF.

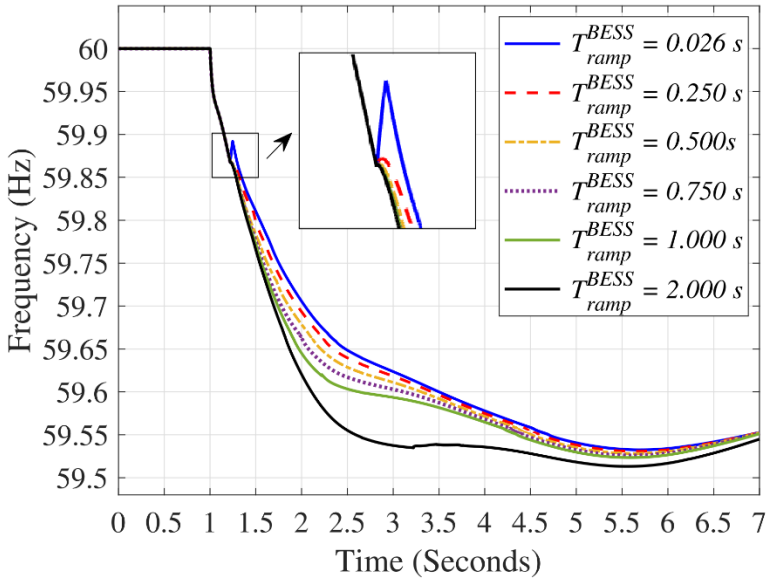

Figure 5.9 Impacts of BESS ramp time on frequency response of the test system.

Time delay is an intrinsic feature of each physical system and the inertia response by VPPs is not an exception. The delay in VPP response for fast frequency regulation mainly includes communication delay and DERs response time delay. In the proposed framework, the aforementioned delay is modeled by T_a. Unlike the small time-delay in local control, in wide-area power systems the time delay can vary from tens to several hundred milliseconds or more [201]. The latency of fiber optic fiber optic digital communication has been reported as approximately

38 milliseconds for one way, while latency using modems via microwave is over 80 milliseconds. Communication systems that entail satellites may have even longer delay, in the order of 500 milliseconds [202].

Figure 5.10 studies the impact of different time delays on inertia response by VPPs. The communication delays between 20 milliseconds and 2 seconds are examined to investigate the performance of the proposed framework. It can be observed that the higher communication delays result in larger frequency deviations and RoCoF. At $T_a = 0.20\,s$ the systems achieve the maximum RoCoF of 386 mHz/s which result will results in tripping the RoCoF relays. Therefore the maximum communication time delay to avoid RoCoF problem is 200 milliseconds. It is also found that the large time delay can cause considerable frequency overshoots in the system. Following a generation/load imbalance, VPPs could have a significant contribution to inertia response and frequency regulation. However, in case the VPP response action is associated with large time delay, during the time delay generators try to compensate the power imbalance, for instance via increasing their generations. Subsequently, when VPP response interferes as a supplementary control and compensates all or a part of the load/generation imbalance, the additional generation, produced during the time delay, may cause considerable frequency overshoots and impose instability to the system performance.

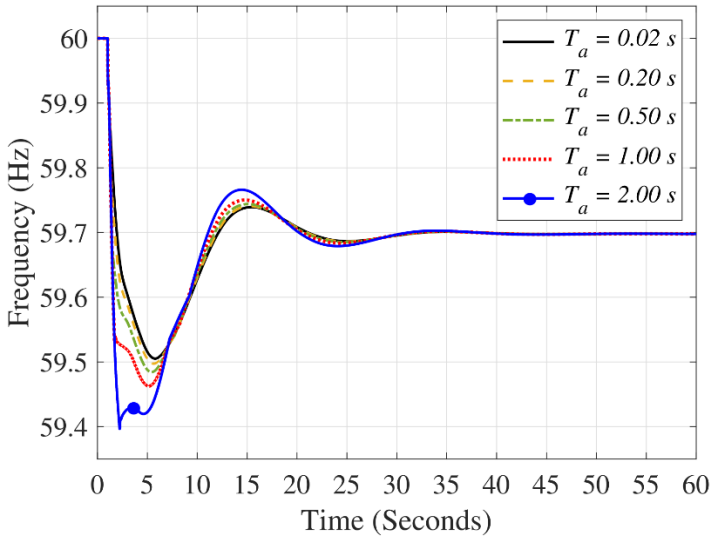

Figure 5.10 Impacts of communication time delay on frequency response of the test system.

5.3.2 Synthetic test cases

Two synthetic grids generated by developed AutoSynGrid toolkit in chapter two are examined in this scenario. The maximum generation capacity and total peak load of AutoSynGrid-100 are 7.94 GW and 5.49 GW, respectively. For AutoSynGrid-200 these values are 19.53 GW and 11.94 GW respectively. In both cases the loss of generation event happens at t = 1 second, tripping the generator at bus 78 (G78) with $P_{G78} = 595\ MW$ in AutoSunGrid-100 and the generator G147 with generation of $P_{G147} = 894\ MW$ in AutoSynGrid-200. To drive comparable results with previous section, the augmented IEEE 69-bus system is utilized as VPP for both synthetic cases. It is considered that every load in the synthetic cases is able to perform as VPP with a maximum capacity equal to 50% of its load. Similar to the previous scenario, it is assumed that the BESSs, DGs, and flexible loads compose 60%, 30%, and 10% of VPPs maximum capacity, respectively. And the participation factor for all the VPPs, β^{vpp}, is equal to 1. Figure 5.11 shows the frequency response of both synthetic grids without VPP participation to loss of generator in different penetration ratio of RES. Similar to the IEEE standard case, reduction of synchronous inertia due

to higher share of RES generation in large-scale synthetic cases increases the RoCoF and decreases the nadir frequency. However, it can be seen that the critical frequency drop happens in slightly higher penetration of RES for larger cases. For instance, 24-bus system reaches the frequency nadir of 59 Hz at RES penetration of 55%; however, 60% of RES penetration results in frequency nadir of 59.05 Hz in 200-bus synthetic grid. Another point is the higher resiliency of the power grids at lower RES penetrations.

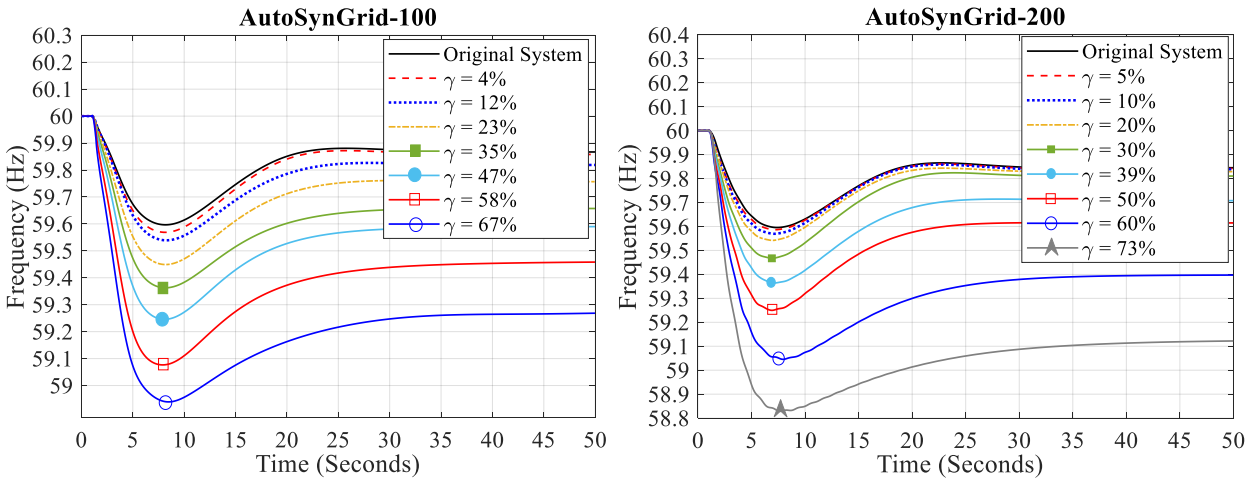

Figure 5.11 Frequency response of large-scale synthetic grids without VPP control for generation imbalance..

The p_{IR} estimation of proposed and conventional methods for different disturbances in the large-scale synthetic cases are provided in Table 5.2. Results show that the proposed approach has considerably smaller estimation errors in comparison with conventional method in large-scale power grids. Despite the size of network, the proposed method is robust to the size of power imbalance and has estimation errors around 0.75%. Table 5.2 also shows the additional cost of the market due to the error of inertia estimation. The average costs of overestimation with conventional method for AutoSynGrid-100 and AutoSynGrid-200 are \$7,501/day and \$11,223/day, respectively. By increasing the size of the network which requires larger generators, the average cost of overestimation increases in conventional method. On the other hand, with proposed method the average overestimation costs are \$268/day and \$274/day for AutoSynGrid-100 and

AutoSynGrid-200, respectively. The total costs of WAMS implementation in the worst case without optimal placement are approximately $670 \times 10^3\$/\text{day}$ and $1400 \times 10^3\$/\text{day}$ for AutoSynGrid-100 and AutoSynGrid-200, respectively. The daily levelized cost of WAMS implementation over 20 years investment period and 5% interest rate using the amortization calculation formula are \$146/day and \$306/day. Therefore, the final average cost of overestimation for proposed method would be \$414/day and \$580/day for AutoSynGrid-100 and AutoSynGrid-200, respectively, which are still significantly less than the conventional method.

Table 5.2 Estimation of p_{IR} for different tripping scenarios in AutoSynGrid cases

			Conventional method				**Proposed method**			
	Tripping event	Size (MW)	Estimation (MW)	Overestimation (%)	Overestimation ($\times 10^3\$/day$)	Cost	Estimation (MW)	Overestimation (%)	Overestimation ($\times 10^3\$/day$)	Cost
AutoSynGrid-100	Gen. @ bus#2	413	512.9	24.2	12.6		416.9	0.94	0.49	
	Gen. @ bus#33	114	126.8	11.3	1.6		114.3	0.26	0.04	
	Gen. @ bus#70	247	292.9	18.6	5.8		248.7	0.68	0.21	
	Gen. @ bus#90	89	95.3	7.1	0.8		89.7	0.84	0.09	
	Gen. @ bus#94	527	659.8	25.2	16.7		531.1	0.77	0.51	
AutoSynGrid-200	Gen. @ bus#4	220	262.0	19.1	5.3		221.6	0.73	0.20	
	Gen. @ bus#13	518	646.5	24.8	16.2		520.3	0.44	0.28	
	Gen. @ bus#100	442	550.3	24.5	13.7		446.0	0.9	0.50	
	Gen. @ bus#144	179	201.9	12.8	2.9		180.0	0.56	0.12	
	Gen. @ bus#161	568	710.6	25.1	18.0		570.2	0.38	0.27	
				$\boldsymbol{\mu}_{\text{con.}}^{\text{over.}} = 19\%$				$\boldsymbol{\mu}_{\text{prop.}}^{\text{over.}} = 0.7\%$		

Figure 5.12 shows the frequency response of test systems for a fixed RES penetration ratio, $\gamma = 58\%$ for AutoSynGrid-100 and $\gamma = 60\%$ for AutoSynGrid-200, and varying total VPP capacity. The participation of VPPs in inertia response reduces both frequency deviation and time to frequency nadir, as it is illustrated in Fig. 5.12. Both of these outcomes are highly desirable. The reduction in frequency nadir reduces the possibility to encounter load shedding or blackouts, while

the reduction in time to frequency nadir reduces the required time for VPPs energy delivery and operate at normal condition. For both synthetic cases participating VPPs in fast frequency response improves the frequency nadir. For AutoSynGrid-100, only 2.5% of VPP penetration can provide enough inertia response to avoid the critical frequency and load shedding. However, AutoSynGrid-200 the minimum VPP penetration to avoid load shedding is 5.4% of VPP participation. Comparing the results of IEEE 24-bus system with large-scale synthetic grids shows that all the networks can accommodate 50% of renewable energy penetration without facing large frequency nadirs in case of loss of generator. However, larger networks show slightly better performance in case of hosting higher renewable energy penetration. For instance, AutoSynGrid-200 reached the critical frequency of 59.1 Hz for underfrequency load shedding around 60% of penetration level. However, to improve the frequency nadir they require higher participation ratios of VPPs.

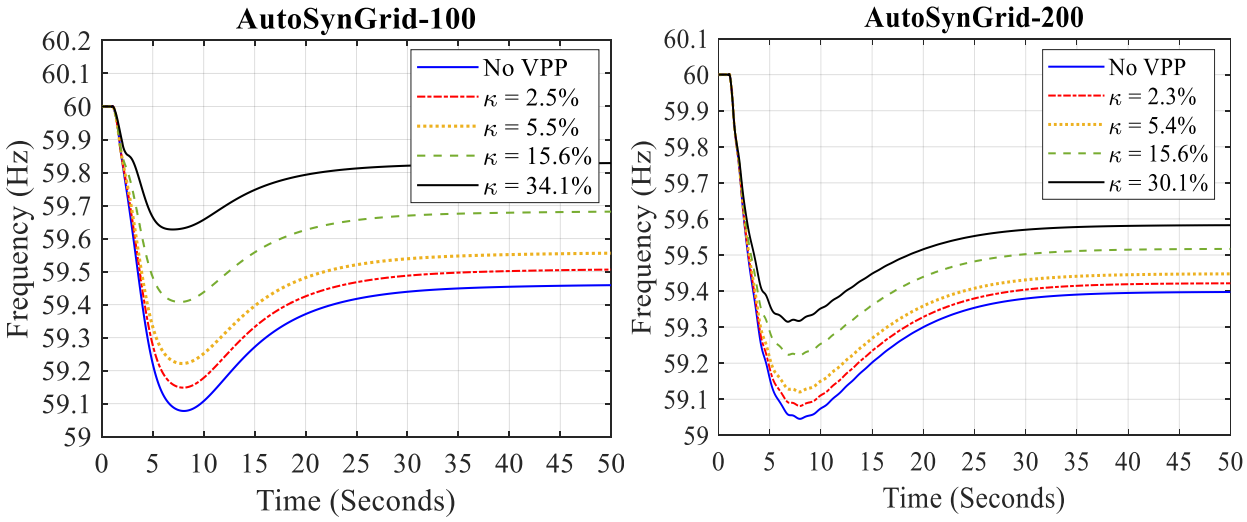

Figure 5.12 Frequency response of large-scale synthetic grids with VPP participation.

5.4 Summary

In this chapter, an inertia response framework was developed to investigate the potential of aggregated DERs in distribution networks for fast frequency regulation. To have an accurate estimation of disturbance and system inertia in case of a load/generation imbalance, an online power disturbance estimation was proposed by introducing new terms in the swing equation. Results showed that the proposed approach has considerably smaller estimation errors in comparison with conventional method in large-scale power grids also. Despite the size of network, the proposed method is robust to the size of power imbalance and has estimation errors around 0.7%. In addition, a real-time optimization framework was developed to control aggregated DERs in a distribution network. It guarantees the fast response of DERs in their feasible operation region while satisfying network operational constraints. Moreover, VPP participation factor and decentralized inertia control were introduced to allocate the active power set-points of VPPs in the power system. It is found that the participation of VPPs in inertia response reduces both frequency deviation and time to frequency nadir. Results showed that the proposed approach has considerably smaller estimation errors in comparison with conventional method. In addition, larger power imbalances result in larger error estimations in conventional method. However, proposed method is robust to the size of power imbalance with estimation errors around 0.70%. It was found that the average cost of overestimation with conventional method is $ 3,114 /day; however, with proposed method the average overestimation cost is $187/day, which is significantly less than the conventional method. It was observed that virtual power plant operation, with a capacity ratio , κ, of 33.1%, improves the frequency deviation by 60%. This improvement is 50% for κ = 16.2%. Moreover, it was found that it is not required to utilize inertia response in all the cases with renewable energy penetration less than 50%. The maximum renewable energy penetration level that system can accommodate without facing problems in frequency nadir increases with

increasing the network size. In addition, it was found that the minimum ramp time for BESS to improve frequency response in our proposed VPP inertia emulation is 500 milliseconds. On the other hand, it was observed that the minimum communication time delay of VPP to participate in inertia response is 200 milliseconds.

6. Overall conclusions and future work

6.1 Conclusion

The objective of this dissertation was to investigate the impediments for renewable energy integration in both transmission and distribution networks and propose novel approaches and frameworks to help to increase hosting capacity and improve inertia response to ensure an efficient and reliable power system with high penetration of renewable energies. We have developed tools and frameworks to facilitate implementation of erratic renewable energy resources in all sections of power grids including generation, transmission and distribution. All the new methods and solutions to address negative impacts of renewable energies should be validated using realistic test cases. However, existing power system models that could be used to test new concepts and methods are mostly dated or insufficient. Therefore, as the first objective, a new framework was developed to generate any number of test cases featuring the same statistical properties of realistic power grids. We proposed a complete framework to generate synthetic power grids and introduced a toolkit based on MATLAB GUI with interactive input/output interface. The proposed AutoSynGrid toolkit is able to generate any number of synthetic power grids with given network size featuring statistical properties of realistic power grids. The generated synthetic cases include data of the system MVA base, bus data, generator data, branch data, generator cost data, type of generators, and fuel types, providing sufficient data that can be used for a variety of analysis such as power flow and optimal power flow studies. Moreover, a full validation process was proposed to assure that the generated synthetic cases satisfy the predefined criteria of multiple metrics that were observed from realistic power grids. Five categories of topology metrics, electrical parameters, state variables, interdependency, and scaling properties were considered as validation metrics to determine how realistic the resulting cases are. It was found that the size of the network has a direct impact on realism of the network in two way. First, by increasing the network size it

is more feasible to generate synthetic grids with high closeness factor. Second, it is more feasible to mimic the characteristics of a reference system with similar network size than a reference system with higher network size difference. Moreover, in synthetic grid modelling it is important to have different layers of information, i.e. bus types, generation settings, etc. in a synthetic grid but it is vital to generate and assign this information in a validated systematic approach. And totally random generation and assignment do not result in a acceptable test case The AutoSynGrid generates the synthetic power grids in MATPOWER format allowing to use the MATPOWER open source package to further studies on the generated cases. The final version of the AutoSynGrid toolkit will be released to the public at VCU's Electric Power and Energy Systems (EPES) laboratory webpage.

Then we focused on integration of small-scale PV systems in the distribution networks to appropriately examine maximum PV installation capacity and propose solutions to improve hosting capacity. A detailed impact assessment framework was proposed to assess the impacts of DPV on a realistic distribution network. Two DPV installation schemes namely customer-based and utility-aided installations were considered. For customer-based installation, a set of Monte Carlo experiments designed to model free installation of DPVs in the network. A multi-objective optimization problem was developed for utility-aided installation to optimize the size and location of aggregated DPVs with the objectives of minimum voltage deviation, voltage fluctuation, total energy loss and eliminating voltage violation and reverse power flow. To perform an accurate impact assessment, solar insolation of all the buildings in the studied area was studied to estimate the DPV installation potential of the distribution network. In addition, we developed synthetic load profile modeling to generate synthetic load profiles based on available realistic load profiles for each building in the network. The framework was applied to a local distribution network. It was

found that for higher CDFs starting from $\beta_{\min}$=0.5 there is not a significant difference in the probability of reverse power flow occurrence. Moreover, it was observed that it is more likely to have a voltage violation in residential feeders. Unlike the general commercial energy-use pattern, which has a good correlation with typical PV power profile, residential energy-use pattern presents a peak value during the nighttime when there is a small or no PV generation resulting in surplus PV generation at noon and initiating reverse power flow and voltage rise. It was also found that with customer-based installation in the studied network, beyond 30% of DPV penetration the network operator needs necessary upgrades in the network to avoid overvoltage and severe reveres power flows. However, by utility-aided installation the network can accommodate 50% of DPV penetration without having overvoltage and reverse power flows and need to system upgrades. It is clear that there will be a tradeoff between network planning by utilities and costs of network upgrades. Distribution network operators can eliminate or postpone system upgrades with interfering in customer decisions in DPV installation to minimize system operation and upgrade costs. In addition, it is shown that utility-based installation can decrees the energy loss in the system by 11.3% at 20% of penetration ratio. Comparing the utility-based and customer-based DPV installations indicates that when the system has a medium renewable penetration ratio, an optimal installation is necessary because it will bring significant improvements in energy loss reduction, voltage fluctuation, and voltage deviation. However, when the renewable integration ratio is lower or very high, there will be less difference between the types of installation.

In addition, demand side management of smart homes as one of the viable solutions to improve hosting capacity was examined. To this end, the interaction of demand side management strategies with rooftop PV systems and novel algorithms to increase renewable energy utilization without negative impacts was investigated. We examined the decentralized DSM strategy for both

commercial and residential loads in a radial distribution network with rooftop PV installation, and compares its impacts and performance in terms of customer benefits and distribution network operation. Customer benefits were measured as electricity cost savings with manageable sacrifice of convenience and for the distribution network operation, PV utilization, system real power loss, and voltage fluctuation are considered. It was found that the PV utilization efficiency can be improved from 68% to 98% by utilizing proposed DSM algorithm. However, with higher penalty price, i.e. $\pi_p = 3$ ¢/kWh for load shifts the PV utilization efficiency drops to 76%. Note that the increasing the PV utilization efficiency results in improving the hosting capacity of the network by eliminating backfeed power to the network due to surplus rooftop PV generation. As we observed in the previous chapter, the reverse power flow has a strong relationship with overvoltage in the system. Therefore, minimizing the reverse power flow with increasing PV utilization efficiency improves the total husting capacity of the network. It was also observed that higher demand side management participations will tend to "flatten" the voltage profile and bring better improvement to voltage fluctuations caused by load variations. It was found that residential DSM, if implemented in a decentralized optimization, exhibits better performance than the commercial DSM in terms of all the four aforementioned measures. In fact, for the commercial customers due to their high load profile, the only cost minimization is not suitable for the DSM objective function and the distribution network operation constraints should be considered. For the decentralized DSM, residential DSM usually yields better electricity cost savings due to their higher electricity price. It also results in more improvements in PV usage efficiency, energy loss reduction, and voltage fluctuation. The simulations also indicated that the decentralized commercial DSM may even introduce negative impacts on system energy loss and voltage fluctuation. This implies that coordinated DSM optimization is necessary for commercial loads.

In the last objective, we investigated low inertia of power system due to the high penetration of large-scale renewable energies in the transmission networks. We combined the previous findings of this dissertation and proposed a novel framework to address the low inertia, as one of the most important challenges of power grids with high penetration of renewable energies. An online framework to provide inertia emulation and fast frequency response using aggregated DERs was developed. A precise inertia estimation method was proposed by introducing new terms in the swing equation to have an accurate estimation of required system inertia in case of a large generator/load imbalance. The reduction of inertia due to the loss of unknown generator along with load deviation due to frequency deviation were considered to have a more accurate estimation of required inertia. Moreover, a distributed inertia control was developed to efficiently allocate inertia response to the available VPPs. In addition, a real-time optimization framework was proposed to control aggregated DERs in the active distribution network to reliably and securely emulate inertia response. The objective of DERs optimization was to track the set-point with minimum tracking error at the substation while enforcing distribution network operational constraints along with the feasible operation region of DERs. The performance of the proposed framework was verified using modified IEEE 24-bus and 69-bus systems. Our simulation results showed that the proposed approach has considerably smaller estimation errors in comparison with conventional method. In addition, larger power imbalances result in larger error estimations in conventional method. However, proposed method is robust to the size of power imbalance with estimation errors around 0.70%. It was found that the average cost of overestimation with conventional method is $ 3,114 /day; however, with proposed method the average overestimation cost is $187/day, which is significantly less than the conventional method. It was observed that virtual power plant operation, with a capacity ratio , κ, of 33.1%, improves the frequency deviation by 60%. This improvement

is 50% for $\kappa = 16.2\%$. Moreover, it was found that it is not required to utilize inertia response in all the cases with renewable energy penetration less than 50%. The maximum renewable energy penetration level that system can accommodate without facing problems in frequency nadir increases with increasing the network size. In addition, it was found that the minimum ramp time for BESS to improve frequency response in our proposed VPP inertia emulation is 500 milliseconds. On the other hand, it was observed that the minimum communication time delay of VPP to participate in inertia response is 200 milliseconds. The investigation on communication delay time showed that as the time delay increase, the power system may experience considerable frequency overshoots and impose instability on the power system.

6.2 Future works

The work that is presented in this dissertation can be extended, by pursuing a number of directions such as:

- Develop a framework to generate combined transmission and distribution synthetic network models. These models can be used to analyze the interactions between transmission and multiple distribution systems, such as the provision of ancillary services by active distribution grids, the co-optimization of planning and operation, the development of emergency control and protection schemes spanning over different voltage levels, the analysis of combined market aspects, etc.
- Annual analysis along with economic analysis of customer-based PV systems to suggest the best strategy for distributed PV installation.
- Study the fast dynamics of renewable distributed generation and their impacts on the voltage regulations and transient stability of distribution networks.

- Develop a framework for distribution network operator or aggregator to utilize the electric vehicles' storages in the demand side management. Demand side management algorithm can optimize total costs by modifying electric vehicles' charging/discharging schedules.
- Considering electricity market in inertia response of VPPs. A participation algorithm may be developed to coordinate the exchange power between the he multi-VPP and the main grid with objective of minimum cost for power grid operator and maximum profit for VPPs.

References

[1] "U.S. Solar Market Insight | SEIA." [Online]. Available: https://www.seia.org/us-solar-market-insight. [Accessed: 02-Apr-2019].

[2] Z. Wang, S. H. Elyas, and R. J. Thomas, "A novel measure to characterize bus type assignments of realistic power grids," *2015 IEEE Eindhoven PowerTech, PowerTech 2015*, 2015.

[3] R. D. Zimmerman, C. E. Murillo-Sanchez, and R. J. Thomas, "MATPOWER: Steady-State Operations, Planning, and Analysis Tools for Power Systems Research and Education," *IEEE Trans. Power Syst.*, vol. 26, no. 1, pp. 12–19, 2011.

[4] F. P. Vahl, R. Rüther, and N. Casarotto Filho, "The influence of distributed generation penetration levels on energy markets," *Energy Policy*, vol. 62, pp. 226–235, 2013.

[5] T. Ackermann and T. Ackermann, "Distributed Generation : A Definition Distributed generation : a definition," vol. 7796, no. August 2016, pp. 195–204, 2001.

[6] A. Colmenar-Santos, C. Reino-Rio, D. Borge-Diez, and E. Collado-Fernández, "Distributed generation: A review of factors that can contribute most to achieve a scenario of DG units embedded in the new distribution networks," *Renew. Sustain. Energy Rev.*, vol. 59, pp. 1130–1148, 2016.

[7] W. H. Kersting, *Distribution system modeling and analysis*. CRC press, 2006.

[8] U. Sultana, A. B. Khairuddin, M. M. Aman, A. S. Mokhtar, and N. Zareen, "A review of optimum DG placement based on minimization of power losses and voltage stability enhancement of distribution system," *Renew. Sustain. Energy Rev.*, vol. 63, pp. 363–378, 2016.

[9] M. M. Aman, G. B. Jasmon, H. Mokhlis, and A. H. A. Bakar, "Optimal placement and sizing of a DG based on a new power stability index and line losses," *Int. J. Electr. Power Energy Syst.*, vol. 43, no. 1, pp. 1296–1304, 2012.

[10] M. M. Aman, G. B. Jasmon, A. H. A. Bakar, and H. Mokhlis, "A new approach for optimum DG placement and sizing based on voltage stability maximization and minimization of power losses," *Energy Convers. Manag.*, vol. 70, pp. 202–210, 2013.

[11] W. M. da Rosa, J. C. Teixeira, and E. A. Belati, "New method for optimal allocation of distribution generation aimed at active losses reduction," *Renew. Energy*, vol. 123, pp. 334–341, 2018.

[12] U. Eminoglu and M. H. Hocaoglu, "A voltage stability index for radial distribution networks," *2007 42nd Int. Univ. Power Eng. Conf.*, pp. 408–413, 2007.

[13] A. Keane *et al.*, "State-of-the-art techniques and challenges ahead for distributed generation planning and optimization," *IEEE Trans. Power Syst.*, vol. 28, no. 2, pp. 1493–1502, 2013.

[14] A. Ameli, M. R. Farrokhifard, E. Davari-Nejad, H. Oraee, and M. R. Haghifam, "Profit-based DG planning considering environmental and operational issues: A multiobjective approach," *IEEE Syst. J.*, vol. PP, no. 99, pp. 1–12, 2015.

[15] S. Hashemi and J. Østergaard, "Methods and strategies for overvoltage prevention in low voltage distribution systems with PV," *IET Renew. Power Gener.*, vol. 11, no. 2, pp. 205–214, 2016.

[16] P. Mohammadi and S. Mehraeen, "Challenges of PV Integration in Low-Voltage Secondary Networks," *IEEE Trans. Power Deliv.*, vol. 32, no. 1, pp. 1–1, 2016.

[17] P. P. Barker and R. W. De Mello, "Determining the impact of distributed generation on power systems. I. Radial distribution systems," *Power Eng. Soc. Summer Meet. 2000. IEEE*, vol. 3, no. c, pp. 1645–1656 vol. 3, 2000.

[18] M. A. Eltawil and Z. Zhao, "Grid-connected photovoltaic power systems: Technical and potential problems—A review," *Renew. Sustain. Energy Rev.*, vol. 14, no. 1, pp. 112–129, 2010.

[19] A. Rabiee and S. M. Mohseni-Bonab, "Maximizing hosting capacity of renewable energy sources in distribution networks: A multi-objective and scenario-based approach," *Energy*, vol. 120, pp. 417–430, 2017.

[20] L. K. Estorque and M. Pedrasa, "Utility-scale DG Planning using Location-specific Hosting Capacity Analysis," pp. 1–6, 2016.

[21] V. Quintero-Molina, M. Romero-L, and A. Pavas, "Assessment of the hosting capacity in distribution networks with different DG location," *2017 IEEE Manchester PowerTech, Powertech 2017*, 2017.

[22] P. Denholm, K. Clark, and M. O'Connell, "On the Path to SunShot: Emerging Issues and Challenges in Integrating Solar with the Distribution System," *Natl. Renew. Energy Lab.*, no. May, p. 55, 2016.

[23] R. Meeker *et al.*, "High Penetration Solar PV Deployment Sunshine State Solar Grid Initiative (SUNGRIN) Final Report," 2015.

[24] S. M. Ismael, S. H. E. Abdel Aleem, A. Y. Abdelaziz, and A. F. Zobaa, "State-of-the-art of hosting capacity in modern power systems with distributed generation," *Renew. Energy*, vol. 130, pp. 1002–1020, 2019.

[25] P. H. Divshali and L. Söder, "Improving Hosting Capacity of Rooftop PVs by Quadratic Control of an LV-Central BSS," vol. 3053, no. c, pp. 1–9, 2017.

[26] F. Ding and B. Mather, "On Distributed PV Hosting Capacity Estimation, Sensitivity Study, and Improvement," *IEEE Trans. Sustain. Energy*, vol. 8, no. 3, pp. 1010–1020, 2017.

[27] J. Seuss, M. J. Reno, R. J. Broderick, and S. Grijalva, "Improving distribution network PV hosting capacity via smart inverter reactive power support," *IEEE Power Energy Soc. Gen. Meet.*, vol. 2015-Septe, no. 1, pp. 0–4, 2015.

[28] Accenture consulting, "Power Surge Ahead; How Distribution Utilities Can Get Smart with

Distributed Generation," 2017.

[29] N. E. M. Association, *American National Standard for Electric Power Systems and Equipment-Voltage Ratings (60 Hertz)*. National Electrical Manufacturers Association, 2016.

[30] P. Palensky and D. Dietrich, "Demand side management: Demand response, intelligent energy systems, and smart loads," *IEEE Trans. Ind. Informatics*, vol. 7, no. 3, pp. 381–388, 2011.

[31] E. Yao, P. Samadi, V. W. S. Wong, and R. Schober, "Residential Demand Side Management Under High Penetration of Rooftop Photovoltaic Units," *IEEE Trans. Smart Grid*, vol. 7, no. 3, pp. 1597–1608, 2015.

[32] H. Shakouri G. and A. Kazemi, "Multi-objective cost-load optimization for demand side management of a residential area in smart grids," *Sustain. Cities Soc.*, vol. 32, pp. 171–180, 2017.

[33] S. M. Alhejaj and F. M. Gonzalez-Longatt, "Impact of inertia emulation control of grid-scale BESS on power system frequency response," *2016 Int. Conf. Students Appl. Eng. ICSAE 2016*, pp. 254–258, 2017.

[34] V. Knap, S. K. Chaudhary, D. Stroe, M. Swierczynski, B. Craciun, and R. Teodorescu, "Sizing of an Energy Storage System for Grid Inertial Response and Primary Frequency Reserve," vol. 31, no. 5, pp. 3447–3456, 2016.

[35] H. Karbouj, Z. H. Rather, D. Flynn, and H. W. Qazi, "Non-synchronous fast frequency reserves in renewable energy integrated power systems: A critical review," *Int. J. Electr. Power Energy Syst.*, vol. 106, no. November 2018, pp. 488–501, 2019.

[36] G. A. Pagani and M. Aiello, "The Power Grid as a complex network: A survey," *Phys. A Stat. Mech. its Appl.*, vol. 392, no. 11, pp. 2688–2700, 2013.

[37] S. Soltan and G. Zussman, "Generation of Synthetic SpSpatial Embedded Power Grid Networks," in *Power and Energy Society General Meeting (PESGM)*, 2016.

[38] T. Xu, A. B. Birchfield, K. M. Gegner, K. S. Shetye, and T. J. Overbye, "Application of Large-Scale Synthetic Power System Models for Energy Economic Studies," pp. 3123–3129, 2017.

[39] A. B. Birchfield, T. Xu, K. M. Gegner, K. S. Shetye, and T. J. Overbye, "Grid Structural Characteristics as Validation Criteria for Synthetic Networks," *IEEE Trans. Power Syst.*, vol. 32, no. 4, pp. 3258–3265, 2017.

[40] K. M. Gegner, A. B. Birchfield, T. Xu, K. S. Shetye, and T. J. Overbye, "A methodology for the creation of geographically realistic synthetic power flow models," *2016 IEEE Power Energy Conf. Illinois, PECI 2016*, pp. 1–6, 2016.

[41] A. B. Birchfield, K. M. Gegner, T. Xu, K. S. Shetye, and T. J. Overbye, "Statistical Considerations in the Creation of Realistic Synthetic Power Grids for Geomagnetic Disturbance Studies," *IEEE Trans. Power Syst.*, vol. 32, no. 2, pp. 1502–1510, 2017.

[42] “Electric Grid Test Case Repository.” [Online]. Available: https://electricgrids.engr.tamu.edu/. [Accessed: 02-Jan-2018].

[43] D. Krishnamurthy, W. Li, and L. Tesfatsion, “An 8-Zone Test System Based on ISO New England Data: Development and Application,” *IEEE Trans. Power Syst.*, vol. 31, no. 1, pp. 234–246, 2015.

[44] N. Pilatte, P. Aristidou, and G. Hug, “TDNetGen: An Open-Source, Parametrizable, Large-Scale, Transmission, and Distribution Test System,” *IEEE Syst. J.*, pp. 1–9, 2017.

[45] E. Cotilla-Sanchez, P. D. H. Hines, C. Barrows, and S. Blumsack, “Comparing the topological and electrical structure of the North American electric power infrastructure,” *IEEE Syst. J.*, vol. 6, no. 4, pp. 616–626, 2012.

[46] D. Ciechanowicz, D. Pelzer, B. Bartenschlager, and A. Knoll, “A modular power system planning and power flow simulation framework for generating and evaluating power network models,” *IEEE Trans. Power Syst.*, vol. 32, no. 3, pp. 2214–2224, 2017.

[47] H. Sadeghian and Z. Wang, “AutoSynGrid: A MATLAB-based toolkit for automatic generation of synthetic power grids,” *Int. J. Electr. Power Energy Syst.*, vol. 118, no. November 2019, p. 105757, 2020.

[48] V. Krishnan *et al.*, “Validation of Synthetic U.S. Electric Power Distribution System Data Sets,” *IEEE Trans. Smart Grid*, vol. 3053, no. c, pp. 1–1, 2020.

[49] C. Coffrin, D. Gordon, and P. Scott, “NESTA, The NICTA Energy System Test Case Archive,” pp. 1–26, 2014.

[50] D. J. Watts and S. H. Strogatz, “Collectivedynamics of ‘small-world’ networks,” *Nature*, vol. 393, no. 6684, pp. 440–442, 1998.

[51] Z. Wang, A. Scaglione, and R. J. Thomas, “Generating statistically correct random topologies for testing smart grid communication and control networks,” *IEEE Trans. Smart Grid*, vol. 1, no. 1, pp. 28–39, 2010.

[52] Z. Wang, R. J. Thomas, and A. Scaglione, “Generating random topology power grids,” *Proc. Annu. Hawaii Int. Conf. Syst. Sci.*, pp. 1–9, 2008.

[53] S. H. Elyas, Z. Wang, and R. J. Thomas, “On Statistical Size and Placement of Generation and Load for Synthetic Grid Modeling,” *10th Bulk Power Syst. Dyn. Control Symp. - (IREP 2017)*, 2017.

[54] Z. Wang and S. H. Elyas, “On the Scaling Property of Power Grids,” *Hawaii Int. Conf. Syst. Sci. HICSS*, pp. 3148–3155, 2017.

[55] Z. Wang and R. J. Thomas, “On bus type assignments in random topology power grid models,” *Proc. Annu. Hawaii Int. Conf. Syst. Sci.*, vol. 2015-March, pp. 2671–2679, 2015.

[56] S. H. Elyas and Z. Wang, “A multi-objective optimization algorithm for bus type assignments in random topology power grid model,” *Proc. Annu. Hawaii Int. Conf. Syst. Sci.*, vol. 2016-March, pp. 2446–2455, 2016.

[57] H. Sadeghian, S. H. Elyas, and Z. Wang, “A Novel Algorithm for Statistical Assignment of

Transmission Capacities in Synthetic Grid Modeling," in *IEEE Power and Energy Society General Meeting*, 2018.

[58] S. H. Elyas and Z. Wang, "Improved Synthetic Power Grid Modeling With Correlated Bus Type Assignments," *IEEE Trans. Power Syst.*, vol. 32, no. 5, pp. 3391–3402, 2017.

[59] A. Y. Elrayyah, M. Z. C. Wanik, and A. Bouselham, "Simplified approach to analyze voltage rise in LV systems With PV installations using equivalent power systems diagrams," *IEEE Trans. Power Deliv.*, vol. 32, no. 4, pp. 2140–2149, 2017.

[60] P.-C. Chen *et al.*, "Analysis of Voltage Profile Problems Due to the Penetration of Distributed Generation in Low-Voltage Secondary Distribution Networks," *IEEE Trans. Power Deliv.*, vol. 27, no. 4, pp. 2020–2028, Oct. 2012.

[61] E. Zio, M. Delfanti, L. Giorgi, V. Olivieri, and G. Sansavini, "Monte Carlo simulation-based probabilistic assessment of DG penetration in medium voltage distribution networks," *Int. J. Electr. Power Energy Syst.*, vol. 64, pp. 852–860, 2015.

[62] G. De Carne, G. Buticchi, Z. Zou, and M. Liserre, "Reverse Power Flow Control in a ST-Fed Distribution Grid," *IEEE Trans. Smart Grid*, vol. 9, no. 4, pp. 3811–3819, 2018.

[63] M. Hasheminamin, V. G. Agelidis, V. Salehi, R. Teodorescu, and B. Hredzak, "Index-Based Assessment of Voltage Rise and Reverse Power Flow Phenomena in a Distribution Feeder under High PV Penetration," *IEEE J. Photovoltaics*, vol. 5, no. 4, pp. 1158–1168, 2015.

[64] J. Widén, E. Wäckelgård, J. Paatero, and P. Lund, "Impacts of distributed photovoltaics on network voltages: Stochastic simulations of three Swedish low-voltage distribution grids," *Electr. Power Syst. Res.*, vol. 80, no. 12, pp. 1562–1571, 2010.

[65] Y. Chen, M. Strothers, and A. Benigni, "A Stochastic Approach to Optimum Placement of Photovoltaic Generation in Distribution Feeder," 2016.

[66] M. Alturki, A. Khodaei, A. Paaso, and S. Bahramirad, "Optimization-based distribution grid hosting capacity calculations," *Appl. Energy*, vol. 219, no. March 2017, pp. 350–360, 2018.

[67] C. H. Lin, W. L. Hsieh, C. S. Chen, C. T. Hsu, and T. T. Ku, "Optimization of photovoltaic penetration in distribution systems considering annual duration curve of solar irradiation," *IEEE Trans. Power Syst.*, vol. 27, no. 2, pp. 1090–1097, 2012.

[68] H. Al-Saadi, R. Zivanovic, and S. F. Al-Sarawi, "Probabilistic Hosting Capacity for Active Distribution Networks," *IEEE Trans. Ind. Informatics*, vol. 13, no. 5, pp. 2519–2532, 2017.

[69] M. S. S. Abad, J. Ma, D. Zhang, A. S. Ahmadyar, and H. Marzooghi, "Probabilistic Assessment of Hosting Capacity in Radial Distribution Systems," *IEEE Trans. Sustain. Energy*, vol. 9, no. 4, pp. 1935–1947, 2018.

[70] I. Navigant Consulting, "Virginia Solar Pathways Project. Study 1: Distributed Solar Generation Integration and Best Practices Review," Richmond, Virginia, 2016.

[71] Horizon Power, "Renewable Energy: Available Hosting Capacity, Australia," 2017. [Online]. Available: https://www.horizonpower.com.au/media/1592/hosting-capacities-fact-sheet-030317.pdf.

[72] Z. Abdmouleh, A. Gastli, L. Ben-Brahim, M. Haouari, and N. A. Al-Emadi, "Review of optimization techniques applied for the integration of distributed generation from renewable energy sources," *Renew. Energy*, vol. 113, pp. 266–280, 2017.

[73] R. Viral and D. K. Khatod, "An analytical approach for sizing and siting of DGs in balanced radial distribution networks for loss minimization," *Int. J. Electr. Power Energy Syst.*, vol. 67, pp. 191–201, 2015.

[74] N. Acharya, P. Mahat, and N. Mithulananthan, "An analytical approach for DG allocation in primary distribution network," *Int. J. Electr. Power Energy Syst.*, vol. 28, no. 10, pp. 669–678, 2006.

[75] A. M. Abd-El-Motaleb and S. K. Bekdach, "Optimal sizing of distributed generation considering uncertainties in a hybrid power system," *Int. J. Electr. Power Energy Syst.*, vol. 82, pp. 179–188, 2016.

[76] H. HassanzadehFard and A. Jalilian, "Optimal sizing and location of renewable energy based DG units in distribution systems considering load growth," *Int. J. Electr. Power Energy Syst.*, vol. 101, no. January 2017, pp. 356–370, 2018.

[77] E. S. Ali, S. M. Abd Elazim, and A. Y. Abdelaziz, "Ant Lion Optimization Algorithm for optimal location and sizing of renewable distributed generations," *Renew. Energy*, vol. 101, pp. 1311–1324, 2017.

[78] P. Shivwanshi and S. E. Mubeen, "Placement and Sizing of Distributed Generation on Distribution Systems with a Multi-Objective Particle Swarm Optimization and Analytical Approach : A Review," *Int. J. Comput. Appl.*, vol. 132, no. 15, pp. 37–41, 2015.

[79] S. Daud, A. F. A. Kadir, C. K. Gan, A. Mohamed, and T. Khatib, "A comparison of heuristic optimization techniques for optimal placement and sizing of photovoltaic based distributed generation in a distribution system," *Sol. Energy*, vol. 140, pp. 219–226, 2016.

[80] M. M. Aman, G. B. Jasmon, H. Mokhlis, and A. H. A. Bakar, "Optimal placement and sizing of a DG based on a new power stability index and line losses," *Int. J. Electr. Power Energy Syst.*, vol. 43, no. 1, pp. 1296–1304, 2012.

[81] X. Fu, H. Chen, R. Cai, and P. Yang, "Optimal allocation and adaptive VAR control of PV-DG in distribution networks," *Appl. Energy*, vol. 137, pp. 173–182, 2015.

[82] P. Chavali, P. Yang, and A. Nehorai, "A distributed algorithm of appliance scheduling for home energy management system," *IEEE Trans. Smart Grid*, vol. 5, no. 1, pp. 282–290, 2014.

[83] S. Mhanna, G. Verbič, and A. C. Chapman, "A faithful distributed mechanism for demand response aggregation," *IEEE Trans. Smart Grid*, vol. 7, no. 3, pp. 1743–1753, 2015.

[84] A.-H. Mohsenian-Rad, V. W. S. Wong, J. Jatskevich, R. Schober, and A. Leon-Garcia, "Autonomous demand-side management based on game-theoretic energy consumption scheduling for the future smart grid," *IEEE Trans. Smart Grid*, vol. 1, no. 3, pp. 320–331, 2010.

[85] M. A. A. Pedrasa, T. D. Spooner, and I. F. MacGill, "Coordinated scheduling of residential

distributed energy resources to optimize smart home energy services," *IEEE Trans. Smart Grid*, vol. 1, no. 2, pp. 134–143, 2010.

[86] C. O. Adika and L. Wang, "Autonomous appliance scheduling for household energy management," *IEEE Trans. Smart Grid*, vol. 5, no. 2, pp. 673–682, 2013.

[87] B. Bahl, M. Lampe, P. Voll, and A. Bardow, "Optimization-based identification and quantification of demand-side management potential for distributed energy supply systems," *Energy*, vol. 135, pp. 889–899, 2017.

[88] P. Mesarić and S. Krajcar, "Home demand side management integrated with electric vehicles and renewable energy sources," *Energy Build.*, vol. 108, pp. 1–9, 2015.

[89] K. Dietrich, J. M. Latorre, L. Olmos, and A. Ramos, "Demand response in an isolated system with high wind integration," *IEEE Trans. Power Syst.*, vol. 27, no. 1, pp. 20–29, 2011.

[90] R.-S. Liu and Y.-F. Hsu, "A scalable and robust approach to demand side management for smart grids with uncertain renewable power generation and bi-directional energy trading," *Int. J. Electr. Power Energy Syst.*, vol. 97, pp. 396–407, 2018.

[91] B. Lokeshgupta and S. Sivasubramani, "Multi-objective dynamic economic and emission dispatch with demand side management," *Int. J. Electr. Power Energy Syst.*, vol. 97, pp. 334–343, 2018.

[92] M. H. Alham, M. Elshahed, D. K. Ibrahim, and E. E. D. A. El Zahab, "Optimal operation of power system incorporating wind energy with demand side management," *Ain Shams Eng. J.*, vol. 8, no. 1, pp. 1–7, 2017.

[93] F. Ye, Y. Qian, and R. Q. Hu, "A real-time information based demand-side management system in smart grid," *IEEE Trans. Parallel Distrib. Syst.*, vol. 27, no. 2, pp. 329–339, 2015.

[94] K. G. Di Santo, S. G. Di Santo, R. M. Monaro, and M. A. Saidel, "Active demand side management for households in smart grids using optimization and artificial intelligence," *Measurement*, vol. 115, pp. 152–161, 2018.

[95] A. Vaghefi, F. Farzan, and M. A. Jafari, "Modeling industrial loads in non-residential buildings," *Appl. Energy*, vol. 158, pp. 378–389, 2015.

[96] E. Fernandez, M. J. Hossain, and M. S. H. Nizami, "Game-theoretic approach to demand-side energy management for a smart neighbourhood in Sydney incorporating renewable resources," *Appl. Energy*, vol. 232, pp. 245–257, 2018.

[97] B. DeMarco, C. Baone, C. Han, Y. Lesieutre, "Primary and Secondary Control for High Penetration Renewables Primary and Secondary Control for High Penetration Renewables," *PSERC Publ. 12-06*, no. May, 2012, pp. 1–37, 2012.

[98] T. A. Deetjen, H. Martin, J. D. Rhodes, and M. E. Webber, "Modeling the optimal mix and location of wind and solar with transmission and carbon pricing considerations," *Renew. energy*, vol. 120, pp. 35–50, 2018.

[99] U. Tamrakar, D. Shrestha, M. Maharjan, B. P. Bhattarai, T. M. Hansen, and R. Tonkoski,

"Virtual inertia: Current trends and future directions," *Appl. Sci.*, vol. 7, no. 7, p. 654, 2017.

[100] N. Miller, D. Lew, and R. Piwko, "Technology capabilities for fast frequency response," *GE Energy Consult. Tech. Rep.*, 2017.

[101] H. Lund, "Electric grid stability and the design of sustainable energy systems," *Int. J. Sustain. Energy*, vol. 24, no. 1, pp. 45–54, 2005.

[102] Z. Wu, D. W. Gao, H. Zhang, S. Yan, and X. Wang, "Coordinated control strategy of battery energy storage system and PMSG-WTG to enhance system frequency regulation capability," *IEEE Trans. Sustain. Energy*, vol. 8, no. 3, pp. 1330–1343, 2017.

[103] M. Altin, A. D. Hansen, T. K. Barlas, K. Das, and J. N. Sakamuri, "Optimization of short-term overproduction response of variable speed wind turbines," *IEEE Trans. Sustain. Energy*, vol. 9, no. 4, pp. 1732–1739, 2018.

[104] N. R. Ullah, T. Thiringer, and D. Karlsson, "Temporary primary frequency control support by variable speed wind turbines—Potential and applications," *IEEE Trans. Power Syst.*, vol. 23, no. 2, pp. 601–612, 2008.

[105] J. M. Mauricio, A. Marano, A. Gómez-Expósito, and J. L. M. Ramos, "Frequency regulation contribution through variable-speed wind energy conversion systems," *IEEE Trans. Power Syst.*, vol. 24, no. 1, pp. 173–180, 2009.

[106] B.-I. Crăciun, T. Kerekes, D. Séra, and R. Teodorescu, "Frequency support functions in large PV power plants with active power reserves," *IEEE J. Emerg. Sel. Top. Power Electron.*, vol. 2, no. 4, pp. 849–858, 2014.

[107] B.-I. Cr ciun, T. Kerekes, D. S�ra, and R. Teodorescu, "Overview of recent grid codes for PV power integration," in *2012 13th International Conference on Optimization of Electrical and Electronic Equipment (OPTIM)*, 2012, pp. 959–965.

[108] C. Loutan *et al.*, "Demonstration of essential reliability services by a 300-MW solar photovoltaic power plant," National Renewable Energy Lab.(NREL), Golden, CO (United States), 2017.

[109] J. Morren, S. W. H. De Haan, and J. A. Ferreira, "Primary power/frequency control with wind turbines and fuel cells," in *2006 IEEE Power Engineering Society General Meeting*, 2006, pp. 8-pp.

[110] G. Delille, B. Francois, and G. Malarange, "Dynamic frequency control support by energy storage to reduce the impact of wind and solar generation on isolated power system's inertia," *IEEE Trans. Sustain. energy*, vol. 3, no. 4, pp. 931–939, 2012.

[111] "Converters for energy storage and grid stabilization," *ABB*. .

[112] T. Xu, W. Jang, and T. Overbye, "Commitment of Fast-Responding Storage Devices to Mimic Inertia for the Enhancement of Primary Frequency Response," *IEEE Trans. Power Syst.*, vol. 33, no. 2, pp. 1219–1230, 2018.

[113] I. Serban, R. Teodorescu, and C. Marinescu, "Energy storage systems impact on the short-term frequency stability of distributed autonomous microgrids, an analysis using aggregate

models," *IET Renew. Power Gener.*, vol. 7, no. 5, pp. 531–539, 2013.

[114] A. K. Srivastava, A. A. Kumar, and N. N. Schulz, "Impact of distributed generations with energy storage devices on the electric grid," *IEEE Syst. J.*, vol. 6, no. 1, pp. 110–117, 2012.

[115] J. Fleer and P. Stenzel, "Impact analysis of different operation strategies for battery energy storage systems providing primary control reserve," *J. Energy Storage*, vol. 8, pp. 320–338, 2016.

[116] P. Stenzel, J. C. Koj, A. Schreiber, W. Hennings, and P. Zapp, "Primary control provided by large-scale battery energy storage systems or fossil power plants in Germany and related environmental impacts," *J. Energy Storage*, vol. 8, pp. 300–310, 2016.

[117] C. Pradhan, C. N. Bhende, and A. K. Samanta, "Adaptive virtual inertia-based frequency regulation in wind power systems," *Renew. energy*, vol. 115, pp. 558–574, 2018.

[118] A. Delavari and I. Kamwa, "Improved optimal decentralized load modulation for power system primary frequency regulation," *IEEE Trans. Power Syst.*, vol. 33, no. 1, pp. 1013–1025, 2018.

[119] A. Molina-García, F. Bouffard, and D. S. Kirschen, "Decentralized demand-side contribution to primary frequency control," *IEEE Trans. Power Syst.*, vol. 26, no. 1, pp. 411–419, 2011.

[120] L.-R. Chang-Chien, L. N. An, T.-W. Lin, and W.-J. Lee, "Incorporating demand response with spinning reserve to realize an adaptive frequency restoration plan for system contingencies," *IEEE Trans. Smart Grid*, vol. 3, no. 3, pp. 1145–1153, 2012.

[121] M. R. V. Moghadam, R. T. B. Ma, and R. Zhang, "Distributed frequency control in smart grids via randomized demand response," *IEEE Trans. Smart Grid*, vol. 5, no. 6, pp. 2798–2809, 2014.

[122] S. Weckx, R. D'hulst, and J. Driesen, "Primary and secondary frequency support by a multi-agent demand control system," *IEEE Trans. Power Syst.*, vol. 30, no. 3, pp. 1394–1404, 2014.

[123] C. Zhao, U. Topcu, and S. H. Low, "Optimal load control via frequency measurement and neighborhood area communication," *IEEE Trans. Power Syst.*, vol. 28, no. 4, pp. 3576–3587, 2013.

[124] B. Biegel, L. H. Hansen, P. Andersen, and J. Stoustrup, "Primary control by ON/OFF demand-side devices," *IEEE Trans. Smart Grid*, vol. 4, no. 4, pp. 2061–2071, 2013.

[125] D. Trudnowski, M. Donnelly, and E. Lightner, "Power-system frequency and stability control using decentralized intelligent loads," in *Transmission and Distribution Conference and Exhibition, 2005/2006 IEEE PES*, 2006, pp. 1453–1459.

[126] M. Donnelly, D. J. Trudnowski, S. Mattix, and J. E. Dagle, "Autonomous demand response for primary frequency regulation," 2012.

[127] A. Wickramasinghe, S. Perera, A. P. Agalgaonkar, and L. Meegahapola, "Synchronous mode operation of DFIG based wind turbines for improvement of power system inertia,"

Renew. Energy, vol. 95, pp. 152–161, 2016.

[128] T. Inoue, H. Taniguchi, Y. Ikeguchi, and K. Yoshida, "Estimation of power system inertia constant and capacity of spinning-reserve support generators using measured frequency transients," *IEEE Trans. Power Syst.*, vol. 12, no. 1, pp. 136–143, 1997.

[129] P. M. Ashton, C. S. Saunders, G. A. Taylor, A. M. Carter, and M. E. Bradley, "Inertia estimation of the GB power system using synchrophasor measurements," *IEEE Trans. Power Syst.*, vol. 30, no. 2, pp. 701–709, 2015.

[130] M. Kuivaniemi *et al.*, "Estimation of System Inertia in the Nordic Power System Using Measured Frequency Disturbances," in *Cigre Conference*, 2015, pp. 27–28.

[131] P. Wall, F. Gonzalez-Longatt, and V. Terzija, "Estimation of generator inertia available during a disturbance," in *2012 IEEE Power and Energy Society General Meeting*, 2012, pp. 1–8.

[132] D. P. Chassin, Z. Huang, M. K. Donnelly, C. Hassler, E. Ramirez, and C. Ray, "Estimation of WECC system inertia using observed frequency transients," *IEEE Trans. Power Syst.*, vol. 20, no. 2, pp. 1190–1192, 2005.

[133] P. Wall, V. Terzija, and S. Member, "Simultaneous Estimation of the Time of Disturbance and Inertia in Power Systems," vol. 29, no. 4, pp. 2018–2031, 2018.

[134] D. Zografos and M. Ghandhari, "Estimation of power system inertia," in *2016 IEEE Power and Energy Society General Meeting (PESGM)*, 2016, pp. 1–5.

[135] A. Ketabi and M. H. Fini, "An Underfrequency load shedding scheme for hybrid and Multiarea power systems," *IEEE Trans. Smart Grid*, vol. 6, no. 1, pp. 82–91, 2015.

[136] R. Azizipanah-abarghooee, M. Malekpour, and S. Member, "A New Approach to the On-line Estimation of the Loss of Generation Size in Power Systems," *IEEE Trans. Power Syst.*, vol. PP, no. c, p. 1, 2018.

[137] E. Muljadi, V. Gevorgian, and A. Hoke, "Energy storage opportunities and capabilities of a type 3 wind turbine generator," in *2016 IEEE Energy Conversion Congress and Exposition (ECCE)*, 2016, pp. 1–5.

[138] M. F. M. Arani and E. F. El-Saadany, "Implementing virtual inertia in DFIG-based wind power generation," *IEEE Trans. Power Syst.*, vol. 28, no. 2, pp. 1373–1384, 2012.

[139] Y. Ma, W. Cao, L. Yang, F. F. Wang, and L. M. Tolbert, "Virtual synchronous generator control of full converter wind turbines with short-term energy storage," *IEEE Trans. Ind. Electron.*, vol. 64, no. 11, pp. 8821–8831, 2017.

[140] L. Miao, J. Wen, H. Xie, C. Yue, and W.-J. Lee, "Coordinated control strategy of wind turbine generator and energy storage equipment for frequency support," *IEEE Trans. Ind. Appl.*, vol. 51, no. 4, pp. 2732–2742, 2015.

[141] J. Liu, J. Wen, W. Yao, and Y. Long, "Solution to short-term frequency response of wind farms by using energy storage systems," *IET Renew. Power Gener.*, vol. 10, no. 5, pp. 669–678, 2016.

[142] J. C. Hernandez, P. G. Bueno, and F. Sanchez-Sutil, "Enhanced utility-scale photovoltaic units with frequency support functions and dynamic grid support for transmission systems," *IET Renew. Power Gener.*, vol. 11, no. 3, pp. 361–372, 2017.

[143] Y. J. A. Zhang, C. Zhao, W. Tang, and S. H. Low, "Profit-maximizing planning and control of battery energy storage systems for primary frequency control," *IEEE Trans. Smart Grid*, vol. 9, no. 2, pp. 712–723, 2016.

[144] Y. Liu, W. Du, L. Xiao, H. Wang, and J. Cao, "A method for sizing energy storage system to increase wind penetration as limited by grid frequency deviations," *IEEE Trans. Power Syst.*, vol. 31, no. 1, pp. 729–737, 2015.

[145] L. A. C. Lopes, "Self-tuning virtual synchronous machine: A control strategy for energy storage systems to support dynamic frequency control," *IEEE Trans. Energy Convers.*, vol. 29, no. 4, pp. 833–840, 2014.

[146] S. Pulendran and J. E. Tate, "Energy storage system control for prevention of transient under-frequency load shedding," *IEEE Trans. Smart Grid*, vol. 8, no. 2, pp. 927–936, 2015.

[147] Z. Wang, A. Scaglione, and R. J. Thomas, "The node degree distribution in power grid and its topology robustness under random and selective node removals," *2010 IEEE Int. Conf. Commun. Work. ICC 2010*, no. 1, 2010.

[148] "U.S. Energy Information Association. Form EIA - 860, 2016." [Online]. Available: https://www.eia.gov/electricity/data/eia860/. [Accessed: 30-May-2018].

[149] "Western Electricity Coordinating Council (WECC)." [Online]. Available: https://www.wecc.biz/Pages/home.aspx. [Accessed: 08-Jan-2018].

[150] "Electric Reliability Council of Texas (ERCOT)." [Online]. Available: http://www.ercot.com/. [Accessed: 08-Jan-2018].

[151] "MATPOWER Test Cases | DR POWER." [Online]. Available: https://egriddata.org/group/matpower-test-cases. [Accessed: 06-Jun-2018].

[152] "ACTIVSg synthetc grids." [Online]. Available: https://electricgrids.engr.tamu.edu/. [Accessed: 01-Feb-2020].

[153] T. van Erven and P. Harremoes, "Rényi Divergence and Kullback-Leibler Divergence," *IEEE Trans. Inf. Theory*, vol. 60, no. 7, pp. 3797–3820, Jul. 2014.

[154] B. E. Flores and D. W. Wichern, "Evaluating forecasts: a look at aggregate bias and accuracy measures," *J. Forecast.*, vol. 24, no. 6, pp. 433–451, 2005.

[155] F. Katiraei and J. R. Aguero, "Solar PV Integration Challenges," *IEEE Power Energy Mag.*, vol. 9, no. 3, pp. 62–71, 2011.

[156] "Index of /datasets/files/961/pub." [Online]. Available: http://en.openei.org/datasets/files/961/pub/.

[157] J. Widén, M. Lundh, I. Vassileva, E. Dahlquist, K. Ellegård, and E. Wäckelgård, "Constructing load profiles for household electricity and hot water from time-use data-Modelling approach and validation," *Energy Build.*, vol. 41, no. 7, pp. 753–768, 2009.

[158] M. Nijhuis, M. Gibescu, and J. F. G. Cobben, "Bottom-up Markov Chain Monte Carlo approach for scenario based residential load modelling with publicly available data," *Energy Build.*, vol. 112, pp. 121–129, 2016.

[159] F. M. Figueiredo, J. A. Jardini, S. U. Ahn, C. M. V. Tahan, and M. R. Gouvea, "Daily load profiles for residential, commercial and industrial low voltage consumers," *IEEE Trans. Power Deliv.*, vol. 15, no. 1, pp. 375–380, 2002.

[160] D. Fischer, A. Härtl, and B. Wille-Haussmann, "Model for electric load profiles with high time resolution for German households," *Energy Build.*, vol. 92, pp. 170–179, 2015.

[161] C. Bucher and G. Andersson, "Generation of Domestic Load Profiles - an Adaptive Top-Down Approach," *12th Int. Conf. Probabilistic Methods Appl. to Power Syst.*, no. June 2012, pp. 436–441, 2012.

[162] N. Good, L. Zhang, A. Navarro-Espinosa, and P. Mancarella, "High resolution modelling of multi-energy domestic demand profiles," *Appl. Energy*, vol. 137, pp. 193–210, 2015.

[163] H. Li, A. L. Bornsheuer, T. Xu, A. B. Birchfield, and T. J. Overbye, "Load modeling in synthetic electric grids," *2018 IEEE Texas Power Energy Conf. TPEC 2018*, vol. 2018-Febru, pp. 1–6, 2018.

[164] "Energy Information and Data | OpenEI.org." [Online]. Available: http://en.openei.org/wiki/Main_Page. [Accessed: 30-Apr-2017].

[165] M. Starke and D. Eere, *Assessment of Industrial Load for Demand Response across U.S. Regions of the Western Interconnect*, no. September. 2013.

[166] A. Duffy, F. McLoughlin, and M. Conlon, "The Generation of Domestic Electricity Load Profiles through Markov Chain Modelling," *3rd Int. Sci. Conf. Energy Clim. Chang.*, pp. 18–27, 2010.

[167] H. Sadeghian and Z. Wang, "Photovoltaic Generation in Distribution Networks : Optimal vs . Random Installation," in *2018 IEEE PES Innovative Smart Grid Technologies, ISGT*, 2018.

[168] A. Medina, J. C. Hernández, and F. Jurado, "Optimal placement and sizing procedure for PV systems on radial distribution systems," *2006 Int. Conf. Power Syst. Technol. POWERCON2006*, 2007.

[169] Z. F. Hongxing Yang, Wei Zhou, Lin Lu, "Optimal sizing method for stand-alone hybrid solar–wind system with LPSP technology by using genetic algorithm," *Sol. Energy*, vol. 82, no. 4, pp. 354–367, Apr. 2008.

[170] "The NSRDB Data Viewer." [Online]. Available: https://maps.nrel.gov/nsrdb-viewer.

[171] S. Wen, H. Lan, Q. Fu, D. C. Yu, and L. Zhang, "Economic allocation for energy storage system considering wind power distribution," *IEEE Trans. Power Syst.*, vol. 30, no. 2, pp. 644–652, 2015.

[172] E. kianmehr, S. Nikkhah, and A. Rabiee, "Multi-objective stochastic model for joint optimal allocation of DG units and network reconfiguration from DG owner's and DisCo's

perspectives," *Renew. Energy*, vol. 132, pp. 471–485, 2019.

[173] J. Pollock and D. Hill, "Overcoming the issues associated with operating a distribution system in reverse power flow," in *5th IET International Conference on Renewable Power Generation (RPG) 2016*, 2016, pp. 31 (6 .)-31 (6 .).

[174] J. W. Smith, R. Dugan, and W. Sunderman, "Distribution modeling and analysis of high penetration PV," *IEEE Power Energy Soc. Gen. Meet.*, pp. 1–7, 2011.

[175] Z. W. Seyyed Hamid Elyas, Hamidreza Sadeghian, Hayder O Alwan, "Optimized Household Demand Management with Local Solar PV Generation," in *North American Power Symposium*, 2017.

[176] C. Seneviratne and C. Ozansoy, "Frequency response due to a large generator loss with the increasing penetration of wind/PV generation - A literature review," *Renew. Sustain. Energy Rev.*, vol. 57, pp. 659–668, 2016.

[177] A. Fernández-Guillamón, E. Gómez-Lázaro, E. Muljadi, and Á. Molina-García, "Power systems with high renewable energy sources: A review of inertia and frequency control strategies over time," *Renew. Sustain. Energy Rev.*, vol. 115, no. January, p. 109369, 2019.

[178] K. O. Adu-Kankam and L. M. Camarinha-Matos, "Towards collaborative Virtual Power Plants: Trends and convergence," *Sustain. Energy, Grids Networks*, vol. 16, pp. 217–230, 2018.

[179] M. Eremia and M. Shahidehpour, *Handbook of Electrical Power System Dynamics: Modeling, Stability, and Control*. 2013.

[180] J. Machowski, J. Bialek, and J. Bumby, *Power system dynamics: stability and control*. John Wiley & Sons, 2011.

[181] J. Schiffer, P. Aristidou, and R. Ortega, "Online Estimation of Power System Inertia Using Dynamic Regressor Extension and Mixing," *IEEE Trans. Power Syst.*, vol. PP, no. c, p. 1, 2018.

[182] P. W. Sauer and M. A. Pai, *Power system dynamics and stability*, vol. 101. Prentice hall Upper Saddle River, NJ, 1998.

[183] F. Milano, A. Ortega, and A. J. Conejo, "Model-agnostic linear estimation of generator rotor speeds based on phasor measurement units," *IEEE Trans. Power Syst.*, vol. 33, no. 6, pp. 7258–7268, 2018.

[184] J. Machowski, J. W. Bialek, and J. R. Bumby, *Power system dynamics: stability and controlJohn Wiley & Sons,*. 2011.

[185] S. Hashemi and J. Østergaard, "Efficient Control of Energy Storage for Increasing the PV Hosting Capacity of LV Grids," *IEEE Trans. Smart Grid*, vol. 9, no. 3, pp. 2295–2303, 2018.

[186] M. Nick, R. Cherkaoui, and M. Paolone, "Optimal Planning of Distributed Energy Storage Systems in Active Distribution Networks Embedding Grid Reconfiguration," *IEEE Trans. Power Syst.*, vol. 33, no. 2, pp. 1577–1590, 2018.

[187] A. Soroudi, P. Siano, and A. Keane, "Optimal DR and ESS scheduling for distribution losses payments minimization under electricity price uncertainty," *IEEE Trans. Smart Grid*, vol. 7, no. 1, pp. 261–272, 2016.

[188] P. V. Brogan, R. J. Best, D. J. Morrow, K. McKinley, and M. L. Kubik, "Effect of BESS Response on Frequency and RoCoF During Under Frequency Transients," *IEEE Trans. Power Syst.*, vol. 34, no. 1, pp. 575–583, 2018.

[189] K. E. Martin *et al.*, "An overview of the IEEE standard C37. 118.2—synchrophasor data transfer for power systems," *IEEE Trans. Smart Grid*, vol. 5, no. 4, pp. 1980–1984, 2014.

[190] P. Romano and M. Paolone, "Enhanced interpolated-DFT for synchrophasor estimation in FPGAs: Theory, implementation, and validation of a PMU prototype," *IEEE Trans. Instrum. Meas.*, vol. 63, no. 12, pp. 2824–2836, 2014.

[191] A. Bagchi, L. Goel, and P. Wang, "Adequacy Assessment of Generating Systems Incorporating Storage Integrated Virtual Power Plants," *IEEE Trans. Smart Grid*, vol. 10, no. 3, pp. 3440–3451, 2019.

[192] H. Thiesen, C. Jauch, and A. Gloe, "Design of a system substituting today's inherent inertia in the European continental synchronous area," *Energies*, vol. 9, no. 8, p. 582, 2016.

[193] B. K. Poolla, S. Bolognani, L. Na, and F. Dörfler, "A market mechanism for virtual inertia," *IEEE Trans. Smart Grid*, 2020.

[194] "Firm Frequency Response (FFR) | National Grid ESO," *National Grid ESO*. .

[195] M. Cheng, S. S. Sami, and J. Wu, "Benefits of using virtual energy storage system for power system frequency response," *Appl. Energy*, vol. 194, pp. 376–385, 2017.

[196] Z. H. Rather, Z. Chen, P. Thøgersen, P. Lund, and B. Kirby, "Realistic approach for phasor measurement unit placement: Consideration of practical hidden costs," *IEEE Trans. Power Deliv.*, vol. 30, no. 1, pp. 3–15, 2014.

[197] N. N. Barish, "Capital Investment and Amortization Policies in the USSR," *Eng. Econ.*, vol. 7, no. 2, pp. 39–56, 1962.

[198] W. J. Cole and A. Frazier, "Cost projections for utility-scale battery storage," 2019.

[199] A. Dyśko, I. Abdulhadi, X. Li, and C. Booth, "Assessment of Risks Resulting from the Adjustment of ROCOF Based Loss of Mains Protection Settings Phase II," *Univ. Strat. ref NGC/LOM/TR/2013-001b*, 2013.

[200] K. E. Martin, "Synchrophasor measurements under the IEEE standard C37. 118.1-2011 with amendment C37. 118.1 a," *IEEE Trans. Power Deliv.*, vol. 30, no. 3, pp. 1514–1522, 2015.

[201] H. Wu, K. S. Tsakalis, and G. T. Heydt, "Evaluation of time delay effects to wide area power system stabilizer design," *IEEE Trans. Power Syst.*, vol. 19, no. 4, pp. 1935–1941, 2004.

[202] C. W. Taylor, M. V Venkatasubramanian, Y. Chen, and others, "Wide-area stability and voltage control," in *Proc. VII Symp. Specialties Electr. Oper. Expansion Planning*, 2000,

pp. 21–26.

Vita

Hamidreza Sadeghian

Professional Summary

Experienced power system engineer and researcher with a great deal of experience in both electric transmission and distribution utility industry. My expertise involves power system operation and planning, electricity market and economics, integration of renewable energies, synthetic power grid modeling, demand side management (DSM), distributed energy resources (DERs), and optimization. I love coding and automation. Skilled in PSS/E, PowerGEM TARA, PowerWorld, PSCAD, RTDS, MATLAB and Python.

Education

- **Virginia Commonwealth University**, Richmond, VA, USA, fall 2016 – present
  Ph.D. Candidate, Electrical Engineering, GPA: 4.0
  Dossertation: Improving Grid Hosting Capacity and Inertia Response with High Penetration of Renewable Generation
  Advisor: Dr. Zhifang Wang
- **Amirkabir University of Technology (Tehran Polytechnic)**, Tehran, Iran, 2014
  M.S. in Electrical Engineering (Energy management), GPA: 3.9
  Thesis: Profit Based Unit Commitment of Combined Heat and Power Systems.
  Advisor: Dr. Morteza Mohammadi Ardehali
  Co-advisor: Dr. Seyyed Hossein Hosseinian
- **University of Tabriz**, Tabriz, Iran, 2012
  B.S. in Electrical Engineering, GPA: 3.6
  Thesis: Design and Simulation of Bi-directional Convertor for Hybrid Electric Vehicles
  Advisor: Dr. Ebrahim Babaei

Research Interests

- Integration of renewable energy resources
- Electric transmission planning
- Synthetic power grid modeling
- Inertia emulation and fast frequency response
- Electricity market and economics
- Application of intelligent methods in power systems
- Demand side management
- Power system automation

Work Experience

Graduate Research Assistant, Virginia Commonwealth University, Richmond, VA	Sept. 2016	–present
Graduate Intern at ET Planning and Strategic Initiatives, Dominion Energy, Richmond, VA	May 2019	–Aug. 2019
Operation Manager, Shahid Zerafati's 10 MW power plant, Babolsar, Iran	Oct. 2015	–May 2016
Consulting Engineer, East Azerbaijan Electric Power Distribution Company, Bonab, Iran	Apr. 2015	–Sept. 2015
Lecturer, Islamic Azad University (IAU) - Bonab Branch, Bonab, Iran	Dec. 2014	–Aug. 2015
Graduate Research Assistant, Amirkabir University of Technology, Tehran, Iran	Sept. 2012	–Aug. 2014
Intern, Tabriz Electric Power Distribution Company, Tabriz, Iran	July 2012	–Sept. 2012

Honors and Awards

Dominion Energy Power the Future Innovation Competition, outstanding performance, Oct. 2018
VCU ECE department Outstanding Graduate Research Assistant award, May 2018
VCU College of Engineering's 3MT Competition, people's choice award, Apr. 2018
VCU Dean's Early Research Initiative (DERI) program award, Feb. 2018
VCU Graduate School travel award, Sept. 2017
VCU ECE department travel award, Sept. 2017
Distinguished Teaching Award, Islamic Azad University (IAU), Tabriz, Iran, July 2015

Publications

Journal Publications:

[J1] **H. Sadeghian** and Z. Wang, "AutoSynGrid: A MATLAB-based toolkit for automatic generation of synthetic power grids." International Journal of Electrical Power & Energy Systems 118 (2020): 105757.
DOI: https://doi.org/10.1016/j.ijepes.2019.105757

[J2] **H. Sadeghian** and Z. Wang, "A novel impact-assessment framework for distributed PV installations in low-voltage secondary networks." Renewable Energy 147 (2020): 2179-2194.
DOI: https://doi.org/10.1016/j.renene.2019.09.117

[J3] **H. Sadeghian** and Z. Wang, "Real-Time Virtual Power Plants Control for Inertia Emulation and Fast Frequency Response" International Journal of Electrical Power & Energy Systems, (2020) (under review).

[J4] M. H. Athari, Zhifang Wang, and **Hamidreza Sadeghian**, "GridStat Analysis Toolkit: A Framework for Statistical Analysis of Power System Networks", IET Generation, Transmission & Distribution (2020) (under review).

[J5] **H.R. Sadeghian**, and M.M. Ardehali "A Novel Approach for Optimal Economic Dispatch Scheduling of Integrated Combined Heat and Power Systems for Maximum Economic Profit and Minimum Environmental Emissions Based on Benders Decomposition" *Elsevier. Energy* 2016 May 1;102:10-23.
DOI: https://doi.org/10.1016/j.energy.2016.02.044

Peer-reviewed Conference Papers:

[C1] **H. Sadeghian,** and Z. Wang 'Integration of Rooftop PV Systems with Decentralized Residential and Commercial Demand Side Management. *2019 North American Power Symposium (NAPS), Sept. 2019.*
DOI: 10.1109/NAPS46351.2019.9000290

[C2] **H. Sadeghian**, S. H. Elyas, and Z. Wang, "A Novel Algorithm for Statistical Assignment of Transmission Capacities in Synthetic Grid Modeling," *in IEEE PES General Meeting, 2018*.
DOI: 10.1109/PESGM.2018.8585532

[C3] **H. Sadeghian** and Z. Wang, "Photovoltaic Generation in Distribution Networks: Optimal vs. Random Installation," *in 2018 IEEE PES Innovative Smart Grid Technologies, ISGT, Feb. 2018.*
DOI: 10.1109/ISGT.2018.8403320

[C4] **H. Sadeghian** and Z. Wang, "Decentralized Demand Side Management with Rooftop PV in Residential Distribution Network," *in 2018 IEEE PES Innovative Smart Grid Technologies, ISGT, Feb. 2018*.
DOI: 10.1109/ISGT.2018.8403404

[C5] **H. Sadeghian**, and Z. Wang "Combined Heat and Power Unit Commitment with Smart Parking Lots of Plug-in Electric Vehicles" *, 2017 North American Power Symposium (NAPS), Sept. 2017.*
DOI: 10.1109/NAPS.2017.8107281

[C6] S. H. Elyas, **H. Sadeghian**, H. Alwan, and Z. Wang "Optimized Household Demand Management with Local Distributed Solar Generation" *, 2017 North American Power Symposium (NAPS), Sept. 2017.*
DOI: 10.1109/NAPS.2017.8107411

[C7] **H. Sadeghian**, M.H. Athari, and Z. Wang, "Optimized Solar Photovoltaic Generation in a Real Local Distribution Network," *in 2017 IEEE PES Innovative Smart Grid Technologies, ISGT, Apr. 2017.*
DOI: 10.1109/ISGT.2017.8086067

[C8] **H. Sadeghian**, M.H. Athari, and G.B. Gharehpetian "Improved Multi-Agent System for Intelligent Energy Management of Microgrids in Presence of PHEVs," *23rd Iranian Conference on Electrical Engineering (ICEE2015), Sharif University of Technology, Tehran, Iran, Feb. 2015.*

[C9] M.H. Athari, **H. Sadeghian**, and G.B. Gharehpetian, "Optimized Fuzzy Controller for Charging Algorithms of Plugin Hybrid Electric Vehicles" *23rd Iranian Conference on Electrical Engineering (ICEE 2015), Sharif University of Technology, Tehran, Iran, Feb. 2015.*

[C10] **H.R. Sadeghian**, M.M. Ardehali, and M.E Nazari "Combined Heat and Power Profit Based Unit Commitment Considering Reserve Market Using Imperialistic Competitive Algorithm" *22nd Iranian Conference on Electrical Engineering (ICEE 2014), Shahid Beheshti University, Tehran, Iran, Mar. 2014.*

Professional /Extracurricular Activities

Power the Future Innovation Competition, Dominion Energy – VCU Collage of Engineering, Oct. 2018

- Top 10 for outstanding performance with an innovation solution

Mentor, VCU Dean's Early Research Initiative (DERI) program, July 2017 – Nov. 2017

Student Program Chair, Solar Energy Workshop (SEW) 2015, Bonab, Iran

IEEE Power and Energy Society student membership, since Sept. 2014

Reviewer for IEEE and Elsevier journals and IEEE sponsored conferences

- IEEE Transactions on Sustainable Energy
- IEEE Transactions on Smart Grid
- Energy Conversion and Management (Elsevier)
- Applied Energy (Elsevier)
- International Transactions on Electrical Energy Systems (ETEP)

Professional Presentations and Talks

- Paper presentation at 2019 North American Power Symposium (NAPS2019), Oct. 2019
- Paper presentation at 2018 Innovative Smart Grid Technologies (ISGT2018), Feb. 2018
- Invited talk in VCU department of Electrical Engineering Graduate Seminar, Oct. 2017
- Two paper presentation at 49th North American Power Symposium (NAPS2017), Sep. 2017
- Research presentation for Virginia Dominion Power experts, Apr. 2017

Related Coursework

- Power system operation & control
- Knowledge discovery & data mining
- Renewable energy resources
- Sustainable & eff. power system
- Economy & energy management
- Energy planning
- Micro-grids & smart grids
- Energy storage
- Power system analysis